János Csaba Kun

Methods for improving vehicle interior noise FEM-PEM simulations in the mid-frequency range

Doctoral dissertation

Doctoral School of Multidisciplinary Engineering Sciences

Supervisor:
Dr. Dániel Feszty
Associate Professor
Széchenyi István University

2023

Table of contents

Table of Contents

Abstract

Interior acoustics has become a significant vehicle property influencing purchase decisions especially in the premium segment. Predicting acoustic behavior in the mid-frequency range between 400-1000 Hz with the inclusion of porous elastic materials (PEM), however, poses significant challenges in numerical simulations. Thus, the goal of the research presented in this work was to develop methods addressing specifically the challenges of the acoustic simulations in the mid-frequency range.

A multi-level complexity Finite Element Method (FEM) - PEM simulation campaign was carried out to investigate influences leading to the discrepancy between interior vehicle acoustic measurements and simulations in the mid-frequency range. Three test cases were investigated in untrimmed – body-in-white – and in trimmed configurations: a 650 mm x 550 mm flat plate with 2 mm thickness, a scaled model vehicle interior with acoustically participating walls, and a full-scale production vehicle, a 2015 Audi A3 Limousine.

The investigation required an intermediate complexity level between the highly academic case of a flat plate and the fully praxis-oriented whole vehicle, therefore a custom apparatus was designed that is suitable not only for validating FEM-PEM methodology but also statistical methods in the mid-frequency range. One fully rigid and one acoustically participating version of a scaled and simplified vehicle interior was manufactured, with a fluid volume modal density of minimum 3 modes in each third-octave frequency band from 282 Hz on.

Certain parameters, such as damping and Young's modulus of poroelastic materials exhibit significantly frequency dependent behavior, with up to 300% increase in these values over the investigated frequency range. Hence, the effect of this frequency dependency on acoustic response was quantified. In lightly damped structures with significant trim applications, the combination of frequency dependent damping and Young's modulus can result in up to 10 dB difference in structural response. However, with increasing complexity and cases closer to production vehicles with more damped structures and thinner applied trims, the effect reduces below 2 dB, the audible threshold.

These results prompted an investigation into further reasons for the low correlation in the mid-frequency range. Mass production vehicles are produced to certain tolerances, which is present in the thickness of the sheetmetal they are formed from. Therefore, effects of thickness tolerances were investigated on the flat plate case, with a 5% thickness variation resulting in

resonance frequencies being shifted by up to 50 Hz. This stark effect was noticeable on the model vehicle cavity as well as the full vehicle, but most prominently above 400 Hz.

Kivonat

A beltéri akusztika nagyon fontos járműtulajdonsággá vált, mely elsősorban a prémiumszegmensben vásárlást erősen befolyásoló tényező lett. Ugyanakkor nagy kihívás pontosan számítani a járművek beltéri akusztikai tulajdonságait, különösen a 400-1000 Hz közötti frekvenciatartományon, a poroelasztikus anyagok (PEM) figyelembevételével. Ezért a disszertációban bemutatott kutatás célja olyan módszerek kifejlesztése volt, melyek pontosan ezeket a kihívásokat érintik a középfrekvenciás tartományon.

Egy több komplexitási szintű végeselem-módszerrel végrehajtott, poroelasztikus anyagokat figyelembe vevő (FEM-PEM módszer) szimulációs vizsgálatot terveztem, kimondottan az akusztikai mérések és szimulációk közti eltérések lehetséges okainak feltárására a középfrekvenciás tartományon. Ehhez három teszt eset vizsgálata volt szükséges, nyers karosszéria (body-in-white) és akusztikailag csillapított (“trimmed”) konfigurációkban: egy 650 mm x 550 mm méretű, 2 mm anyagvastagságú acéllemez, egy méretarányos járműbeltér modellje akusztikailag rugalmas falakkal, illetve egy szériagyártású, 2015-ös Audi A3 Limousine karosszériája teljes beltérrel.

A vizsgálathoz szükség volt az akadémiai esetként kezelt síklemez és a teljesen praxisorientált járműmodell között, ezért egy egyedi mérőberendezést terveztem és gyártattam, mely nem csak FEM-PEM módszer validálására, hanem statisztikai módszerekére is alkalmazható a középfrekvenciás tartományban. Az egyedi berendezés befoglalt fluiduma minimum 3 sajátlengési módussal rendelkezik 282 Hz felett harmadoktávonként. A mérőberendezésből egy akusztilaig merev, és egy akusztikailag rugalmas falú változat készült.

Bizonyos paraméterek, mint a csillapítási tényező és a Young-modulus poroelasztikus anyagok esetén nagymértékben frekvenciafüggően viselkedik, akár 300%-os növekedést is mutatva a vizsgált frekvenciatartományon. Emiatt szimulációkkal vizsgáltam ennek a frekvenciafüggő viselkedésnek hatását az akusztikai válaszokra. Alacsony csillapítású szerkezetek esetén e két parameter frekvenciafüggő változása akár 10 dB különbséget okozhat szerkezeti válaszfüggvényekben. Ugyanakkor, növekvő komplexitással és szériaközelibb eseteket vizsgálva nagyobb szerkezeti csillapítással és kevesebb csillapító anyaggal, a hatás a hallható 2 dB határ alá esik.

Ezen megállapítások alapján további, középfrekvenciás eltérést okozó jelenségeket vizsgáltam. Tömeggyártásban készülő járművek gyártási tűrések figyelembe vételével készülnek, mely már az alapanyagukat adó fémlemez vastagságában is megjelenik. A síklemez

eseten a vastagságtűrés vizsgálata kimutatta, hogy a gyártási tűrések bizonyos rezonanciákat akár 50 Hz-cel befolyásolhatnak. Ez a jelentős hatás a kicsinyített és a teljes járműmodellen is észlelhető volt, ugyanakkor leginkább 400 Hz felett.

1. Introduction

1.1. Research motivation

Continuous development in the automotive industry has led customers to expect quieter and more efficient vehicles for their daily commute. Megatrends, such as the need to reduce the environmental footprint of vehicles, urbanisation or the general increase in the need for mobility have shifted paradigms for vehicle producers. Buyers today prefer intelligent, efficient and comfortable cars instead of vehicles requiring the increased level of driver control or exposure to tiring noises, vibrations as well as harsh, intrusive effects in the cabin. As a result of the aforementioned effects, today's mainstream vehicles require engineering sophistication that was formerly typical for luxury cars only. This manifests itself in the need for accurate engineering methods to achieve the desired vehicle characteristics, rather than just the usage of fine materials. To satisfy customers, highly scientific methods have to be applied during the design process of cars. Today, the noise, vibration and harshness (NVH) level is one of the key vehicle properties customers care of. However, the sole development goal is not, in all cases, the absolute reduction of noise. While mainstream vehicle models are expected to be quieter and smoother, their performance-oriented versions need to have a unique sound character, to provide an aural excitement beside driving enjoyment. Both of these development targets mean that achieving the desired acoustic characteristics has gained huge importance within the vehicle development process. Complex simulations and verification measurements have to be carried out to ensure that the final product meets the development requirements and that the development process itself is ready to flexibly engineer outstanding products.

In the current transformation of the automotive landscape, the significance of acoustic methods will not decline. Simply put, just changing the internal combustion powertrain to an electric one will not solve the many acoustic challenges that arise from the vibrations and noises from the various mechanical systems and load exchange flow-induced noises of the conventional power unit. If anything, the significance of accurate and efficient acoustic prediction methods in industry is going to grow. Electric drivetrains introduce fundamentally new challenges with their distinctive acoustic behaviour. Planetary gearsets inside electric motors emit noise at much higher frequencies than internal combustion counterparts, while the rest of the high-voltage system can also be a source of unwanted disturbances. Not to mention that the absence of the base noise emission of an IC engine brings into spotlight previously difficult to notice operating noises of the HVAC system, various servo motors serving the comfort of passengers or the tire- and wind noises at lower speeds. This means that acoustic treatments are expected to perform well not only at low frequencies (where chassis noises “masked” earlier by the combustion powertrain will now be audible) but also at high frequencies, where the excitation from e-motors will dominate (Lennström et.al., 2013). Alongside the improved acoustic performance, however, stricter efficiency goals will dictate continuous weight savings as well. This means that acoustic packages must also be designed in a greatly targeted fashion, applying only the necessary amount of material to highly specified locations. Both above mentioned, conflicting requirements coupled with the accelerated development cycles necessitate accurate numerical methods to determine acoustic properties in the early phases of the design process.

Computer aided design and development has become industry standard, and especially in the case of extensive sound package design, numerical simulations are essential for timely and cost-effective development. Depending on the investigated frequency range, various acoustic methods are available: for higher frequency applications, energy-based methods, such as Statistical Energy Analysis (SEA) are well-suited, while Finite Element Methods (FEM) are appropriate for the lower frequency ranges. Because of the fundamentally different approaches of these solvers and the large variety in the physical attributes of acoustic systems, there is no set frequency boundary for their reliable operation. Therefore, in the so-called mid-frequency range (between 400-1000 Hz), both suffer from limitation. In this range, structures generally do not possess a high enough modal density for SEA and other energy-based methods to be applicable, while the FEM’s frequency range is limited from above by statistical and modal effects. This means, that the high modal density increases the difficulty to identify individual modal contributions in the case of modal frequency response calculations, while the statistical uncertainties in the model also have a more pronounced effect on higher frequency behaviour. Unfortunately, from an excitation standpoint, this frequency range cannot simply be ignored, as disturbing sources exist that emit in these specific regions and the human ear’s acoustic reception is also particularly sensitive in the mid-frequency gap.

Sound packages have become complex since their deliberate introduction in automobiles (Figure 1.), and with their improvement the underlying design practices and engineering methods have followed suit. FEM provides an ideal framework for the abstraction of these packages as it gives almost complete freedom for the available geometries and provides multiple discretization options; however, it was not readily available to accurately model all effects of a sound package. The main material constituents of modern automotive sound packages are foam- and felt-like materials, which are collectively known as Poroelastic Materials (PEM), since they consist of a solid, porous matrix filled with air. After modelling just their mass with non-structural mass elements (the so-called Non-Structural Mass method - NSM), a significant breakthrough was the application of the Biot-theory to model absorptive effects as well. With a variety of parameters, the Biot-parameters based trim modelling allow a high degree of fine-tuning of the acoustic packages of vehicles. However, the determination of these parameters, as well as their behaviour over the various frequency ranges poses several challenges on its own. As such, the combination of finite element method and poroelastic materials into FEM-PEM modelling still opened up significant ways in improving interior acoustic simulations. However, even the addition of the Biot model did not solve the mid- and high-frequency discrepancies between simulation and measurement results.

Figure 1.: Complex interior of a state-of-the-art luxury limousine with elaborate trims (Audi Media Center, 2023).

Despite the challenges of using FEM, it is worthwhile to attempt broadening this method's applicable frequency range. By its vast applicability to structural engineering problems, it has become a standard tool in product engineering pipelines, especially in the automotive industry. As model preparation is one of the major industrial challenges in numerical simulation methods, the use of an already established method, which duplicates use cases for a single model preparation step, shows huge economic potential.

Therefore, the general goal of this work is to investigate the applicability of FEM-PEM methods for predicting the mid-frequency interior acoustic phenomena in automotive structures. In particular, various phenomena will be investigated that limit the applicability of FEM for mid-frequency acoustic problems, such as the frequency dependency of Biot-materials, as well as the potential of an overdeveloped model that is too sensitive for manufacturing tolerances, with the addition of the design of test apparatuses that aid such a research methodology. To provide proper foundations for the work, relevant literature is summarized, and the particularities of automotive interior acoustics are described before elaborating on the research methodology and its findings.

1.2. Peculiarities of vehicle acoustics

Acoustics is present in a variety of engineering fields. Architects and civil engineers must be mindful of room acoustics requirements when laying out buildings, so that in office spaces employees can converse on normal levels without disturbing each other, without the machinery noises of the building disturbing meetings. At the same time, performing venues must be laid out so that the members of the audience can enjoy the production independent of their seats, meaning that the sound pressure levels should be uniform throughout the seating space. In the aerospace industry, sound insulation is a critical factor in the commercialization of air travel. Jet engines in close vicinity produce sound pressure levels beyond our threshold of pain, therefore it is essential that aircrafts are equipped with efficient sound reduction solutions, so that the noise loading on passengers is reduced to acceptable levels. Aircraft interior acoustic challenges are quite close to those encountered in passenger vehicles, as light overall package weights and thin-walled structures are required. However, the excitations are in a vastly different spectrum and the geometric constraints, proportions, and dimensions also stray far away from those in the automotive environment. To understand the specifics that distinguish automotive interior acoustics, the upcoming section discusses particularities that were important to consider throughout the research.

1.2.1. Typical automotive structures

Modern passenger vehicles almost exclusively employ metal monocoque load carrying structures covered cosmetically by non-load-carrying metal panels. The monocoque bodies themselves are a composition of thin, formed metal panels with bonded or welded multi-material strengthening structures. In the past decade, vehicle manufacturers have started to integrate composite load-carrying members in the monocoques, typically using carbon fiber reinforced plastics to better resolve the challenge of light overall weight for strict efficiency targets and adequate handling characteristics versus chassis torsional rigidity and crashworthiness for the comfort and safety of passengers. Figure 2. shows a high-end luxury passenger car's multi-material monocoque bodywork. As the focus of this work will be on the acoustic package, no composite structures will be investigated since their FEM simulation is a topic by itself.

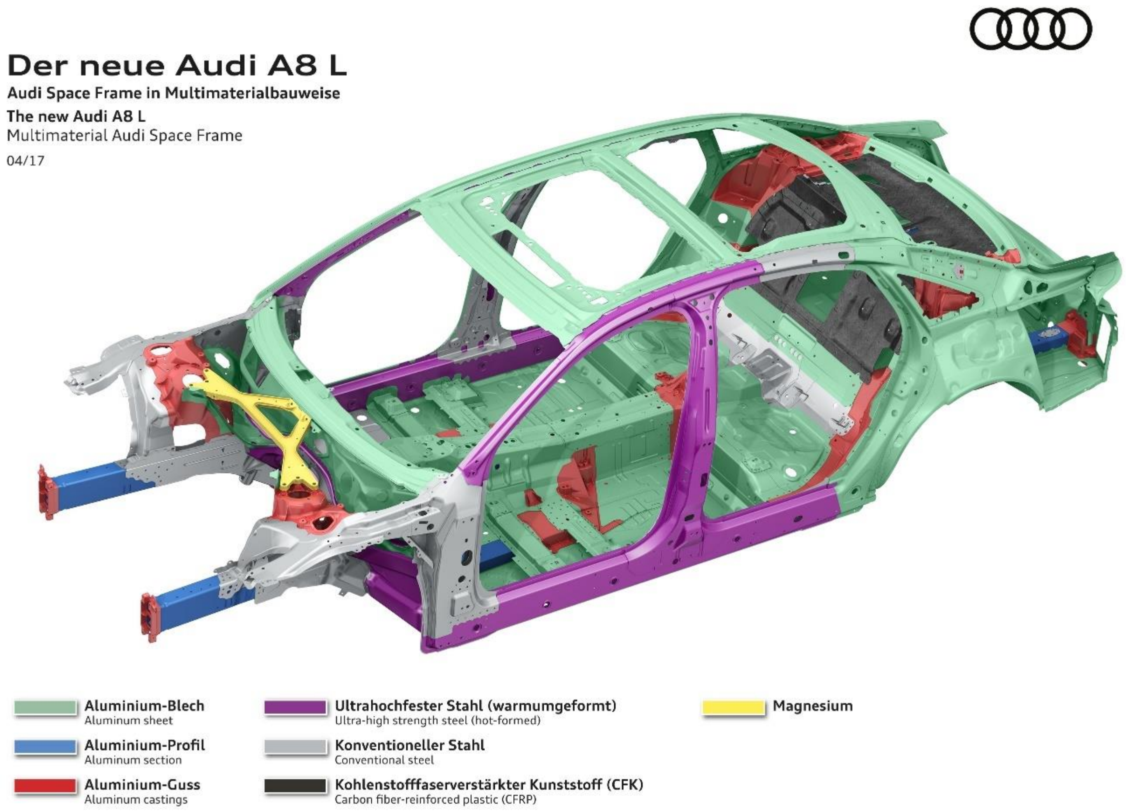

Figure 2.: Multi-material raw bodywork of a conventional passenger vehicle (Audi Media Center, 2023b).

Typical and critical elements of the bodywork are the load carrying longitudinal front chassis legs, which generally continue in a stiffening rib structure welded to the vehicle floor, as well as the doorsills, the roof-carrying A-, B-, C-pillars which form the essential safety cell of the vehicle that may not collapse even in the event of severe accidents, the central drivetrain tunnel providing additional bending stiffness to the structure and the rear chassis legs extending to the rear bulkhead. Figure 3. illustrates these main elements that constitute a vehicle body (Shome and Tulumuru, 2015).

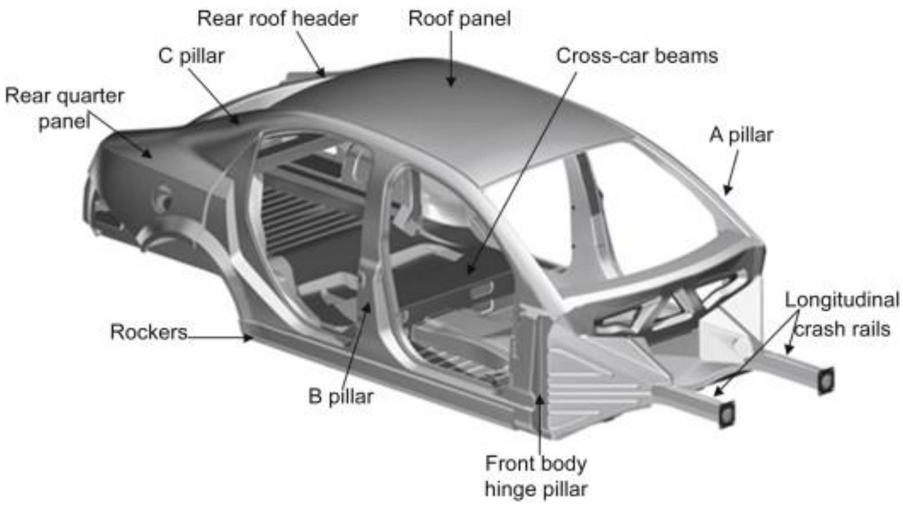

Figure 3.: Most significant elements of a modern passenger car monocoque structure (Shome and Tulumuru, 2015).

These stiffer structures are generally composed of pressed metal sheets (aluminium or steel) bonded permanently together using welding, gluing or riveting (Figure 4.). While forming a kind of skeleton for the vehicle, this structure needs to be complemented with larger sheet metal elements to form a modern, attractive vehicle body that is not only a well-engineered structure but one that grabs the attention of customers to persuade them for a purchase.

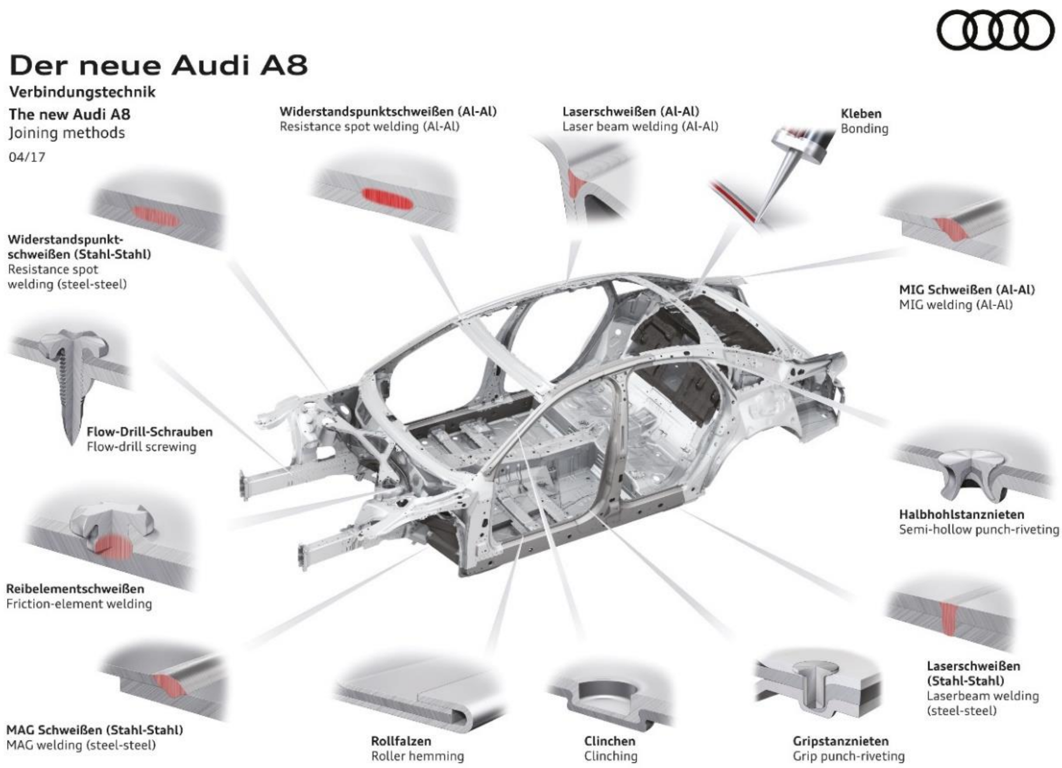

Figure 4.: Various joining methods used in a modern passenger vehicle construction (Audi Media Center, 2023c).

The floorpan, firewall, roof and sidewalls are usually also permanently attached to the bodywork using one of the previously mentioned methods, while the doors, trunk lid, hood and front bodywork components are bolted. These elements altogether enclose a passenger compartment air cavity that is the main object of inquiries and simulations pertaining interior noise, as passengers ultimately perceive the excitations as sound pressure fluctuations inside the enclosed air cavity.

A particular challenge – especially in model buildup – is the accurate discretization of the volume, due to its complex geometry that must follow the contours of the highly irregularly shaped vehicle interior. Even though the sheet metal sections are generally formed and include stiffening ribs and geometric measures to avoid excessively low first resonance modes, this is not a possibility for external panels that compose the final shape of the vehicle since their first design priority is to be attractive to customers. Along with the windscreen and side window panes, such large surfaces act as optimal amplifiers for the input vibration energy into the chassis and interior, therefore the principal objectives of acoustic development target the reduction of this amplification effect either by optimal sheet metal and bare body (or Body-in-White) construction or by the addition of sound package elements. Naturally, this results in simulations and experiments at various complexity levels in industrial environments as well, so that development engineers can understand how effectively each design measure combats unwanted noise components. A further benefit of such multi-level complexity methodology is that the various elements can be introduced into the computational campaigns stepwise as well, which highlights throughout the design process with continuous comparison to experiments the discrepancies at each complexity step. Therefore, problematic modelling methods that introduce errors can be identified from the large number of simulation input components.

1.2.2. Sound packages

The aforementioned sound packages that target interior noise level reduction are component packages composed of parts whose main- or partial goal is to absorb disturbing sound waves within the cabin. Such elements include cosmetic covers such as the floor carpet, headliner and door trims, but also some elements that are not obvious to owners, such as felts and insulators laid under the cosmetic interior covers. Collectively, these elements – that often are made of porous elastic materials (PEM) as well – are called trims. To simplify further discussion of the various complexity stages of automotive bodies, three of the most significant are defined below.

- Body-in-White (BiW): Body-in-White configuration means the completed body structure without subassemblies, trims or even windows. In this stage, the fundamental modal behavior of the metal structure can be understood, and measures can be taken to reduce harmful structure-borne noise emission.
- Body-in-Blue (BiB): A step up in complexity, body-in-blue configurations include windows and sprayed noise reductionfoams on the vehicle structure. With a completely enclosed passenger air cavity, this stage can be used for investigating fluid-structure coupling phenomena on top of modal behavior. However, crucially, porous materials are not included in this configuration.
- Trimmed Body (TB): Closest configuration to that of a roadworthy passenger vehicle, including all body parts, but still without drivetrain, suspension or wheels. Body parts include all interior components with carpeting, door covers, instrument panel and ancillary small trim elements. To accurately assess each component's contribution to the complete package performance, stepwise built-up configurations may occur, i.e. with and without door trims, headliner, firewall insulation, etc. (Fig. 5.)

Representation of trims in computational models is a major topic of interest in the automotive world since they have a profound impact on the interior acoustic behaviour. This is self-explanatory, but the need for accurate modelling stems from the ever-accelerating development cycles and tighter budgets that push manufacturers strongly towards more efficient development methods. In the case of a highly complex product like today's automobiles, costs of product changes increase exponentially along the development timeline, leading to a situation where most of the vehicle's components have to undergo at least some degree of virtual testing before even the first prototypes are built, as the costs of simulations are on a different order of magnitude than re-engineering budget requirements. With accurate modelling, the number of costly prototypes can be drastically reduced and before any physical part is manufactured, hundreds of options can be virtually evaluated, optimizing the initial point of development in the physical realm.

Trims reduce interior noise through two fundamental phenomena:

1. Mass damping: through their inherent added mass, trims change the modal behavior of structures, thereby altering resonant frequencies and/or mode shapes.
2. Absorption: as two-phase materials with a structural matrix and fluid phase, interior trims also absorb and dampen reverberant sound waves in the interior.

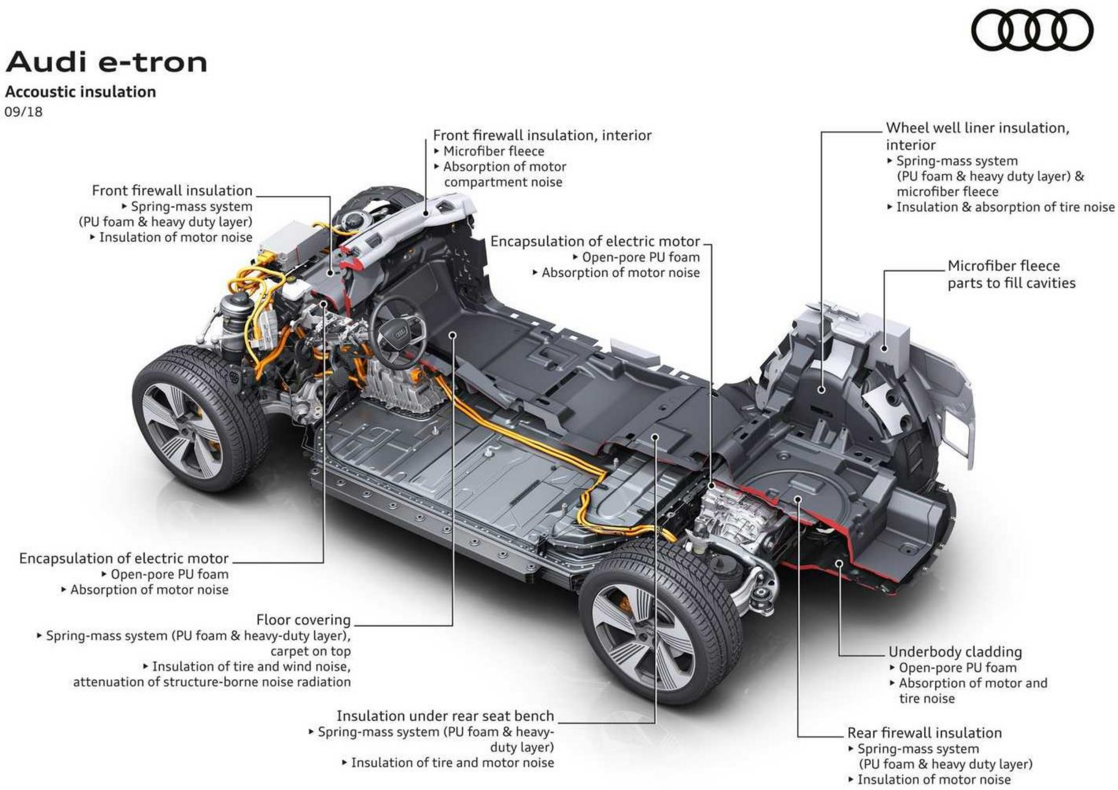

Figure 5.: Acoustic insulation trim elements in a modern electric vehicle (Audi Media Center 2023d).

Naturally, both noise reduction methods should be implemented in virtual testing methods to make them applicable on a broader scale in industry. In initial attempts at acoustic simulations, trims were represented only as non-structural masses, which greatly simplifies calculations and models their mass damping effect. In case of FEM simulations, this simply means that masses are added to specific nodes on the structure, locally. Such methodology can be sufficient for very preliminary investigations or where absorptive effects are not relevant (for instance in the case of local added masses to panels, this modelling method is sufficient) and is very useful in approximating basic effects. However, for simulating a complete vehicle interior, using purely non-structural masses would lead to a gross miscalculation of acoustic phenomena. Absorption effects are completely neglected when using non-structural masses, which means that the reverberations of the cabin can easily be over- or underestimated. Accurate modelling of absorption also requires accurate modelling of geometries, something that is also not possible using purely non-structural mass elements. Many trims are composed of multiple layers of vastly different materials, such as a combination of a foam-like underlayer fixed permanently to a heavy damping overlay, which can only be represented very crudely as an averaged material with the non-structural mass method. With the ever-growing complexity of sound packages including multi-layer trims, complex shapes, varying materials, a new method was developed to ensure the quality of calculations.

1.2.3. Biot-Theory

As in the case of solving the Navier-Stokes equations in Computational Fluid Dynamics (CFD), the new method was not developed fully from scratch for this purpose, rather it was the application of a method used in another discipline to acoustic problems that brought a significant advancement in trim modelling. This method was the application of the Biot-theory in acoustic simulations. Biot-theory, or the theory of poroelasticity was originally developed by Maurice Biot in the 1940's for modelling wave propagation in porous materials composed of a solid matrix filled with a fluid (Biot, 1956). The theory found its initial use in determining settlement of structures on porous soils saturated with fluid in the pursuit and discovery of oil fields. Since the theory aims to describe the elastic behaviour of a porous medium, it is also named as the theory of poroelasticity, and thereby such two-phase materials applied in vehicles are also called Poroelastic Materials (PEM). Three underlying physical theories lay the fundaments of Biot theory: linear elasticity (of the solid matrix), Navier-Stokes equations (to describe the viscous fluid) and Darcy's law (to account for fluid flow in the pores). Altogether these theories are used to assemble the governing equations of the theory of poroelasticity, which describe wave propagation in porous media. Three waves are assumed to propagate through the material: a shear component within the solid matrix, as well as pressure components in the solid matrix and the fluid medium. The original formulation uses six translational variables – $\boldsymbol{u^s}$, $\boldsymbol{u^f}$ vectors for solid and fluid displacements – to express strain- and kinetic energies as well as stress tensors. Biot's original theory culminates in the following set of equations for time-harmonic waves with $\boldsymbol{\omega}$ frequency (Dazel, 2011):

$$\boldsymbol{\nabla\sigma^s}\left(\boldsymbol{u^s},\boldsymbol{u^f}\right) = -\omega^2\,\tilde{\rho}_{11}\boldsymbol{\ddot{u}^s} - \omega^2\tilde{\rho}_{12}\boldsymbol{\ddot{u}^f} \tag{1}$$

$$\boldsymbol{\nabla\sigma^f}\left(\boldsymbol{u^s},\boldsymbol{u^f}\right) = -\boldsymbol{\omega^2}\,\boldsymbol{\tilde{\rho}_{12}}\boldsymbol{\ddot{u}^s} - \boldsymbol{\omega^2}\boldsymbol{\tilde{\rho}_{22}}\boldsymbol{\ddot{u}^f} \tag{2}$$

$$\boldsymbol{\sigma^s}\left(\boldsymbol{u^s},\boldsymbol{u^f}\right) = \left[\boldsymbol{\tilde{P}\nabla u^s} + \boldsymbol{\tilde{Q}\nabla u^f}\right]\boldsymbol{\delta} + \boldsymbol{2N\varepsilon^s}(\boldsymbol{u^s}) \tag{3}$$

$$\boldsymbol{\sigma^f}\left(\boldsymbol{u^s},\boldsymbol{u^f}\right) = \left[\boldsymbol{\tilde{Q}\nabla u^s} + \boldsymbol{\tilde{R}\nabla u^f}\right]\boldsymbol{\delta} \tag{4}$$

These equations account for dissipative effects of three kinds: viscous, structural and thermal dissipation are all considered:

- Viscous dissipation: determined by the square of the relative fluid translation and the flow resistance;

- Structural dissipation: accounted for using complex and frequency dependent coefficients $\tilde{P}, \tilde{Q}, \tilde{R}$;
- Thermal dissipation: included through the fluid's complex, frequency dependent compression modulus $\tilde{K}^f$.

With two distinctive phases present, their interaction cannot be neglected, therefore visco-inertia coupling terms ($\tilde{\rho}_{11}, \tilde{\rho}_{12}, \tilde{\rho}_{22}$) – equivalent densities – are also included in the equation set. These are calculated using the inertia coupling coefficients ($\rho_{11}, \rho_{12}, \rho_{22}$), the fluid-solid coupling density-type measure ρ_a , the material densities of the fluid ρ_f and the solid matrix ρ_s as well as the high-frequency limit of tortuosity α_∞ and porosity θ (explained later, together with the other Biot-parameters) as follows:

$$\boldsymbol{\rho_{11} = \rho_1 + \rho_a,\ \rho_{12} = -\rho_a,\ \rho_{22} = \rho_2 + \rho_a} \tag{5}$$

where

$$\boldsymbol{\rho_1 = (1-\theta)\rho_s,\ \rho_2 = \theta\rho_f,\ \rho_a = (\alpha_\infty - 1)\theta\rho_f} \tag{6}$$

Using $\tilde{b}$ complex coefficient of viscous effects, the visco-inertial coupling terms are computed using the following formulae:

$$\boldsymbol{\tilde{\rho}_{11} = \rho_{11} + \frac{\tilde{b}}{j\omega},\ \tilde{\rho}_{12} = \rho_{12} - \frac{\tilde{b}}{j\omega},\ \tilde{\rho}_{22} = \rho_{22} + \frac{\tilde{b}}{j\omega},} \tag{7}$$

Since their formulation, this set of equations have been revised to reduce the number of operations and thereby enable the efficient use of the theory in today's computational campaigns. Atalla's 1998 revision replaced the fluid translation vector with scalar pressure (*p*), which resulted in the equation set that is widely used by today's commercial FEM-PEM simulation software, including ESI VPS and Nastran-Actran, the two solvers used in this work's simulations (Atalla et.al., 1998). The resulting set of three equations for the displacements, pressure and stresses, often referred to as the *u-p* formulation, are written below:

$$\boldsymbol{\nabla\sigma^s\,(u^s\,,p) = -\omega^2\,\tilde{\rho}_s u^s - \gamma\nabla p} \tag{8}$$

$$\boldsymbol{\nabla p = -\omega^2\,\frac{\tilde{\rho}_{22}}{R}\,p - \omega^2\,\frac{\tilde{\rho}_{22}}{\theta^2}\,\gamma u^s} \tag{9}$$

$$\boldsymbol{\sigma^s\,(u^s\,,p) = \delta\left(K_b - \frac{2}{3}N\right)\nabla u^s + 2N\varepsilon^s(u^s)} \tag{10}$$

, wherein

$$\gamma = \theta\left(\frac{\tilde{\rho}_{12}}{\tilde{\rho}_{22}} - \frac{\tilde{Q}}{\tilde{R}}\right), \tilde{\rho}_s = \tilde{\rho}_{11}\frac{\tilde{\rho}_{12}{}^2}{\tilde{\rho}_{22}} \tag{11}$$

Various formulations exist for determining the complex effective density as well as the compression modulus. Of these, however, the Johnson-Champoux-Allard formulation is most commonly used in commercial codes, such as those used in this work (Allard and Atalla, 2009). As a result, the following material parameters are required to describe poroelastic material behaviour in the discussed formulation (Figure 6. illustrates a generic cross-section):

Phase parameters of constituting materials:

1. Fluid density
2. Speed of sound in fluid
3. Solid matrix structural density: full mass divided by full volume

Specific, porous elastic material parameters:

4. Porosity: ratio of solid and fluid phase volume
5. Flow resistivity: describes viscous losses
6. Tortuosity: provides the coupling between matrix and fluid
7. Viscous characteristic length: another measure of viscous losses
8. Thermal characteristic length: describes thermal losses
9. Damping loss coefficient of the matrix: provides information on structural losses
10. Young's modulus of matrix: elastic behavior descriptor of the matrix
11. Poisson-coefficient of matrix: describes volume change under stress in the matrix

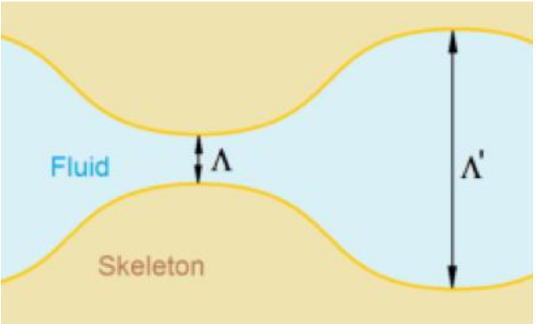

Figure 6.: Sample cross-section of a generic poroelastic material (Allard and Atalla, 2009).

Measurement and determination of these parameters is an ongoing topic of interest due to their wide application in the automotive industry. Fundamentally, they can be measured using three techniques:

- Direct measurement: experiments yield the parameter of interest directly as a result
- Indirect measurement: the parameter of interest is determined analytically or empirically from two or more directly measured quantities
- Inverse measurement: the parameter of interest is a result of an optimisation scheme carried out over a function defined as the difference of measured and modelled data.

With two of the three fundamental measurement methods being an abstraction from a direct measurement, it is evident that the determination of the parameters is a topic of itself, not being the focus of the current work.

Although the original topic of Biot's theory and its vehicle acoustic application on the surface appear vastly different, the basic phenomenon of a fluid interacting with a solid matrix and influencing its mechanical behaviour is very similar, albeit completely on another scale. In vehicles, the used foams have macroscopic external dimensions, and so do the vehicle structures as well – just like in the case of the originally intended soils as well, however, the applied trims' interiors are on the microscopic scale. This means that wave propagation phenomena inside the material are also on such a small scale. As the physical phenomena of sound dissipation within poroelastic materials is that of wave propagation in a fluid constrained by a solid skeleton, Computational Fluid Dynamics could also provide a mathematical language to interpret solutions. Despite exponential growth of available computational power, however, the Biot-theory cannot be exchanged by a coupled FEM-CFD solution on a full-scale vehicle, as the pores would require discretization levels unfeasible for the whole vehicle interior.

1.2.4. Typical excitations

Excitations are quite distinctive in the case of road vehicles. They are perceived by passengers as pressure waves transmitted to their ear drums through air in the cabin compartment. However, these pressure waves can be induced through two fundamentally different transfer paths, which is the classical distinction between noise sources in road vehicles (Kohners and Lehmann, 2014):

- Structure-borne noise: Noise induced by the physical impact of an object on a structure and this signal travelling within the structure. For vehicles, this would correspond to time varying loads (i.e. vibrations) entering the vehicle chassis from the road and tyres, or elements of the powertrain. An example can be the vibratory load entering the chassis through the tyres, rims and suspension due to uneven road, or the vibrations entering the chassis from the engine vibrations. Typical frequency range is between 20-400 Hz.
- Airborne noise: Noise induced by aerodynamic loads or the acoustic radiation of an object and entering the structure of interest via air. For vehicles, this corresponds to time-varying loads (i.e. vibrations) entering the vehicle chassis through the air around the vehicle. Examples are the vibration of the roof due to turbulent flow around it, the pressure waves radiated by the engine in the engine bay, or the tyre surfaces as the tyre is periodically deformed at the tyre-road interface Typical frequency range is 500 Hz and above.

All significant excitation sources of the vehicle are bolted to the skeleton formed by the stiffeners described in a previous section. Suspension- and drivetrain subsystems are the major noise sources directly attached to the vehicle body. Primarily, the structure borne noise elements, like road surface unevenness is damped but still transmitted into the cabin through the suspension arms, shock absorbers and subframe mounting points into the strut towers and through the chassis legs, while powertrain vibrations pass through the mountings directly into the main structure.

These two noise categories are distinctively important as their frequency ranges differ, therefore solvers are more suited to accurate prediction in one or the other. Figure 7. illustrates frequency ranges where certain noises are dominant.

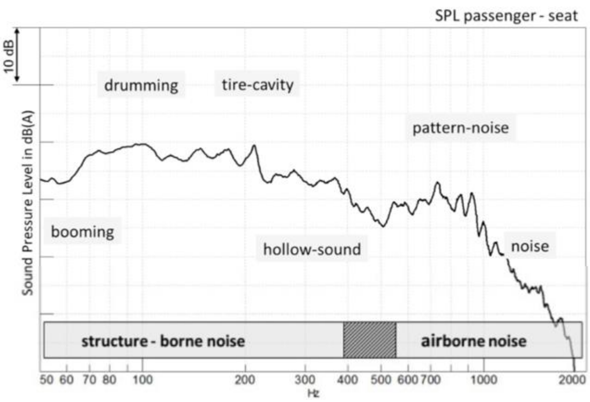

Figure 7.: Frequency range of structure-borne and airborne noise components (Kohners and Lehmann, 2014).

Both structure- and airborne noise sources lead to the vibration of the chassis elements, which create specific boundary conditions for vehicle acoustics. As the bare vehicle structure with large, exposed plate-like surfaces is acoustically unacceptable, acoustic packages comprising of trim elements described in Section 1.2.1. serve the purpose of reducing interior noise as well. Figure 8. shows a schematic cutaway model of a fully trimmed luxury car, which is a great example of the level of complexity that needs to be considered for a whole vehicle. With environmental impact in the focus, lightweight design of these sound packages is paramount.

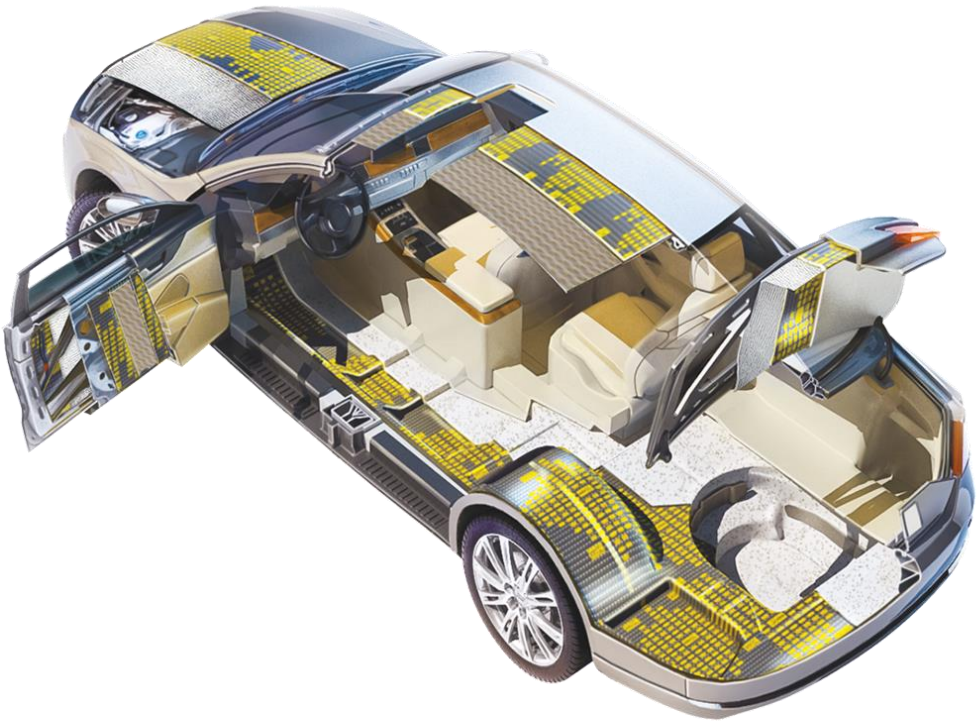

Figure 8.: Multi-layer trim components in a modern luxury vehicle (SGM-Techno, 2023).

All of the above results in a highly complex vibrational system that poses challenges not only in material property modelling but in determining appropriate geometric abstractions.

1.3. Literature review

In order to position current work in today's research space, this section provides a comprehensive overview of simulating vehicle interior acoustics using FEM-PEM methods. To appropriately place the current work, scientific literature must be reviewed, citing the most significant works pertaining the topic at hand, leading to the identification of the gaps in knowledge which will form the basis of the original contribution detailed in the work.

1.3.1. Fundamentals of Finite Element Methods for acoustics

Finite Element Methods (FEM) can be used not only for stress and strength analysis, but also for predicting the acoustic behaviour of structures. Structural problems are solved using a stiffness matrix as well as a displacement- and a load vector, while in acoustic dynamic analyses these are supplemented by mass and damping matrices, as well as acceleration and velocity vectors. Detailed description of structural FEM can be found in (Zienkewicz and Taylor, 2003) and (Thomas, 2007), while the acoustic coupling theory is expanded in (Marburg and Nolte, 2008) and (Ihlenburg, 1998).

For acoustic simulations, it is necessary to model the air surrounding the vibrating solid object. To determine the pressure field in air, coupled solutions are used where the stiffness matrix contains the coupling between the structure and air cavity. Song et al. and Kim et.al. worked extensively on developing acoustic coupling formulations (Song et.al., 2003; Kim et.al., 1999). For solving these equations, multiple solution schemes exist, with modal frequency analysis being the most predominant in vehicle industry. Modal frequency analysis will be elaborated with the specifics employed in the applied solvers for this dissertation's numerical campaign.

1.3.2. Academic cases focusing on simplified geometries

Flat plates as an academic case have been the subject of discussion from the early days of finite element methods and structural computation. As many automotive and especially aerospace acoustics and vibration issues can be modelled with a flat plate setup, various boundary conditions and excitations have been investigated. As large, thin plates with reinforcements are common in aircraft, Strawderman and Brand investigated plate response to airborne noise by determining cross-power spectral densities and plate velocity statistics (Strawderman and Brand, 1969). Their excitation model agreed well with experiments, however, the spectral density results could not be compared with measurement data at the time, only the peak spectrum, which showed good accuracy. In their academic case, the plate was isotropic, simply supported and mounted in an infinite, rigid baffle, with air flowing over one side, corresponding to the typical excitation case experienced in airplanes. Graham has worked on a similar problem, considering a single aircraft panel of 0.5 m width and 0.2 m depth (Graham, 1996a). Turbulent airflow was used for a uniform excitation over the plate, however, plate acoustic radiation was also considered. The developed model used three components (structural, acoustic and hydrodynamic), whose interactions and the wavenumber scattering were all included in the final calculations. Using parameter variation, effects of structural damping, critical frequency, hydrodynamic coincidence and structural inhomogeneity on the response were studied, although not compared with experiments. Acoustic emission of a flat plate concerned Prosser et. al., whose research evaluated a normal mode and dynamic finite element method solution to determine emitted waveforms (Prosser et.al., 1999). Isotropic and composite materials both were under scrutiny, and the DFEM method`s versatility was highlighted as the results from the two techniques tended to correlate well. Flat plates were also the focus of investigation for Farag and Pan. Both flexural and in-plane vibrations of single and coupled flat plates with free and simply supported boundary conditions were considered. Focus was to find natural frequencies, mode shapes and responses, both in terms of displacement and power flows (Farag and Pan, 1998). Frequencies ranged from 0-500 Hz region to 1500-2000 Hz range, where the upper limit lies roughly twice higher than considered in this dissertation. Generally, these investigations employed only numerical schemes.

A major interest in sound insulation and lightweighting is the use of composite panels, either metal-polymer sandwich of fiber-reinforced plastic. Ege et al. compared multiple methods to obtain an equivalent plate model for multilayer plates over an extremely wide frequency range (40 Hz – 20 kHz) (Ege et.al., 2015). The main goal of the work was to be able to determine the frequency dependent complex Young`s modulus of the polymer core, which has successfully been achieved using an inverse technique. The authors highlight that this enables a more accurate prediction of damping characteristics over a broad frequency range, signifying the importance of frequency dependent materials. Liu and Li applied a forced excitation and thermal loading to a sandwich plate and determined its vibration response using the non-classical medium and thick plate theory and modal superposition. Results were compared to FEM/BEM calculations, however, the most emphasis was placed on the parametric study of the Young`s modulus as well as core/face ratio. Frequency dependent parameters were not applied (Liu and Li, 2013). Eshmatov investigated a nonlinear computation method based on the Kirchhoff-Love and Reissner-Mindlin plate theories. Various influencing parameters of the developed procedure were studied, and the author concluded that viscoelastic properties and accurate deformation models were the key to good agreement with experiments (Eshmatov, 2007). Burlayenko et.al. focused on determining the natural frequency of composite plates, however with a lesser focus on vibration response (Burlayenko et.al., 2015). In the second part of his research, Graham included trim over the investigated panel, however, without the use of the Biot-theory (Graham, 1996b). Two layers of insulation and a single layer of plastic trim panel were added to the plate. Naturally, the results indicated high attenuation levels as expected, however, the method was very novel and not used later. Simulations results were not compared with measurements.

As thickness of a plate has a major influence on its bending moment and thereby natural frequency, variable thickness plates have also garnered attention. B. Raju used a finite difference approximation to evaluate eigenfrequencies of a plate with linearly varying thickness which proved to be effective until larger amplitudes introduced nonlinearities (B. Raju, 1966). Another similar research was carried out on a circular plate as well by K. Raju, however, focusing on larger amplitudes, showing further interest in the topic (K. Raju, 1977). Roy and Ganesan studied a square plate`s vibration behavior with variable thickness, postulating that a variable thickness plate can be an effective tool for lowering vibration amplitudes (Roy and Ganesan, 1992a; Roy and Ganesan, 1992b; Roy and Ganesan, 1993). Tapered plates may also be combined with damping foil patches, as investigated by Kumar et.al. (Kumar et.al., 2016; Kumar et.al., 2020). Interestingly, their research was conducted both in air and water media, however, the frequency range of interest was way below the mid-frequency spectrum of interest of the current investigation, and no direct measurement correlation was presented.

Flat plates on their own hardly ever occur in vehicles, therefore a more complex approach is needed to investigate an enclosed air cavity, bounded either by acoustically participating, i.e. flexible or non-participating, rigid walls. Early research of such test cases was performed by Wolf and Nefske, investigating a vehicle interior with modal analysis, as well as Dowell and Voss, focusing on a cavity backed plate system (Wolf and Nefske, 1975; Dowel and Voss, 1963). To model the geometry of a vehicle interior more closely, cavities with tilted walls are often looked into, either with a single or multiple flexible panels (Li and Cheng, 2004; Sum and Pan, 2006; Li and Cheng, 2007). Fully flexible walled cavities in general are the closes in acoustic behavior to a real vehicle structure, yet their possible smaller size and simpler geometry streamline studies on them. Martin and Bodrero, and Jin et.al. investigated such systems, while Peretti and Dowell employed a single flexible wall to research a cavity (Peretti and Dowell, 1992; Martin and Bodrero, 1997; Jin et.al., 2009). Liu et.al. used a rigid walled cavity with a single flexible panel and added porous material to study transmission into the cavity through an excitation on the flexible plate. Relatively good agreement between measurement and simulation was achieved, however the upper frequency limit in the investigation was 500 Hz. (Liu et.al., 2015)

1.3.3. Trim modelling using non-structural mass

Even though Biot`s theory was available from the middle of the 20th century (Biot, 1956a; Biot, 1956b), his findings were not implemented into porous material modelling until the advancements in computing power (Johnson et.al., 1987; Hörlin et.al., 2001, Rigobert et.al., 2003). Such high-effort methods could only gain importance with the increasing sophistication of vehicle design and the higher allowed development costs to increase product substance.

Despite the difficulty in applying the modelling equations, engineers still desired to approximate the acoustic effects of trims. The earliest estimation was done by adding non-structural mass elements on panels where trims would be installed. Depending on the model, locally increased stiffness and damping values complemented the addition of extra masses. One of the earliest examples for this technique is the work done by Priebsch et al. The detailed study examined noise levels emitted by an inline five cylinder engine using finite element calculations (Figure 9.). Poroelastic engine trims were modelled as extra mass without influencing the structural properties of the system. As trim elements were not the focus of this study, their effect was not quantified separately, however, the relatively good comparison between simualtion and measurements proved that the non-structural mass idea had merit in this particular application (Priebsch, et.al., 1990).

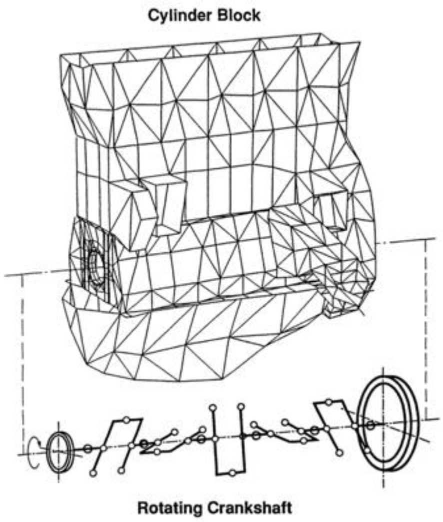

Figure 9.: finite element model of a 5-cylinder engine and crankshaft (Priebsch et.al., 1990)

While trim elements are used on engines as well, their most prominent acoustic role is in the interior. Various damping mats as well as door cards, instrument panels and the seats themselves are used to attenuate disturbing noise from outside. Therefore, the application of non-structural mass models for interior poroelastic materials was a straightforward choice. An example for such a case is the work done by Sung et.al. in 1999. As part of a series of investigations on trimmed bodies, the eigenmodes of a vehicle body were calculated, along with the frequency response. Besides their computational campaign, frequency response functions (FRFs) were also measured, shown on Figure 10. (Sung et.al., 1999).

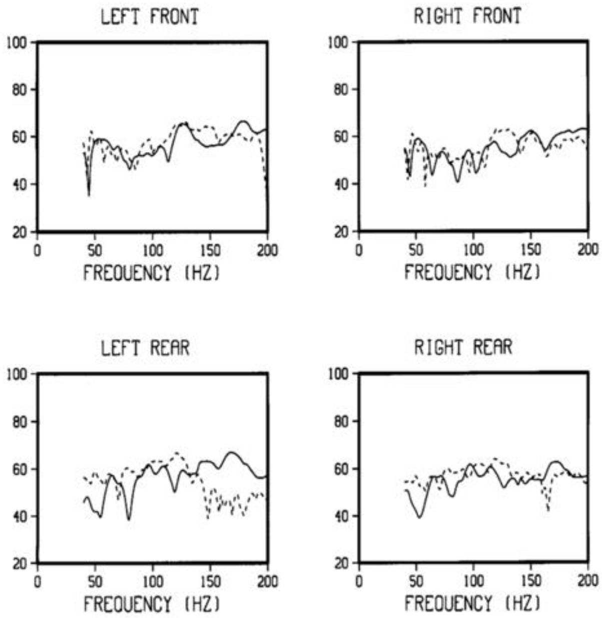

Figure 10.: Comparison of measured (- - -) and calculated (–) SPL (Sung et.al., 1999)

Using 24 reference points over the vehicle body and a single excitation input location, a spatially averaged FRF was compared with the calculated values (Figure 9.). As this was an early attempt at a trimmed body investigation, quite a number of simplifying assumptions were made during the simulation. Trim elements were represented only as non-structural mass, while the doors, hood and trunklid were reduced to point masses and replaced with rigid elements, joined to the bodywork through coupling factors. The relatively small amount of cells (35000 for the body model and 2500 for the acoustic cavity) also reduced accuracy, which manifested itself in the results. Trends were captured correctly, but – especially with increasing frequency – differences between measured and calculated results reached more than 5 dB both in FRF and sound pressure levels inside the cabin.

While this method has a lot of limitations in such a complex case, its quick computation time warrants its use in certain campaigns where short turn-around times are required. Subramanian et al. performed a damping material optimization on a full-size truck cabin. Using a finite element solver, strain energy contours were calculated for treated body panels (Figure 11.). The contours were used to identify extreme energy points, where treatment was increased. By running this process in a feedback loop, the optimization was completed. Although the accuracy of the results was not perfect, the identified locations and treatment increases were proven useful later in the product development cycle. The overall goal of the optimization was achieved, as the production model received a damping treatment with reduced volume and mass (Subramanian et.al., 2003).

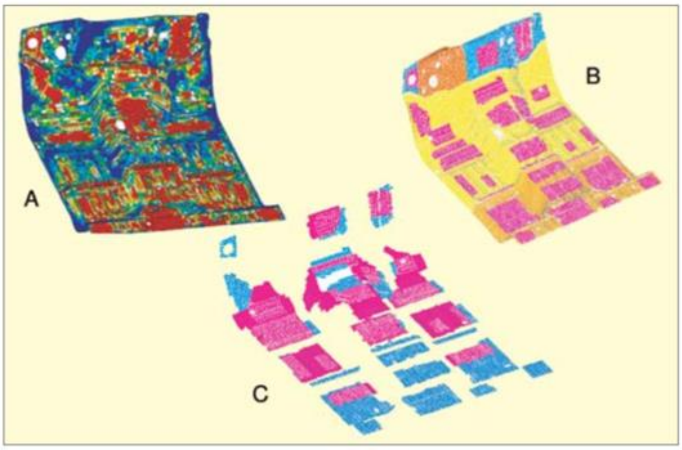

Figure 11.: Composite strain energy contour (A) and damping layer treatment optimization (B: original damping layer, C: optimized damping layer) of a vehicle floor panel (Subramanian et.al., 2003)

Despite being useful in predicting trends, this approximate method has very limited usage. As Sung and Nefske also point out, its main advantage is the quick computational time and relatively good correlation with measurements below 50 Hz. Such limited frequency range means that it cannot be reliably used for meaningful interior noise assessments (Sung and Nefske, 2001).

1.3.4. Biot theory used in automotive acoustics problems with FEM

As available computational capacity started to grow exponentially, the more complex poroelastic formulations started to receive more popularity. Biot-theory describes the behaviour of PEM materials using about 13 macroscopic parameters (the number depends on the equation formulation), which are extracted from measurements (Champoux and Allard, 1991; Atalla et.al., 2006a; Atalla et.al., 2006b; Hamdi et.al., 2000; Hamdi et.al. 2001). Since most of the Biot-parameters are both material- and frequency-dependent, their accurate measurement and application in numerical campaigns poses considerable challenges (Wolkesson, 2013; Berardi et.al., 2016; Jocker and Smeulders, 2016). However, the use of the Biot-theory in FEM simulations improves the comparison between experiments and numerical simulations greatly, especially when compared to the non-structural mass approach. FEM-PEM results match the experiments to higher frequencies, which justifies the extra computational cost imposed.

One of the earliest to approach the Biot theory in Finite Element Methods was Panneton and Atalla. Their 1997 paper describes a method where the Biot equations are formulated for a finite element solution approach, but simplified by mathematically separating the independent fluid and solid degrees of freedom and approximating the low-frequency material behaviour on the basis of air properties. Despite the mathematical efficiency, the method was only used in the 100-500 Hz region on a geometrically simple model seen on Figure 12., and no practical application of this exact scheme was published (Panneton and Atalla, 1997). Göransson also attempted a simplified FE solution of Biot`s equations by taking advantage of matrix symmetries between porous frame and pore fluids. The fully symmetric formulation, however, still requires five unknowns per node to solve for poroelastic effects, which is why its use was not shown in the paper above 160 Hz (Göransson, 1998).

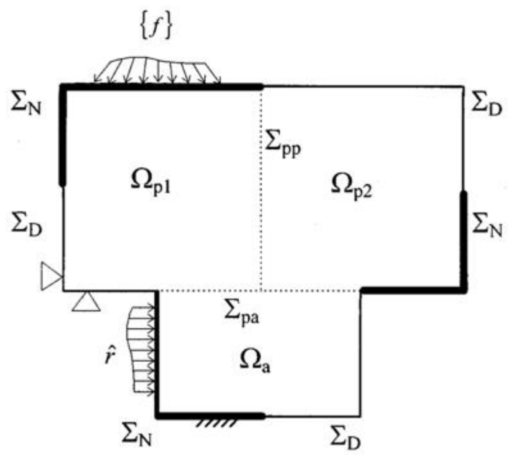

Figure 12.: Geometric setup of the problem posed by Panneton and Atalla: three-dimensional finite domain with acoustic- and poroelastic media (Ω_{pi} and Ω_a) with three different boundary conditions: Σ_{pa} and Σ_{pp} as interfaces between domains, Σ_N and Σ_D as boundaries with Neumann- and Dirichlet-conditions (Panneton and Atalla, 1997)

Deckers et al. provide an excellent summary of the various formulations of the Biot-theory and their numerical applications into a solution scheme (Deckers et.al., 2014). This work is important as a milestone for summarizing the possible numerical ways to include poroelastic modelling. The authors detail various approximation schemes, where either the PEM matrix is assumed to be fully rigid, or an equivalent fluid represents the material. To illustrate the complexity of Biot modelling, Deckers et al. lists seven different formulations that can be used in numerical solvers, with varying numbers of degrees of freedom. Transfer Matrix Method

(TMM) is also described as a viable solution for higher frequency problems. Higher frequencies cause problems in FEM simulations due to the small element sizes necessitated by short wavelengths, a problem exacerbated by the presence of porous cavities which further impose wavelength restrictions. TMM alleviates this issue by describing wave propagation through a multi-layered medium. By assuming an infinite number of layers and keeping in mind that only two dilatational and one transversal wave can propagate through a poroelastic medium, the transfer matrix describes the wave field using a limited number of variables. However, the description of the exact coupling system to the boundaries and originally assuming a plane wave means that TMM`s limitations must be considered. The work of Jain et. al. focusing on optimization of seat materials and their acoustic response also shows the merits of TMM as a component optimization scheme (Jain et.al., 2013). Dejaeger et al. used this method in an effective mass optimization study for an instrument panel insulator. Their goal was to retain or improve the acoustic properties of a firewall damping material while reducing its overall weight. Instead of performing detailed analysis of the entire firewall-insulator-instrument panel system in FEM for each iteration with exactly modelled poroelastic effects, the transfer matrix method was used to evaluate multiple concepts in a shorter timeframe, and only the best of those was validated using a complex FE simulation. The optimization loop developed in their paper is shown on Figure 13. Measurements confirmed the validity of the approach, with the optimized insulator providing improved transmission loss as well as lower weight than the baseline configuration (Dejaeger, 2012).

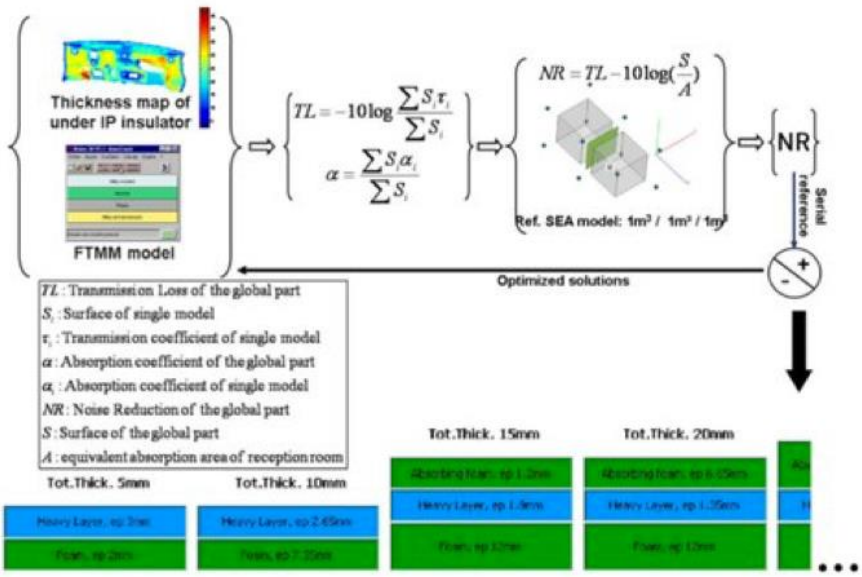

Figure 13.: Optimization loop involving TMM for an instrument panel (Dejaeger, 2012).

A similar optimization scheme was carried out by Rondeau et al., however on a wider topic breadth: Biot parameter and transmission loss measurements were also carried out on a complex instrument panel model, while the numerical campaign involved FEM, boundary element method and poroelastic modelling as well. Correlation between measurement and simulation was overall good, especially in the above 1000 Hz frequency range, as shown on Figure 14. (Rondeau et.al., 2014).

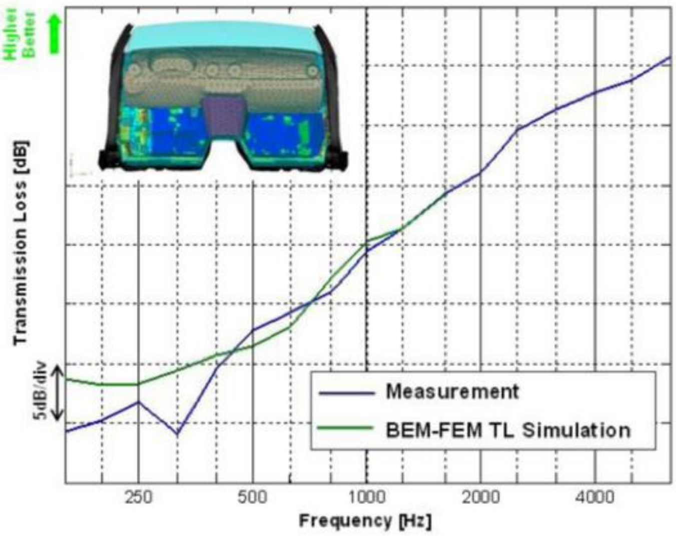

Figure 14.: Transmission loss of instrument panel insulator configuration – measurement and simulation (Rondeau et.al., 2014).

While TMM is useful in the component optimization scheme, its limits are reached when dealing with multiple trim elements in a single acoustic system. For a more complex system, Biot equations or a model thereof is needed. In a 2015 publication, Pietrzyk attempted to predict transmitted airborne noise into a vehicle passenger cabin (Pietrzyk, 2015). For the research, a body-in-blue configuration car model was used (no interior trim, doors and enclosures trimmed) with and without porous carpet material. By starting the investigation with a measurement campaign, baseline values were established. Calculations carried out with the porous carpet used the built-in Biot modeler of MSC Actran. Out of the 4 internal microphones, results for the chosen one show questionable accuracy, with differences reaching 10-20 dB in the worst locations. Frequency range was higher here, as expected for airborne noise transmission, however the maximum test frequency was only 400 Hz. Computational results followed measurement curves better in the 0-200 Hz region than above as Fig. 15. shows, although it should be noted that this model needs more refinement to obtain closer results. As mentioned before, the sheer number of material parameters influencing the Biot-model, as well as their frequency dependency can introduce large discrepancies into simulations, and possibly with more correctly set values, this calculation could also arrive at a better conclusion.

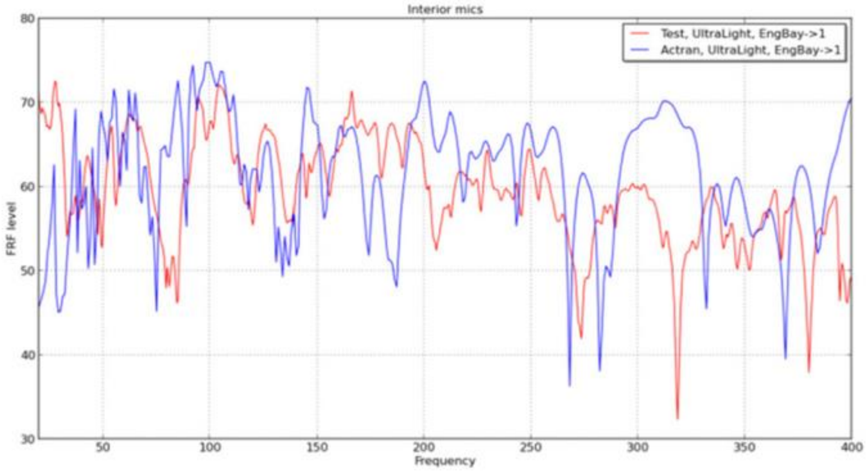

Figure 15.: Resulting FRFs at microphone 1 from measurement (red) and simulation (blue) of a body-in-blue configuration vehicle with interior carpet (Pietrzyk, 2015)

The built-in capabilities of MSC Actran for poroelastic modelling were used by Guellec et al. to perform trim element optimization on a passenger car (Guellec et.al., 2018). As one of the more recent published works on the FEM-PEM topic, it contains the latest simulation results obtained for a trimmed vehicle setup with floor insulator carpet. Two different calculation methods are presented and compared in their work. One involves MSC NASTRAN for a traditional modal solution, which includes calculation of the reduced impedance matrix in Actran. The other, however, takes place fully in Actran and starts with the computed cavity- and structural modes, with the ability to add frequency dependent damping – either globally, or node by node. As the amount of modes can increase rapidly, only a select number of them are stored for computational efficiency. During the carpet optimization, both solution strategies are used since changing embossments retains the originally calculated impedance matrix, while for changed trim material properties, the NLOPT sequence is used to obtain a new impedance matrix for the original modes. Using the NLOPT model enabled the mass optimization of the trim, and resulted in a 1.7 kg weight gain but 2.5 dB reduced power spectral density level over the whole frequency range up to 250 Hz (Figure 16.). As future work it is recommended to investigate the high-frequency behavior of the optimized trim and the process itself as well.

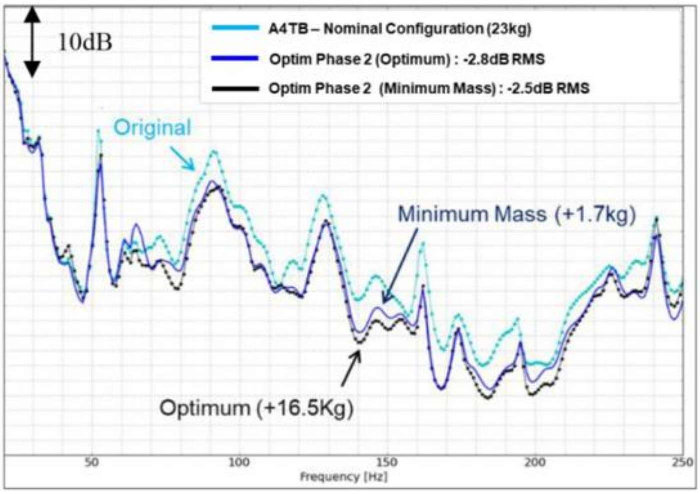

Figure 16.: Trim optimization results showing baseline (light blue), acoustically optimized (dark blue) and minimal mass (black) trim packages [27]

Not focused on trim elements per se but on an entire design process from high-level targets to execution, Bergen et al. presents a whole development strategy for vehicle manufacturing to deal with the challenge of designing an acoustic sound package (Bergen et.al., 2018). Their recommendation is to use panel participation method (or panel contribution analysis) and transfer path method to establish component goals based on overall design targets and use more computationally costly procedures like FE models on smaller substructures, so they can be investigated in detail. However, the introduced example is only looking at the finite element results and does not mention the variety of errors that can be introduced into the process at the beginning with the establishment of component goals.

1.3.5. Frequency dependent material parameters in acoustic FEM simulations

With the relatively large number of material parameters present in the Biot-model, the accuracy of the model is related to the exact understanding of said parameters. Frequency dependency of certain parameters, especially that of the Young's modulus of porous materials has been a topic of interest with the adoption of Biot-modelling in acoustic simulations in recent years.

Although not explicitly implemented in a Biot-theory context, but Bonfiglio et.al. used measured frequency-dependent complex Young's moduli in a transfer matrix method-based computation campaign to determine transmission loss through a flat plate (Bonfiglio and Pompoli, 2016). Specifically in the mid-frequency range, their method did not improve accuracy significantly.

A numerical modification to the standard displacement-pressure formulation of the Biot-theory is the shift cell technique introduced by Magliacano and collegaues, which introduces periodicity to improve the prediction quality and account for frequency dependency (Magliacano et. al., 2021). The method is promising for very small scale geometries but its use in automotive structures has not yet been demonstrated, and its main benefits lie in the low-frequency region.

A recurring issue with the Biot-model has been its complexity with over 10 parameters depending on its formulation. Schrader et.al.et al. attempted a simplification as well as the inclusion of frequency dependency by accounting for porous media effects on insertion loss and sound pressure levels through a complex, frequency dependent Young’s modulus (Schrader et.al., 2018). Despite the simplification in calculation effort, when compared to measurements, no significant improvement was achieved to a classic Biot-formulation.

In the automotive field, one of the most significant research campaigns on the application of frequency dependent material properties was carried out by Lloret et al. in partnership with BMW AG (Lloret et. al., 2017; Lloret et. al., 2020). In a series of publications, researchers have designed a characterization method for frequency dependent Young’s modulus to be applied in the Biot-model (Duvigneau et. al., 2018) and compared the behavior of materials using the determined properties under various conditions (Figure 17. shows a window bench setup aiming to measure insertion loss, for example).

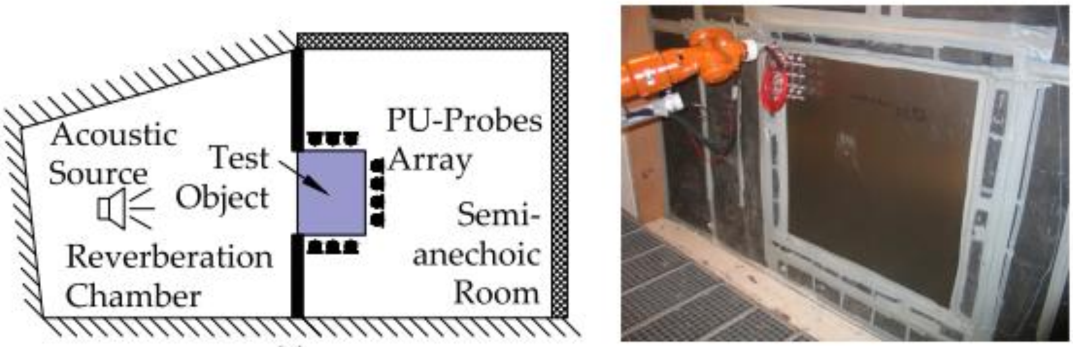

Figure 17.: Window test bench setup for measurement and simulation campaign of foam-heavy layer trim with frequency dependent parameters (Lloret et.al., 2019).

Although the measured Young’s modulus showed significant change (up to 300% increase) within the mid-frequency range, its application improved correlation only slightly. In the investigation in Lloret et. al., 2020, measurements and simulations were carried out in a window test bench setup, with a foam-heavy layer (spring-mass system) trim configuration, fixed to a steel plate specimen, focusing on the determination of insertion loss through the plate-trim system. Of the three investigated methods to account for trim effects (pure porous, pure elastic and porous-elastic – i.e. Biot-model), none could convincingly improve upon the Biot-model's prediction capabilities, which the results on Figure 18. show.

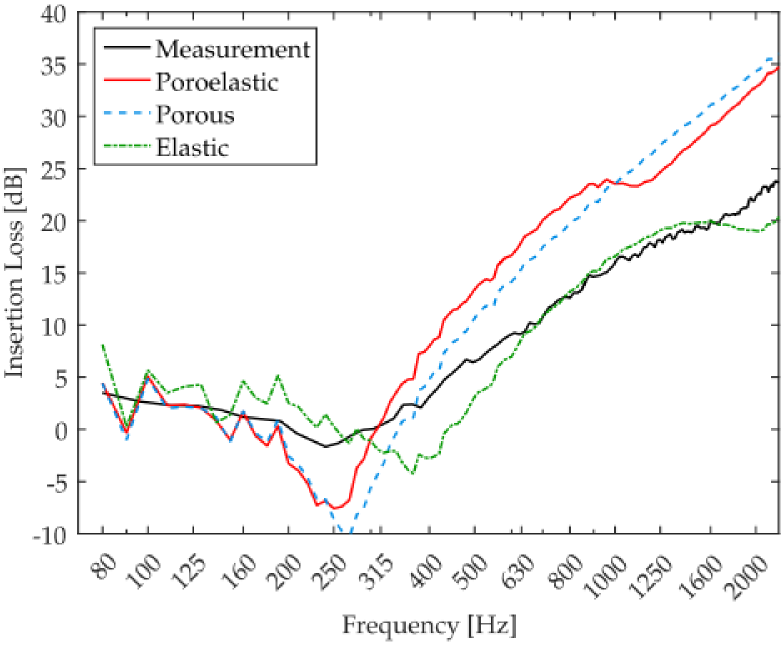

Figure 18.: Insertion loss determined in a window test bench setup with measurement and three different simulation strategies (Lloret et.al., 2020)

1.3.6. Hybrid and alternative methods

High computational costs arising from the complexity of Biot`s theory have driven engineers to develop alternative methods to account for trim behaviour in acoustic models, while the already showcased frequency-range limitations of FEM, as well as its highly deterministic nature in relation to the statistical effects in a real manufacturing environment also called for the application of alternative computational models. This section highlights the most significant alternative acoustic – and trim modelling methods as well as prediction of real-world manufacturing statistics on acoustic performance.

Panel acoustic participation is a finite element-based method, as presented by Wang et al. (Wang et.al., 2017). This method calculates resultant pressures from node vibration, which are summed over each panel to account for their individual pressure contributions. Then, all surrounding panel induced pressures are summed to obtain the resultant pressure for the whole cavity. Thereby the panel participation is defined as the projection of the sound pressure of individual panels in the direction of the overall sound pressure. In their investigation, the panel participation method is used to identify large contributors to interior noise among the panels in contact with the interior cavity on a four seat family car with hammer excitations. Figure 19. shows panel divisions used in the study. Despite good agreement between measurement and simulation, the used frequency range is really narrow (20-50 Hz) and severely limits the applicability of this method.

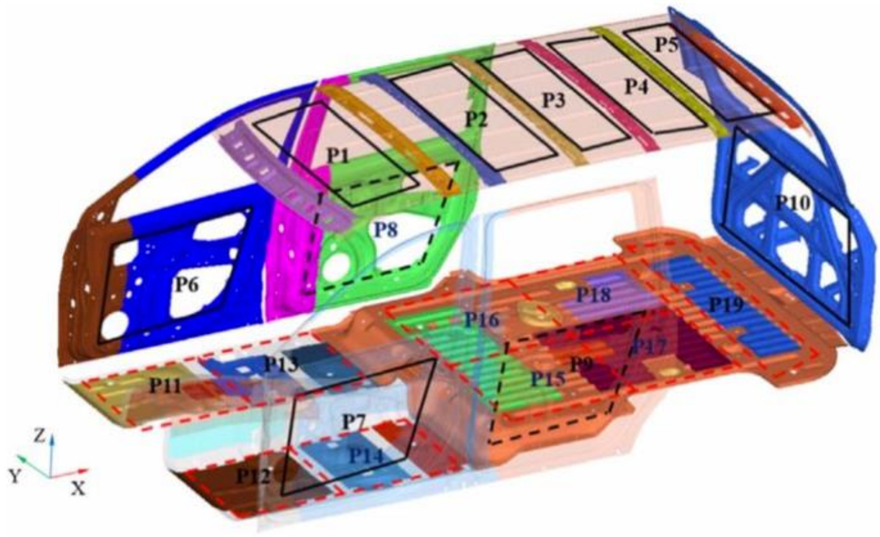

Figure 19.: Panel division in the investigated car for panel acoustic participation method study (Wang et.al., 2017).

Duval et.al. also worked on an energy based hybrid method to obtain sound pressure levels for a trimmed body (Duval et.al., 2004). The goal of the study was the implementation of a new sound package for a diesel hatchback car. In order to do so, acoustic power and transfer functions were measured in a fully lined interior with acoustic treatment and used to calculate sound pressure level at the driver`s ear level. The measurements resulted in an acoustic map of the interior, so the optimization could start with the most contributing elements. Figure 20. shows the acoustic power map of the interior panels investigated in the study. Even though the results were quite good, such an optimization relies on measurements on an actual prototype, so it cannot advise designers upstream in the design process.

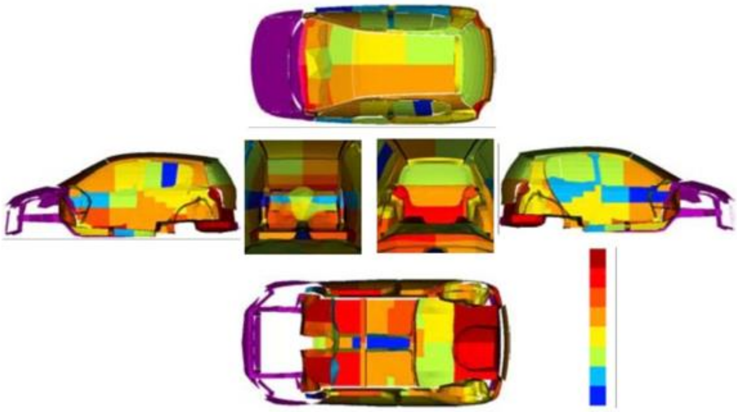

Figure 20.: Acoustic power map of interior trim panels in a small hatchback car (blue: lowest acoustic power; red: highest acoustic power) (Duval et.al., 2004).

Not focused on trim elements per se but on an entire design process from high-level targets to execution, Bergen et al. present a whole development strategy for vehicle manufacturing to deal with the challenge of designing an acoustic sound package (Bergen, 2018). Their recommendation is to use panel participation method (or panel contribution analysis) and transfer path method to establish component goals based on overall design targets, and use more computationally costly procedures like FE models on smaller substructures, so they can be investigated in detail. However, the introduced example is only looking at the finite element results and does not mention the variety of errors that can be introduced into the process at the beginning with the establishment of component goals.

Especially at higher frequency ranges where automotive structures possess orders of magnitude more modes as well as high modal densities, energy based methods return convincing results. Most prominently, Statistical Energy Analysis (SEA) has been successfully used in predicting high-frequency behavior (Musser et.al., 2012; Chen et.al., 2010). SEA calculates acoustic response based on subsystems. Structural and acoustic systems are subdivided into subsystems, and their behavior is described using power balance equations, where excitations are represented as power inputs, stored acoustic energy as modal energy density and the interactions between subsystems are described using damping and coupling loss factors. (Liu et.al., 2020). Due to the highly simplified nature of the geometries involved, few applications exist in the automotive field. Lee et.al. performed a contribution analysis to determine participation of various vehicle parts in the overall noise, successfully including uncertainties in the process (Lee et.al., 2019). However, their focus was not on the mid-frequency field and when compared with experiments, results in the mid-frequency range did not coincide with measurements. To better understand the mechanics of SEA, Liu et.al. set up a scaled, model vehicle with plexiglass walls and an engine compartment and studied the transmission of sound through the firewall (Liu et.al., 2020). Radcliffe et.al. used analytical SEA to simplify the computation effort in the high-frequency domain (Radcliffe and Huang, 1997). SEA was applied to overcome acoustic challenges of train carriages (Zhang et.al., 2016; Forssén et.al., 2012; Sun et.al., 2022) and aircraft interiors as well (Miller et.al., 1983; Dandaroy et.al., 2004; Moeller and Miller, 2013; Petrone et.al., 2019;), however, due to the favorable geometry of these structures, SEA results cannot directly be interpreted in the automotive domain. SEA has been proven to work for higher frequencies and simpler geometries, but its application to mid-frequency automotive acoustics phenomena is still an active research field.

Finite element models today in the automotive industry are highly detailed and represent all connections and parts of a highly compley physical product. Due to the nature of the calculation however, only a nominal structure can be evaluated. In structural calculations, realistic manufacturing tolerances may not be significant, but research indicates, that in acoustics, this is not the case (Luegmair and Schmid, 2020; Schmid et.al., 2020; Cram et.al., 2022). A series of papers in partnership with BMW AG highlight the importance of considering manufacturing tolerances especially in FEM calculations, as with the current trend of increasing simulation dexterity (as is the case with the Biot parameters), virtual models become „overfit" and due to their complexity may be unable to properly estimate an average acoustic response for produced real cars, as shown on Figure 21. (Luegmair and Schmid, 2020).

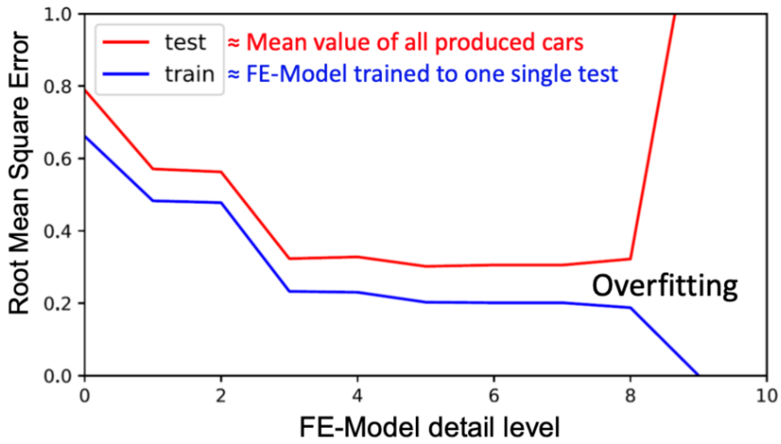

Figure 21.: RMS error of acoustic predictions for production mean and single test case versus FE-detail (Luegmair and Schmid, 2020).

Their method proposes generalized polynomial chaos expansion to estimate result bands, however determination of relevant input parameters is still an open challenge, as their research only includes general observations (Schmid et.al., 2020; Cram et.al., 2022).

1.4. Gaps in knowledge

To summarize the literature review in a broader picture, the significance of FEM in vehicle acoustics and its evolution is clear. Initially, in the 1980's, very simple methods were employed for subassemblies and acoustic calculations were a novel application of FEM in the automotive industry. By the 2000's, it has become standard across the industry to use finite element methods for interior acoustics, which manifested in a significantly larger academic interest in the topic as well, resulting in a large amount of journal articles and research papers with significant results. However, the physics of interior acoustic packages were represented only partially by employing Non-Structural Mass (NSM) models for the trim elements. For such methods, the missing physics of the trim elements (i.e. damping, stiffness, absorption) is compensated for by adjusting the damping of the air in the interior cavity to obtain results comparable to experiments. Since around 2015, poroelastic material (PEM) models have been introduced to represent the trim elements' physics more accurately. These are based on representing the full physics of trim elements, - i.e. mass, damping, stiffness as well as acoustic absorption – via the so-called Biot-parameters, which describe these properties via 11 macroscopic parameters. This has led to the so-called FEM-PEM simulation methods becoming the new industry standard for vehicle acoustic simulations. Even if these methods are acceptable for a range of applications, some deficiencies still exist in the critical mid-frequency range (400 – 1000 Hz), as explained in Section 1.3. . These include

- The lack of such validation tools dedicated specifically for the mid-frequency range, which can enable the comparison of simulation methods with experiments for all key physical phenomena individually or together, i.e. with the gradual inclusion of vibrational energy propagation in solid, in fluid, at solid-fluid interface, through PEM materials, or at any combinations of these.
- In general, the agreement between measurement and simulations with FEM-PEM methods becomes less reliable with increased frequency and model complexity. A particular decrease in accuracy is observed above 400 Hz, to which the following two identified knowledge gaps also may contribute:

- Frequency dependent behavior of porous-elastic materials, which constitute a significant portion of automotive trims has been well-proven and established by multiple sources. However, the inclusion of the frequency dependency of the PEM material parameters, if any, has not yet been considered.
- In production, vehicles lie within certain statistical manufacturing tolerance breadth. The overall influence of this tolerance has been shown, however, its particular mechanics and parameter sensitivity is an area open to be explored, especially for whole vehicle structures.

1.5. Goals of the work

After thorough analysis of available literature in the topic of FEM-PEM simulation methods and their applications to solve interior vehicle acoustics challenges, gaps in the current state-of-the-art have been identified in Section 1.4. Derived from those explained deficiencies, this dissertation aims to investigate the following three aspects:

1. Design a test apparatus system fit for the validation of multiple simulation methods within the mid-frequency range, with and without the application of trim materials.
2. Examine the effect of frequency dependent poroelastic material parameters on a variety of vehicle-like structures through the mid-frequency range.
3. Identify the influence of manufacturing inaccuracies on the acoustic response of various vehicle-like structures.

The upcoming chapters will elaborate on the investigated test cases, the applied simulation methods and the solvers that translate them, as well as the individual original contributions to each of the above described three goals.

2. Test cases and testing methods

As introduced in Section 1.2, vehicle structures in general contain various joining methods, complex geometries, as well as a large number of modes. Therefore, on their own, vehicle bodies are not ideal candidates for methodology development. To thoroughly understand simulation methods, vehicle structures must be simplified into schematic but representative academic cases, where simulated components can be studied on lower complexity levels. However, the simplified geometries eventually must still include phenomena that are also present in real vehicle bodies.

To conceptualize the multi-level complexity of the test apparatuses, it is important to identify the fundamental building blocks of vehicle bodies from an acoustical perspective. Three such blocks make up acoustic vehicle systems:

1. **Structure:** consisting for the moment mainly of metal materials (steel or aluminium). Geometrically, structures can be divided into cosmetic (panel-like) and load bearing (box section-like) elements.
2. **Air Cavity:** the enclosed air cavity interacts with the structure and the sound package, as well as provides the actual medium for sound transmission to occupants' ears.
3. **Trim:** all sound deadening porous-elastic components whose aim is to reduce interior noise levels are called trims, which are the main objectives of a FEM-PEM simulation.

These conceptual blocks will be used to define test apparatuses of increasing complexity, leading up to a fully trimmed vehicle model.

2.1. Test Cases

A set of test cases have been identified, which follow each other in increasing complexity. These are illustrated in Fig. 22. below and explained in detail in the following sections. The logic was to test key concepts first on lower complexity models, followed by medium and full complexity models.

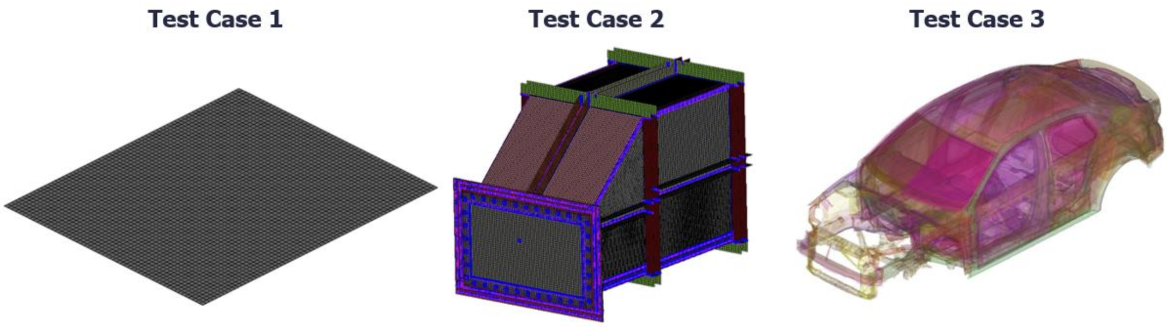

Figure 22.: Test cases 1-3 showing the increasing complexity of models.

2.1.1. Test Case 1 – Flat Plate

Firstly, a lightly damped structure is needed to see the most pronounced effects. A simple, homogeneous flat plate, Test Case 1, in a free-free condition is ideal for these investigations, with dimensions of 650 mm x 550 mm, and 2 mm nominal thickness. Material is structural steel with nominal density of 7850 kg/m3, 210 GPa E-Modulus and Poisson's ratio of 0.3. Figure 23. shows the meshed FE-model of Test Case 1. This simple structure provides a perfect vessel to investigate purely structural response. While a flat plate as an academic case provides a great research vessel, it also highly magnifies the effects of trim materials. Without any reinforcement, a flat plate can be considered as a lightly damped structure, magnifying any possible changes that the use of either frequency-dependent trim material parameters or manufacturing tolerances would have on the acoustic response. These effects, however, may not be so pronounced for stiffer, heavier damped structures which more closely model a vehicle, therefore more representative test cases are required to draw conclusions.

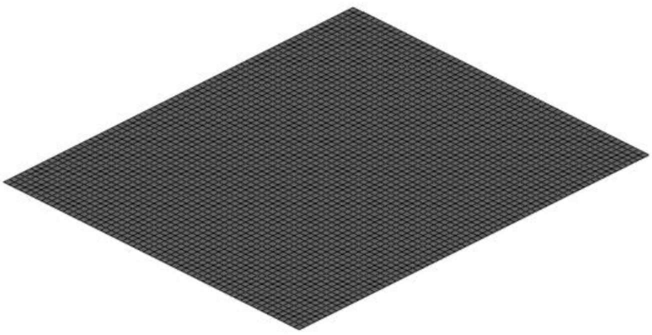

Figure 23.: 650 x 550 mm sized flat steel plate with 2 mm nominal thickness served as Test Case 1, the most fundamental investigation platform.

2.1.2. Test Case 2 – Scaled vehicle cavity

An essential element of a real vehicle's interior acoustic behaviour is the interaction between the trim and the enclosed air cavity. To be able to study such phenomena, a whole vehicle could be considered a useful tool, however, with computing times in FEM on the order of days instead of hours for a large frequency domain, an intermediate solution was created. This intermediate solution took the form of a trapezoidal cavity, however, in two different configurations: one with acoustically rigid, non-participating walls, while another with acoustically flexible walls that are excited in the investigated frequency range and interact with the interior air cavity. Both test cases, Test Case 2a with rigid and Test Case 2b with flexible walls had the same interior volume. To ensure rigidity for any frequency range, Test Case 2a was manufactured out of reinforced concrete, with a removable front concrete wall. Test Case 2b with acoustically participating walls was manufactured out of steel panels with varying thickness (Fig. 24. shows Test Case 2b in reality and with its FE-mesh). A detailed guide to the design and properties of these test cases will be shown later, in Section 3. Stiffener U-sections divide up the flat cavity boundaries, with the stiffeners riveted to the cavity walls. These ensure a similar acoustic behavior to a vehicle chassis. A good indicator for this is that the metal cavity has eigenmodes on the same order of magnitude as a real vehicle body-in-white. The sections on the side can be thought of as front and rear doors, while the other boundaries represent the firewall, windshield, rear end, floor and headliner sections of a real vehicle. 6 response points were selected inside the cavity to provide sound pressure level information.

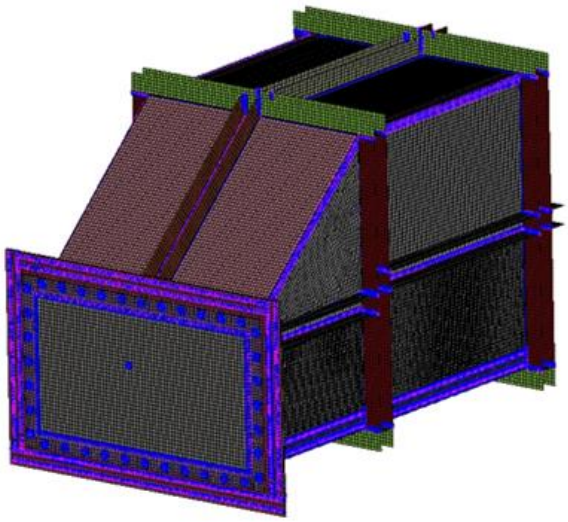

Figure 24: Untrimmed cavity manufactured test specimen (left) and finite element model (right)

2.1.3. Test Case 3 – Trimmed vehicle

As the ultimate goal of the study was to draw conclusions for a full vehicle structure, the final test case, Test Case 3 was a fully trimmed vehicle structure, provided by Audi Hungaria, one of the key partners of the research effort. As a prominent contender in the premium segment, where interior acoustics is one of the key purchase decision factors for customers, the provided vehicle model employed significant amounts of porous materials for sound deadening purposes. The investigated vehicle was a 2015 Audi A3 Limousine in trimmed body configuration. This included a complete interior model with all trim elements, such as door cards, instrument panel, headliner, rear seats and carpeting. Test Case 3 was only investigated in fully trimmed configuration. Whole vehicle and its FE-representation are shown on Figure 25. A detailed description of the model can be found in Section 4.

Figure 25.: Test Case 3 shown in reality (top) and as a FE-representation (bottom) (Buy-a-car, 2023).

2.1.4. PEM trim materials in Test Cases

To understand the effect frequency dependent Biot parameters have, sound absorbing materials (trims) are applied to both apparatuses, as the third complexity level conceptual block. Applied trim was the same for test cases 1, 2a and 2b, composed of an absorbing foam with 55 kg/m^3 density and thickness of 20 mm. Biot-parameters of the foam are standard industrial values. Test Case 3 uses foams that were applied to the series production vehicle with manufacturer provided material parameter values for density, geometry and all relevant Biot parameters. While many of these parameters are frequency dependent, current investigation only considers the impact of frequency dependent Young's modulus and damping. Both the frequency dependent Young's modulus, as well as the frequency dependent damping have been experimentally measured on a foam sample using a Dynamic Mechanical Analyzer (DMA). As the sample could only be excited in the 20-60 Hz region, time-temperature superposition was used to obtain the full material parameter curve for the entire frequency range. Exact details of the measurement procedure are detailed in Schweighardt and Vehovszky, 2021 (Schweighardt and Vehovszky, 2021). This parameter curve was then scaled for the various foam types in Test Case 3 as well to introduce frequency dependency in the full scale vehicle model.

For Test Case 1, the entire plate was covered with the applied trim, in three thicknesses: 10, 30 and 50 mm. Test Case 2, being a more complex geometry, replicated a real vehicle's fully trimmed stage. This means that trim was applied to the representative firewall, floor, front- and rear door card, trunk and headliner areas. In all cases, the same 20 mm foam trim was used. Figure 26. illustrates the trimmed models.

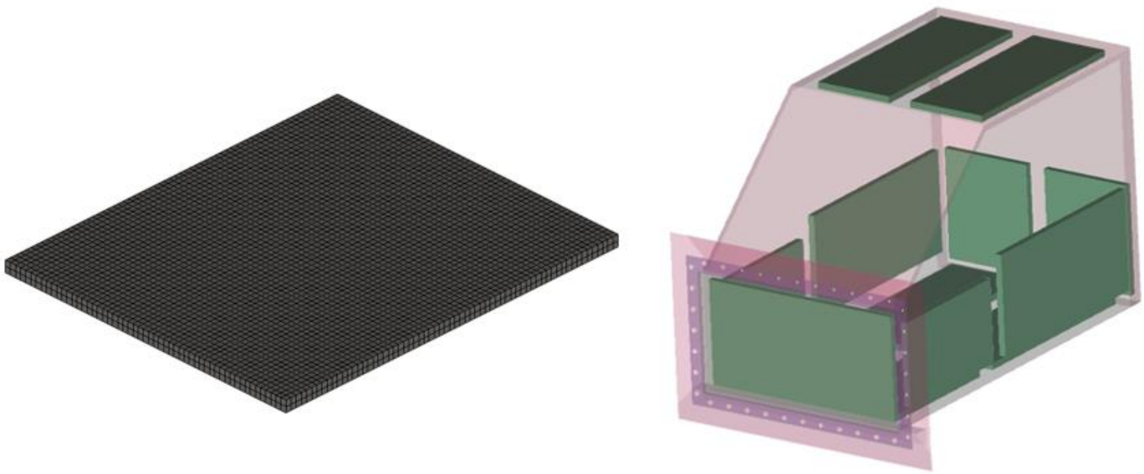

Figure 26: Trimmed plate and cavity models.

2.1.5. Load Cases

To illustrate the effect of the applied trims, the goal was to investigate the overall responses of the apparatuses with quantities that can be easily measured in a future validation campaign.

Test Case 1 – Flat Plate

For the flat plate (Test Case 1, shown on Figure 27.), the overall RMS average velocity was a good indicator of the trim effect, so 20 response points were scattered over the plate surface in random locations. To be comparable with measurements, accelerometer masses were added to response- and driving points as well (1.5 grams each). As its load case, a unit force in perpendicular direction to the plate's plane was applied in the single excitation point with an impulse hammer.

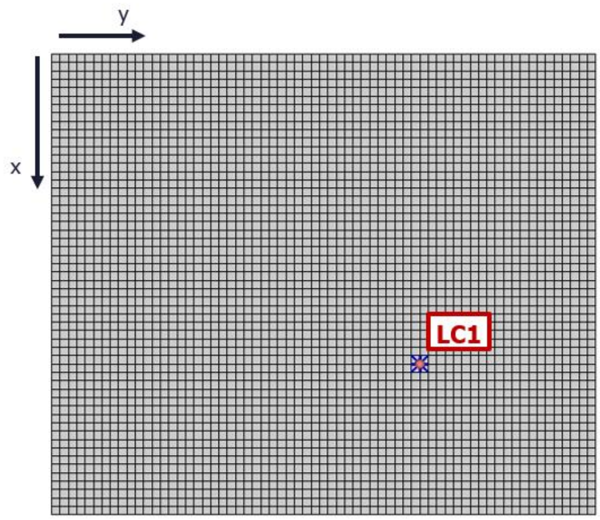

Figure 27: Test Case 1 load case (marked LC1 on figure) in FE representation

Test Case 2 – Scaled vehicle cavity

Overall response in case of the cavity is better characterized by interior sound pressure levels, which furthermore are also the quantity of interest in full vehicles as well. Therefore 6 response points were selected in the fluid medium, close to the walls and corners, in three planes along the width of the cavity. Overall RMS average sound pressure levels were then evaluated in the simulations, as responses to a unit force excitation. The cavity was excited in the -X direction with a unit force using an impulse hammer, to engage all modes throughout the spectrum. Figure 28. illustrates the load cases, while Figure 29. shows response point locations in the flexible walled model cavity.

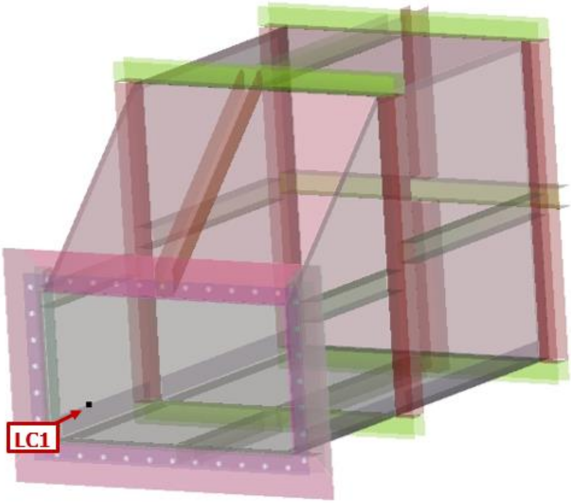

Figure 28.: Load case in -X direction on Test Case 2b. Unit force excitation was applied.

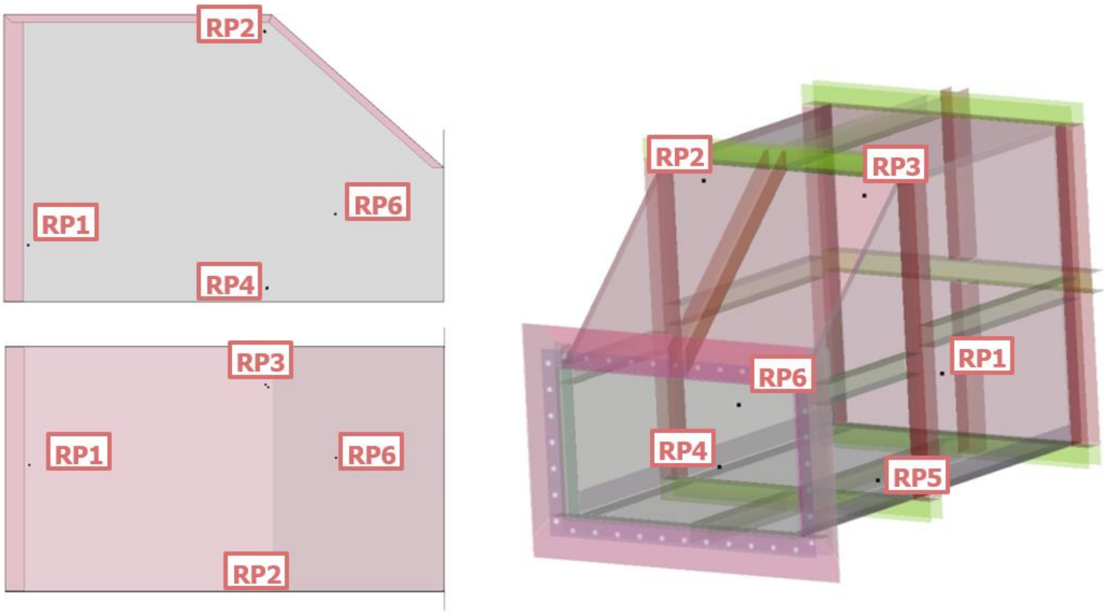

Figure 29.: Acoustic response point locations within Test Case 2b.

<u>Test Case 3 – Trimmed Vehicle</u>

As a significantly more complex structure, load cases and responses were different for the full vehicle study. Test Case 3 used standard excitations transferred directly from industrial simulations, in the +Z direction in the locations shown on Figure 30. These energy input locations include a front lower crossmember under the radiator, connecting the front two chassis legs (marked with 24 on Figure 30.), a longitudinal stiffener as an extension of the front chassis legs underneath the driver's seat (marked with 1 on Figure 30) and a rear subframe mounting point (marked with 34 on Figure 30). These standard input points were used so that the available measurement data could be directly compared with simulation outputs of the computational campaign carried out in this research.

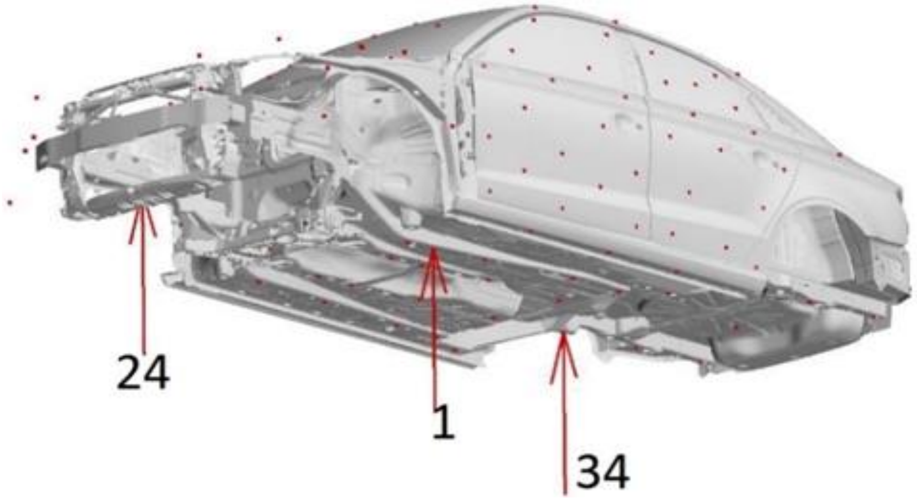

Figure 30: Excitation locations for Test Case 3

Experimental investigation of Test Case 3 was beyond the scope and possibilities of this research, and was deemed unnecessary as validated measurement data was available for the vehicle for all three excitation locations. Response was examined through 30 acoustic response points within the interior cavity, which included the ear positions of all passengers. Response locations are shown on Figure 31.

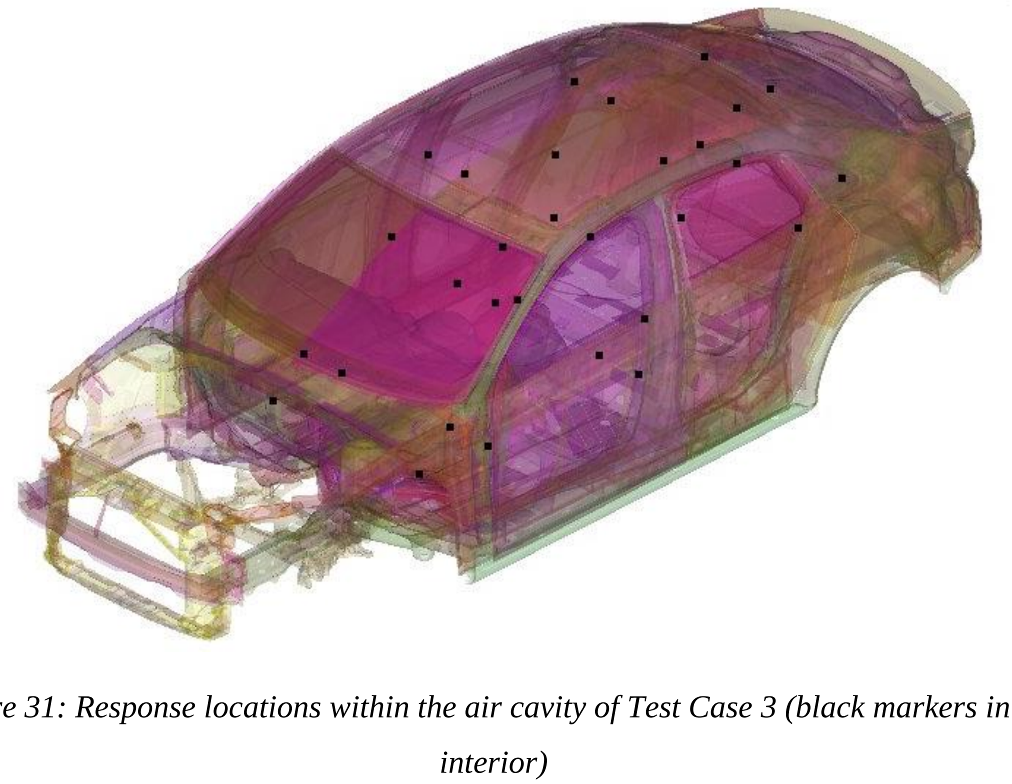

Figure 31: Response locations within the air cavity of Test Case 3 (black markers in the interior)

2.2. Measurement methods

In order to evaluate the proposed methods in simulation compared to experimental data, measurements on the test cases were carried out. Acoustic responses on Test Case 1 and Test case 2b were recorded. The industrial partner provided experimental results for Test Case 3, therefore a separate campaign for a full-scale car was not carried out.

Measurements on Test Case 1 were carried out in purely body-in-white configuration. Objectives were twofold: record the response of the plate and determine its damping loss factor (DLF). The applied measurement method is described in detail in (Kun et.al., 2020), but for the sake of completeness, a summary is also included here. Power Injection Method (PIM) was used for the DLF determination, which is based on power-balance equations in Statistical Energy Analysis. Damping loss factor is calculated as the ratio of the input power and of the product of the total energy of the subsystem and angular frequency. As the input power must be determined exactly from the measurement, input force and input velocity must be simultaneously measured. An impedance hammer was used for excitation, therefore an accelerometer had to be applied close to the impact point. To identify the total energy of the subsystem, spatial averaging over multiple, randomly located response points on the structure was applied.

Theoretically, all modes should be excited to get the correct DLF of a structure, and to get as close to this idealized situation, a total of 20 randomly located response points and 5 load cases were used for this specific measurement. The required number of load cases and response points were determined from a study aiming to establish the minimum number of load- and response points statistically representative of mid-frequency vibration phenomena [21]. 4 response points were measured for a single load case to limit relative added mass to the plate. That resulted in five sensors in total per loadcase: one for measuring excitation, and four for the responses. To ensure that the plate was in free-free boundary conditions, it was hung from a frame using a bungee cord and silicone dampening inserts. The focus frequency range of the investigation was between 400 and 1000 Hz, however, the plate was excited from 0-1600 Hz.

A schematic representation of the measurement setup, including the impact hammer used for the excitation, the plate and the additional equipment used in measurements are shown on Figure 32.

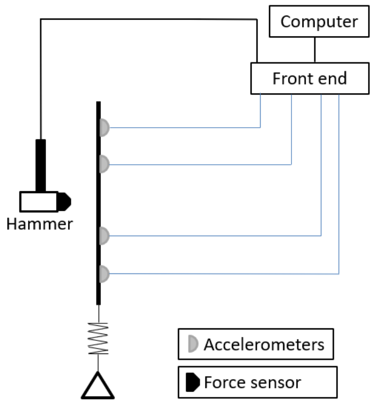

Figure 32.: Schematic diagram of the measurement system.

A Siemens LMS data acquisition system was used in the measurements. Lightweight ICP accelerometer sensors (piezo-electric, B&K, Type 4519-003), weighing 1.5 grams each were used to record responses. A PCB Piezotronics impact rubber with hard rubber head excited the plate. Pre-trigger time was adjusted to ~0.02 s, while trigger force was 20 N. Measurements were recorded from the frequency range between 282 – 1122 Hz, since these are the lower and upper border of the investigated third octave bands (315 – 1000 Hz). Details of the measurement frequency resolution and the calculation of the Damping Loss Factors is explained in Kun et.al., 2020 (Kun et.al., 2020). The obtained damping loss factor values are compiled in Table 1. The plate's frequency response functions were also measured, these will be compared to simulation results in Section 4., along with the application of the frequency dependent DLFs to the plate.

Center frequency	**DLF**
200	0.00116
250	0.00056
315	0.00099
400	0.00058
500	0.00056
630	0.00062
800	0.00050
1000	0.00068

Table 1.: Measured damping loss factors for given third-octave bands with provided center frequencies. These factors are applied to Test Case 1. in Section 4.

Due to the geometry of Test Case 2b, the important metric to describe its acoustic response was the sound pressure level within the enclosed interior air volume. To ensure no influence of external noise sources, experiments on this apparatus were carried out in a semi-anechoic chamber with a lower cut-off frequency of 100 Hz. Isolation from the environment was further realized by setting the apparatus on four air springs, with pressure modulated such that the first rigid body mode was below 20 Hz. Figure 33. shows the measurement setup.

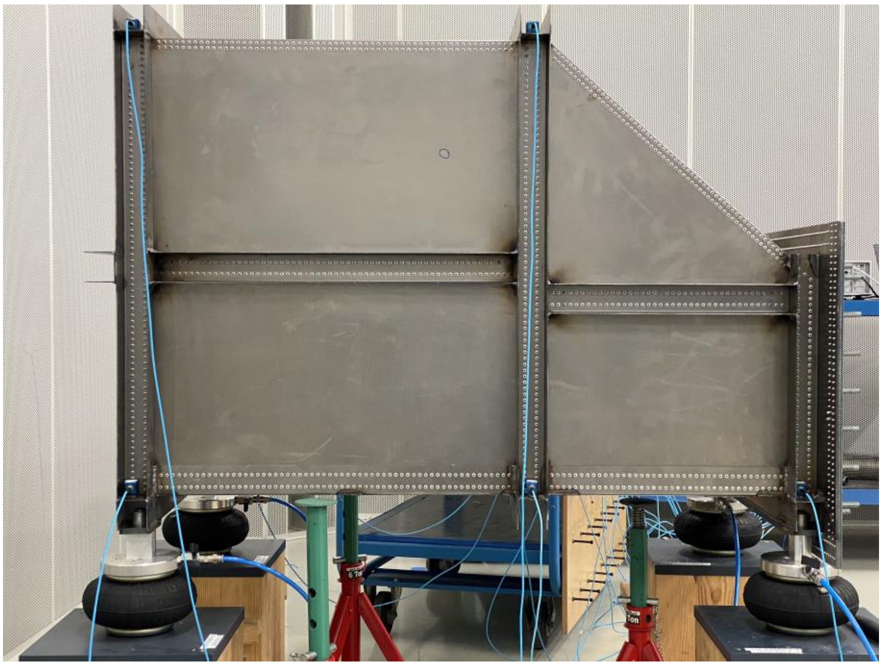

Figure 33.: Test Case 2b set up for experimental measurement in a semi-anechoic chamber on air springs.

1 loadcase in the -X direction was recorded as shown on Figure 28. earlier, with 6 responses within the cavity. Acoustic response was recorded with PCB 378B02 prepolarized free-field condenser microphones with a sensitivity of 50 mV/Pa and frequency range of 3.15 Hz – 20 kHz, and signals were acquired using a Siemens LMS data acquisition system. Impact force excitation was applied using the same PCB Piezotronics impact hammer as for the flat plate experiment. Response was recorded both in body-in-white and in fully trimmed configurations. The contact patch of the front door and the opening of the cavity was sealed with butil adhesive in order to minimize leakage. An interior view of the cavity with the 6 microphones in fully trimmed configuration is shown on Figure 34.

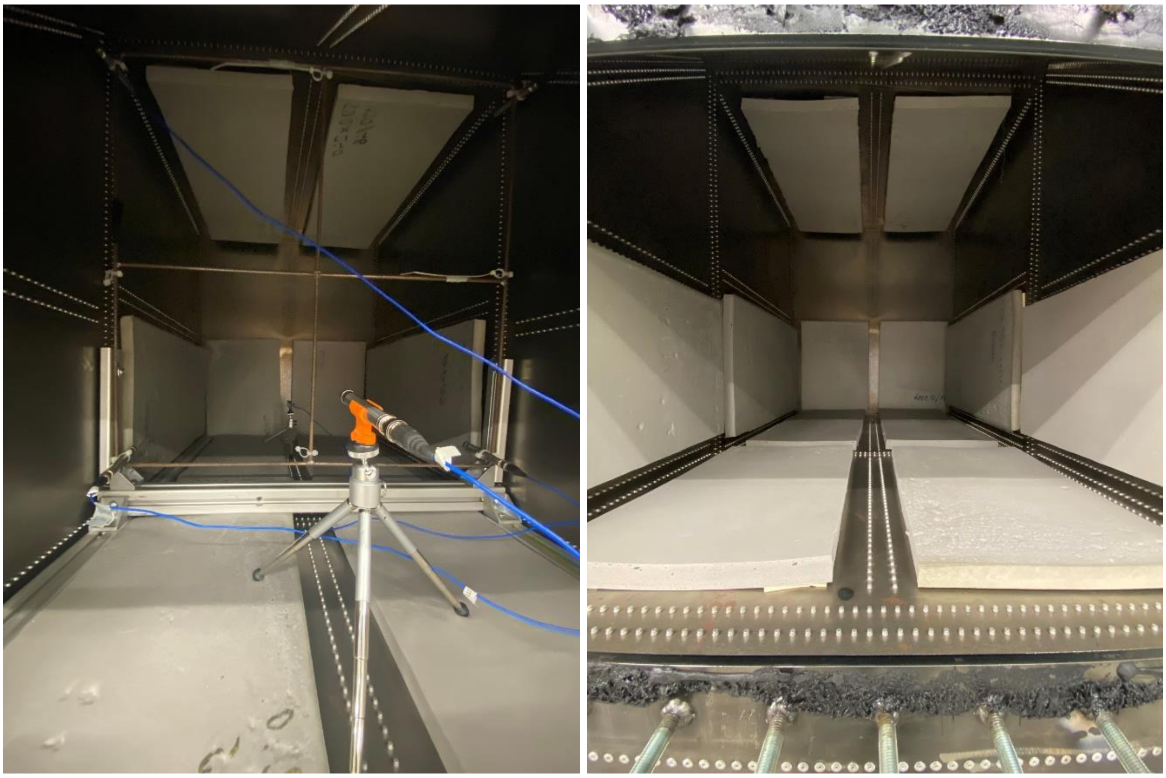

Figure 34.: Trimmed cavity interior setup for measurement with (left) and without (right) interior microphone positions. Microphones in the cavity center were fixed to a welded frame while the front and rear single microphones were fixed in microphone holders with 3D-printed attachments.

2.3. Simulation methods

Fundamental focus in this investigation was on the acoustic response computed using Finite Element Method. Two solvers were used for practical reasons: ESI VPS for test cases 1, 2a and 2b, while NASTRAN-PEM was used for test case 3. ESI VPS was used for the smaller test cases that required full pre-processing including import from raw CAD data through to solution. Data for test case 3 was provided pre-processed for NASTRAN-PEM format, but a significant reason contributed besides the reduced pre-processing time for choosing a different solver was that the large model size required a computer cluster to be able to return results, which means that simulations had to be run on a cluster provided through Audi Hungaria. The industrial partner integrated NASTRAN-PEM into their pipeline, hence its use in the current research. Regardless of the solver, ANSA was used to prepare models including boundary condition and material parameter setting, as well as discretization.

Modal and direct frequency response analysis were both available in both solvers to calculate frequency response functions of structures to given excitations. For this investigation however, modal frequency response is used. Direct frequency response, based on experience of the industrial partner, was unfeasible for a full-scale car model, therefore modal frequency response was chosen as a calculation method to minimize differences in numerical method along the increasing complexity of test cases. Direct frequency response calculates the particular solution to the full equation of motion individually for each requested output frequency. As the studies conducted in this work universally used the frequency range from 20 Hz to 1000 Hz as the range of interest, this would have increased the computation effort – especially for larger models like Test Cases 2a, 2b and 3 – to beyond acceptable levels. This method is particularly useful for single-frequency peak comparisons, which was out of the scope of the investigation conducted here. As industrial problems also generally focus on broader frequency ranges, there is a method that can drastically reduce computational effort by using the orthogonality of structural and fluid eigenmodes to construct a solution.

Modal frequency response analysis extends modal analysis by using mode shapes to uncouple the equations of motion for the structure and compile frequency response results. A trade-off compared to direct frequency analysis is that eigenmodes of both the structure and the fluid have to be calculated before the frequency response calculation. However, modal analysis is a mathematically less intensive method. The calculated modal bases can be used for subsequent calculations, as long as the material and/or geometric properties of the structure and the fluid do not change. As the current investigation focused almost exclusively on varying the material parameters of trims, this advantage of modal frequency response was fully utilized, shortening simulation lead times. Mathematically, the following algorithm is used in the applied solvers. The well-known equation of motion to be solved in FEM is as follows:

$$(-\omega^2\,[M] + i\omega[B] \;+\; [K]\,)\{u\} = \;\{P(\omega)\} \tag{11}$$

The direct solution would involve inverting a large matrix, hence its enormous computational load in the case of millions of degrees of freedom (which can easily occur in a full-scale vehicle). As eigenmodes of a structure are distinct for each eigenfrequency, this orthogonality can be exploited to transform the problem from physical coordinates to modal coordinates, using:

$$\{x\} = [\phi]\{\xi(\omega)\}e^{i\omega t} \tag{12}$$

Above equation only holds if all modes are computed, meaning that the equations are only fully uncoupled if all modes of the structure are included in the calculations. However, for a known excitation in a specific frequency range, a truncated modal base can provide sufficient information, since the contribution of modes far beyond the frequency range of interest is very small. For the structures of interest, a 180% of the upper frequency spectrum limit was used (this means that in the current case, modes were computed up to 1800 Hz for investigations running up to 1000 Hz). To account for the truncation error, residual vectors are calculated. With damping temporarily ignored, substituting physical coordinates for modal ones and pre-multiplying with $[\phi]^T$ uncouples the equations of motion and yields:

$$(-\omega^2\ [\phi]^T[M][\phi]\{\xi(\omega)\} + [\phi]^T[K][\phi]\{\xi(\omega)\}\ )\{u\} =\ [\phi]^T\{P(\omega)\} \qquad (13)$$

By transforming the equations of motion to modal coordinates, a set of single-degree-of-freedom equations have to be solved for modal responses, which are in turn summed to compute the physical responses in complex form (with magnitude and phase).

Presence of structural and viscous damping generally means that the equations of motion are coupled. To circumvent this problem, two possibilities are present. Either the full, coupled equations of motion for the damped system are expressed in modal coordinates and solved directly, or modal damping can be attributed to individual modes (NASTRAN, 2014). To increase computational accuracy and allow for a more detailed investigation, the first option was used for the structural computations conducted in this research campaign, while for the fluid cavities, modal damping was used. This latter simplification was justified by the homogeneity of the fluid, as it was in all cases air.

For modelling trim, the Biot model of PEM was employed, which describes porous media with 11 parameters in its formulation in VPS and NASTRAN-PEM. This equivalence of material model ensures better comparability between the solvers and eliminates conversion errors. Wave propagation within the phases is calculated using parameters of the solid and fluid phases, as well as coefficients that quantify the level of interaction between them. Automotive trim materials, such as foams, felts and fleeces all are bi-phasic materials and can be modelled in acoustic simulations using Biot-theory. The detailed mathematics of the computations carried out were described in Section 1.2.3.

For the given cases in the modal frequency response analysis, simulations consisted of determining the modal bases for the structure and the fluid parts, calculation of trim impedances and solving the frequency response function. Structural and fluid modal bases were re-used for multiple trim configuration calculations, while trim impedances could be re-used if the structure or the fluid was modified. Therefore, computations could be automated to a certain degree.

As different apparatuses were used for calculations, different meshes were applied. In all cases, plates and stiffeners were modelled using shell elements, while trims and the interior fluid cavity were represented as solids. For structures, 10 mm target element size was set for quad shell elements. The fluid cavity and trims were meshed with tetrahedral solid elements, with a 10 mm target size for the trims and 30 mm target for fluid medium. Material damping was applied to structural elements, while modal to the fluid cavity. Riveted and welded connections were modelled accordingly in the structural model of the metal cavity.

3. Cavity apparatus design process

Section 2. elaborated upon the multi-stage test case methodology that would be used throughout the investigation. As these apparatuses are part of a larger scale research focusing on the numerical investigation of the effect of poroelastic materials with both statistical energy analysis (SEA) and finite element method (FEM), each simulation method proposed criteria that had to be considered in the design process. Test Case 1, the basic flat plate could be chosen without much difficulty to be suitable for analysis using both simulation methods, however the design of Test Cases 2a and 2b was significantly influenced by the multi-method approach. This section details these influencing factors and provides the first original contribution to available scientific literature.

The primary goal of a plate-cavity system is to investigate the coupling and interaction of the air volume and the excited plate(s). A common requirement was for the vertical cross-section to be trapezoidal, to introduce a level of irregularity that is present in a vehicle interior on a much larger scale. This introduces a level of complexity and reduces analytically computable resonances.

When simulating an isolated air cavity-single plate configuration in FEM, it is preferred that the walls of the cavity are completely acoustically rigid. This would allow for simulations without the need to model the rigid walls and replacing them with a rigid boundary condition. This simplification reduces the number of degrees of freedom dramatically, as well as eliminates a fluid-structure interface and the coupling issues this may . Such a design would further simplify the system in measurements as well, potentially isolating the pure effects of applied trims. In order to reduce inaccuracies, the plate should be clamped rigidly to the cavity opening, ensuring an airtight enclosure. Such a boundary condition would not require additional modelling elements and joints, which could introduce uncertainties. Acoustically rigid walls can most successfully be achieved by using concrete as a material, which limits practicality of the apparatus due to its eventual large weight and size, however these limitations were overcome with the available infrastructure of the research group. Concrete as a material limited the sizing due to manufacturability: concrete mould panels are made in units of 50 mm width, therefore each perpendicular side of the cavity had to be rounded to the nearest 50 mm measurement.

Replicating a cavity system in SEA poses different requirements. Coupling between multiple subsystems and a cavity is of interest in this case, which requires participating cavity walls. In addition, SEA requires at least 3 modes in every third-octave band for the entire investigated frequency range. In direct conflict with this, the upper limit of the internal modes was set by FEM: modal frequency analysis is much less computationally expensive with minimized number of eigenmodes. Thereby, the target was to design a cavity apparatus with internal dimensions resulting in minimum 3 modes within a third octave band.

The described requirements are highly conflicting: FEM would ideally require perfectly rigid walls, while SEA needs compliance. To resolve this, two separate cavities will be designed, each to suit the individual requirements of the appropriate method: a rigid, concrete-walled cavity for FEM and a steel cavity with reinforcements for SEA investigations. To ensure comparability, the two cavities must have the same volume. This configuration has the added benefit that the steel cavity could be used as a scaled down vehicle body in simpler FEM investigations as well, representing a next step of complexity building upon the knowledge gained from the concrete cavity investigations.

As it has been established that both cavities are needed, additional requirements were defined towards the steel setup to extend its applicability to meaningful FEM research and even beyond that, for example to include the possibility to investigate acoustic power flow. To act as a scaled down vehicle body, plate thicknesses should be close to those used on production vehicles: this means no more than 2 mm thickness in reinforcements and close to 1 mm in the flat plate sections. Although this in turn already has an influence on the modal behavior, it was also defined that the reinforced cavity structure should have modes on the same order of magnitude as a vehicle body-in-white chassis structure. Such similarities in mechanical properties ensure that the studied Test Case 2b will not be a drastically different case to a full vehicle structure.

These design requirements gave the framework for the design process described below.

The basic trapezoidal cross-section shown on Figure 35. was modified using various scaling rules. Its four major exterior dimensions marked by A, B, C and D on the figure were changed in relation to each other resulting in 6 basic cavity shapes, which were then each scaled using factors ranging from 1.5 to 2.0 in five steps. In total, 36 different cavity sizes were examined using modal analysis in ANSA EPILYSIS, using the SOL101 solution protocol. This was used for all calculations throughout the design of both apparatuses.

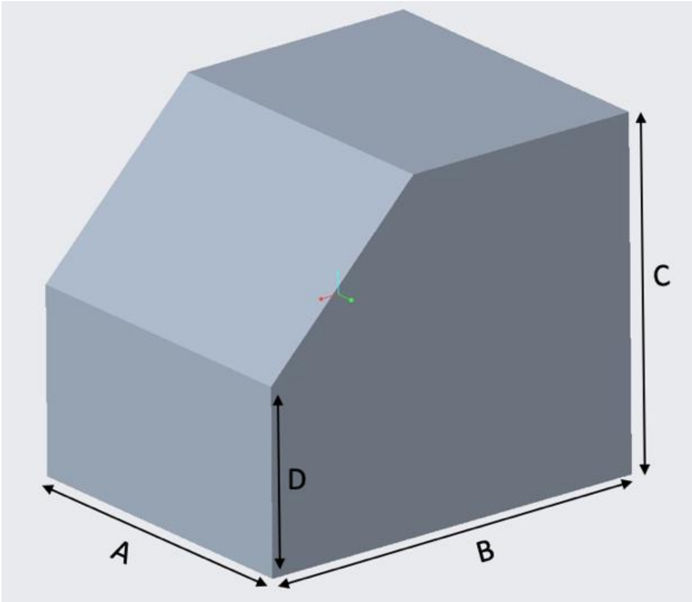

Figure 35: Basic interior shape of cavity with major dimensions for optimization.

The goal of the size definition was to arrive at a cavity size that contained the minimum amount of overall modes up to 1800 Hz, but at least 3 in each third-octave frequency band starting with 250 Hz center frequency, to fulfill demands for SEA application. 1800 Hz was set as the upper limit of the modal analysis investigation, as this would be the maximum frequency of the modal base calculations for the FEM frequency response analysis later on.

Results were then evaluated and tabulated. Figure 36. shows an excerpt of the complete set of results, highlighting the dimensions of the best case with the lowest number of minimum required modes.

Frequency Bands		Modes in band														
		2_1	2_3							2_4						
Lower cutoff frequency (Hz)	Upper cutoff frequency (Hz)	1	1	1,5	1,6	1,7	1,8	1,9	2	1	1,5	1,6	1,7	1,8	1,9
224	282	0	0	0	1	1	2	3	2	1	0	1	2	3	2
282	355	0	1	0	2	3	2	3	3	0	3	4	3	2	5
355	447	2	1	0	3	3	4	3	5	1	5	3	5	5	4
447	562	3	2	0	5	5	7	9	10	4	4	6	5	10	11
562	708	5	3	0	10	12	13	15	16	3	10	14	16	15	18
708	891	7	4	0	17	21	24	26	32	5	18	20	25	29	33
891	1122	14	10	0	31	35	42	50	55	13	32	38	43	53	64
1122	1413	24	16	0	55	67	75	90	105	19	59	68	84	96	113
1413	1778	7	5	0	20	22	30	31	34	7	22	26	30	41	40
	Sum:	62	42	0	144	169	199	230	262	53	153	180	213	254	290
Cavity size (mm)															
	A	350	350,00	525,00	560,00	595,00	630,00	665,00	700,00	350,00	525,00	560,00	595,00	630,00	665,00
	B	900	600,00	900,00	960,00	1020,00	1080,00	1140,00	1200,00	750,00	1125,00	1200,00	1275,00	1350,00	1425,00
	C	400	400,00	600,00	640,00	680,00	720,00	760,00	800,00	400,00	600,00	640,00	680,00	720,00	760,00
	D	175	175,00	262,50	280,00	297,50	315,00	332,50	350,00	175,00	262,50	280,00	297,50	315,00	332,50

Figure 36: Excerpt of complete modal analysis results of 36 different cavity versions, highlighting the final version.

According to the concrete manufacturing requirements, these dimensions were then rounded to the nearest 50 mm, resulting in the final interior cavity dimensions shown in Table 2. Relevant dimensions are highlighted on Figure 34.

Dimension	Value (mm)
A	650
B	1150
C	750
D	350

Table 2.: Final dimensions of the interior cavity volume in the significant directions

As the interior dimension has been defined, the crucial task of the concrete cavity design was to finalize its wall thickness while ensuring its manufacturability. For the given dimensions, the minimum wall thickness required by the manufacturing partner was 100 mm. By increasing the wall thickness, the first natural frequency and the number of modes up to 1800 Hz could be improved, however, with significantly increased weight and thereby reduced practicality. To investigate if this tradeoff would be worthwhile, multiple versions with various wall thicknesses underwent modal analysis. A summary of the results is shown in Table 3.

Frequency Bands		**Modes in band**						
Lower cutoff (Hz)	**Upper cutoff (Hz)**	**300 mm wall**	**300 mm LW**	**300 mm DW**	**200 mm wall CBEAM6**	**160 mm wall CBEAM6**	**160 mm wall CBEAM12**	**100 mm wall CBEAM6**
224	**282**	**0**	**0**	**0**	**0**	**0**	**0**	**0**
282	**355**	**0**	**1**	**1**	**1**	**1**	**1**	**1**
355	**447**	**1**	**0**	**1**	**0**	**1**	**1**	**0**
447	**562**	**1**	**1**	**2**	**1**	**0**	**0**	**4**
562	**708**	**2**	**5**	**8**	**4**	**6**	**6**	**5**
708	**891**	**6**	**6**	**7**	**6**	**5**	**5**	**6**
891	**1122**	**7**	**9**	**11**	**7**	**6**	**7**	**8**
1122	**1413**	**14**	**13**	**19**	**13**	**13**	**13**	**13**
1413	**1778**	**2**	**6**	**5**	**2**	**2**	**2**	**4**
Sum of modes:		**33**	**41**	**54**	**34**	**34**	**35**	**41**
1st natural frequency (Hz):		**371**	**340**	**305**	**314**	**290**	**287**	**208**
Weight (t):		**3.54**	**3.06**	**3.00**	**2.35**	**1.77**	**1.89**	**0.95**

Table 3: Number of modes and total mass of various concrete cavity versions, with varying wall thicknesses, lightened walls and different reinforcement rebar diameters.

The model was meshed and created in ANSA, using only HEXA solid elements with an element target size of 20 mm. Wall thicknesses of 300, 200, 160 and 100 mm were analysed, with various modifications. To reduce the total weight of the 300 mm thick walled structure, double-walls and structurally lightened walls were applied. For the smaller wall thickness, rebar reinforcements were added to the model with CBEAM elements of various circular diameters. An example configuration with cutaway solid elements shows the rebar reinforcements within the structure on Figure 37.

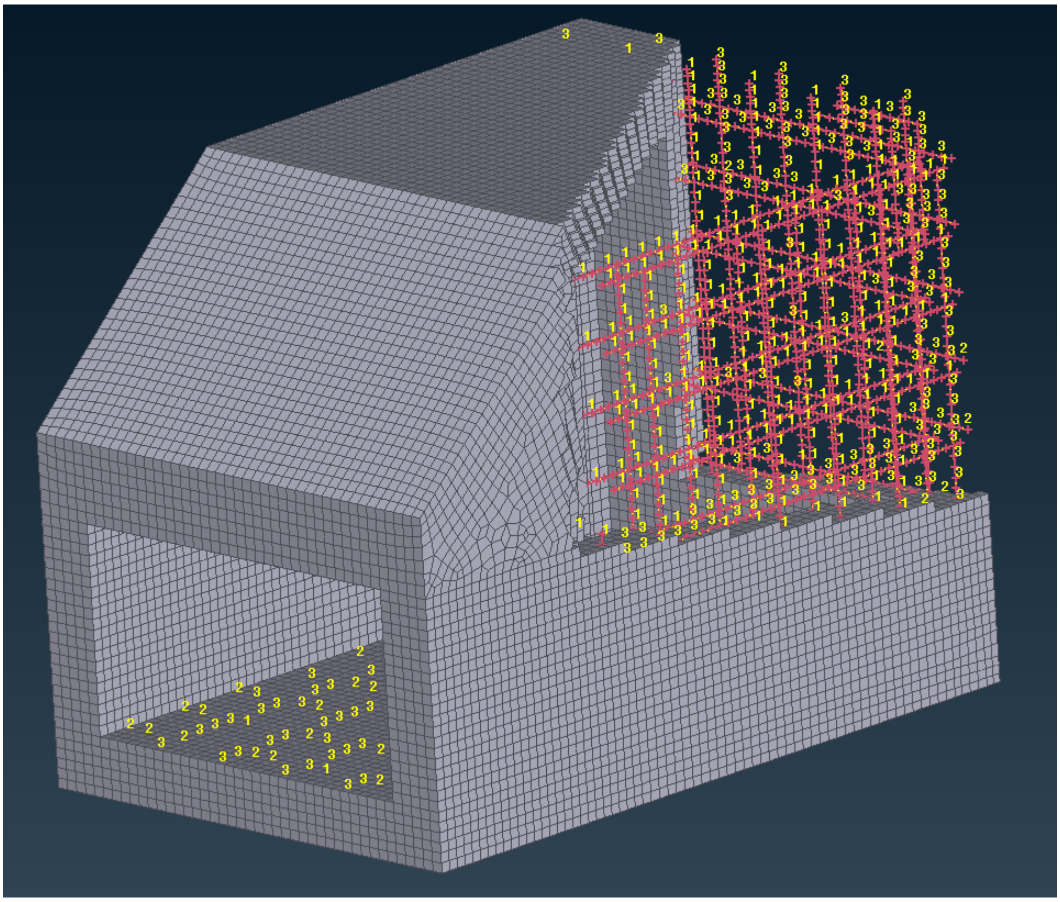

Figure 37: Cutaway of solid mesh used for concrete cavity modal analysis, showing CBEAM elements representing rebar reinforcements.

Table 2. shows the modes in bands as well as the total weight of the analysed structure versions. This was an important factor to consider, as it severely limited the placement and practical usage of the test apparatus. As evident from the results, the major influencing factor of the modal behavior was the wall thickness. Double-walled sidewalls and the structurally lightened solutions created chambers, where more resonance could occur, while the drastically increased total mass of the heavier walls made their choice impractical. In the end, the 100 mm thick walls were chosen as a final solution. As the reinforcements did not have a major effect

on the modal behavior, their location and diameter was determined by the manufacturing`s needs.

The front opening of the cavity is bordered by 5 mm thick steel inserts with welded threaded rods to securely fasten and clamp the investigated plate. Four threaded rods have increased length to hold a 100 mm thick concrete cover plate, which enables investigations of the effects of porous materials on an acoustic cavity. Two openings on the side ensure that interior microphone cables can be connected to receiver channels and acoustic excitations (e.g. white noise machine) have access to the cavity air volume.

During the steel cavity`s design process, similar methods were used to the concrete cavity`s development. However, the models used were more complex due to the various stiffening elements applied as well as due to their joining methods. Initially, the wall thickness` effect was investigated on the modal behaviour. As per the design requirements, the maximum investigated wall thickness was 1.6 mm, which greatly reduced the number of modes within the frequency range. However, since minimizing the number of modes was not the first design priority, a closer approximation of a real vehicle body was instead targeted, and so the thickness for the cavity walls was chosen to be 1 mm. A further reduction to 0.8 mm thickness would have provided even better correlation with vehicle structures purely on sheetmetal thickness, however, its vulnerability and difficulty of manufacturing deterred from its application.

To reinforce the thin metal cavity and to provide additional subsystems for SEA and power flow analyses, stiffeners were added to the structure in multiple locations. For manufacturability, these were 2 mm thick steel U-sections, as they would be joined to the cavity with rivets. Continuous welding was not an option for joining due to the expected high level of geometric distortion this would introduce to the thin steel cavity skin, while spot welding in the required locations was not practically feasible based on the final geometry. Riveting also makes further repairs easier, should the subsequently introduced vibrations cause damage to the structure. Modelling of these joints in ANSA was done using RBE3-HEXA-RBE3 connections, while the structural elements were represented by QUAD shells. Figure 3. shows the applied mesh. In conjunction with the rivets securing the stiffeners to the inner cavity section, the stiffeners themselves were welded together to avoid additional resonant modes with their overhanging ends outside the cavity bounds. These weld lines were also realized with RBE3-HEXA-RBE3 connections. Figure 38. shows the meshed cavity FE-model.

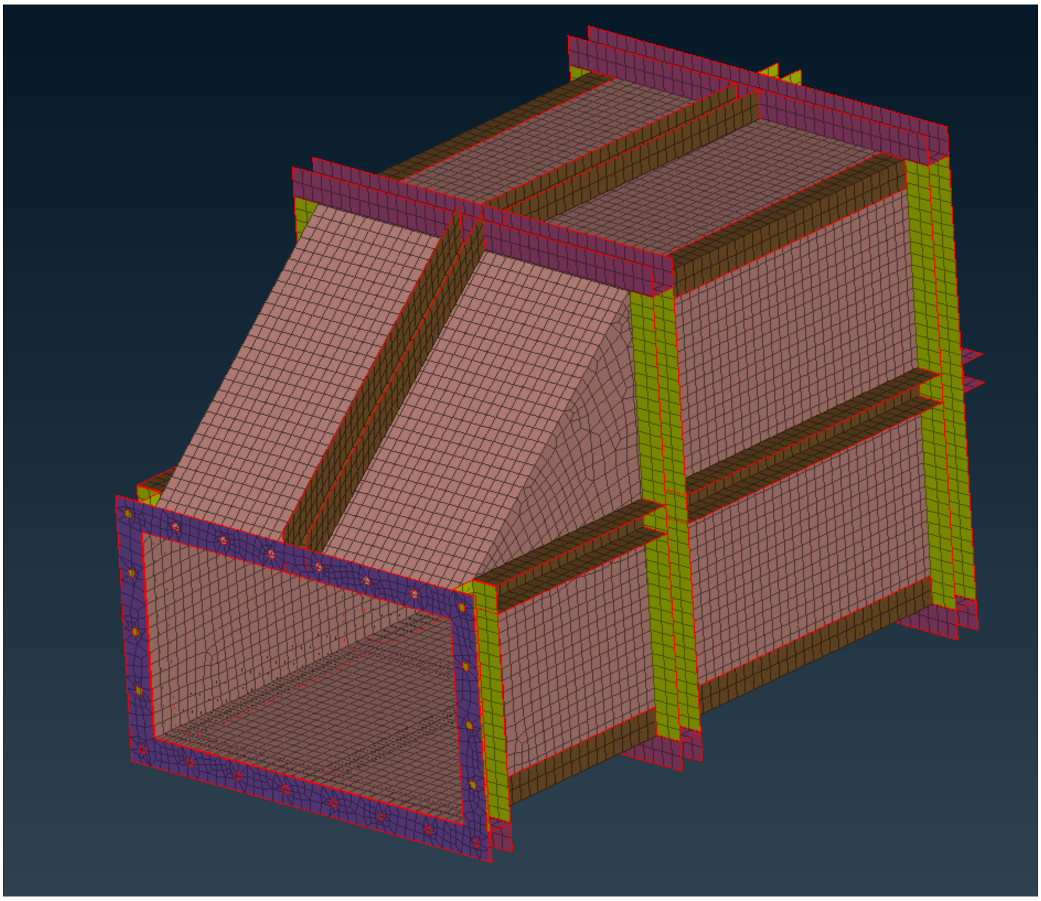

Figure 38.: Shell mesh used for the steel cavity finite element calculations

As the investigation required modal bases to be calculated up to 1800 Hz, element sizes had to be chosen appropriately. Higher frequencies result in shorter wavelengths, thereby the danger exists that too small elements will be used to discretize the model in question. The limiting factor is the bending wavelength in the structure at the given frequency, which can be determined using the formula below:

$$\lambda_b = \sqrt{\frac{\pi c_l h}{\sqrt{3} f \sqrt{(1-\nu^2)}}} \tag{14}$$

In the formula above, f is the frequency of interest, ν is the material's Poisson's ratio, while c_l is the elastic wave velocity, calculated using the Young's modulus and density of the material:

$$c_l = \sqrt{\frac{E}{\rho}} \tag{15}$$

Using structural steel's material properties (the material used for the test apparatus), the wavelength equals 0.104 m. Based on experience and recommendation of the industrial partner, in order to accurately capture the movement of the structure, six nodes must be contained within one wavelength. With first order elements used in the campaign, this meant a maximum element size of 12 mm for 1 mm sheetmetal thickness, and 17 mm for the stiffeners. As computational capacity was available, as well as to account for possible material variations without the need to re-mesh the model, a 10 mm target element size was used for the entire model.

No solid elements except for the representative welds were used in the model. As all stiffeners were manufactured using sheetmetal bending, the bending radii were modelled in FEM as well for the sake of accuracy, with two rows of QUAD elements in all cases. To ensure compatible and non-conflicting boundary conditions, the welded connections were realized with fixed orientation, a maximum aspect ratio of 8, constant width and constant cross-section. Figure 39. shows an example for a realized connection between stiffeners, with the two-row bend model and non-conflicting connection condition.

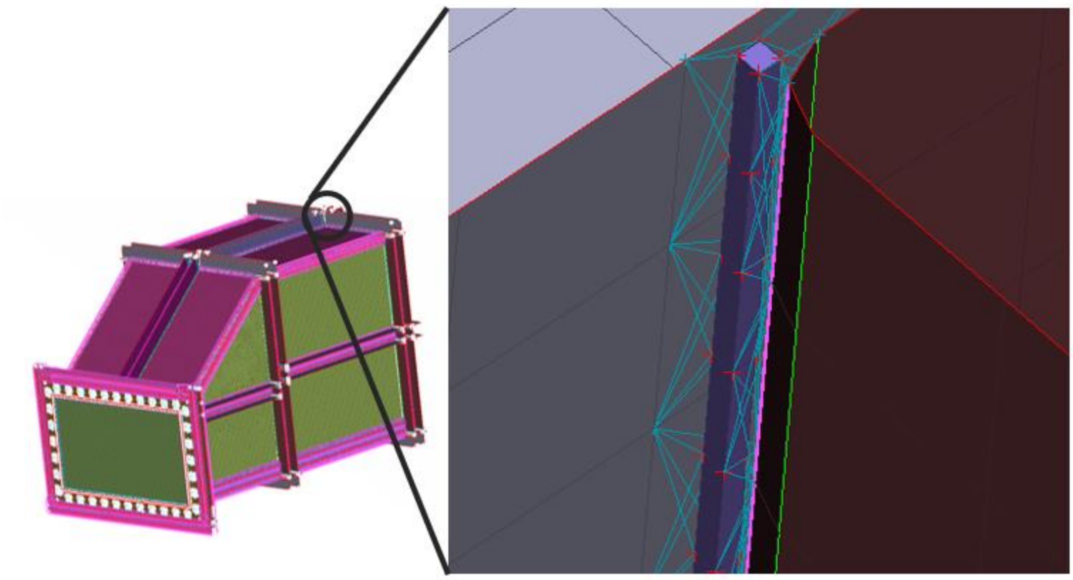

Figure 39.: Illustration of the FE-realization of a bent stiffener edge and its welded connection. RBE3-HEXA-RBE3 representations were chosen for weldlines.

Multiple versions of reinforcements were tested virtually, but in the end, stiffeners placed at the edges of the cavity and a single central reinforcement to the angled cavity wall were chosen, as these allowed the cavity panels to be associated with lower frequency, distinctive modes. The effect of using 5 mm stiffeners was investigated in an effort to lower the modal density, which they successfully did indeed. However, the increased weight would have resulted in an impractical setup (due to safety guidelines, the version with 5 mm reinforcements would have to be moved using a crane) and the modal density reduction was after all not needed, as the thicker reinforcements mostly eliminated local modal behavior of the reinforcing skeleton. A summary of multiple versions` modal behaviour is shown in Table 4.

Frequency Bands		Modes in band					
Lower cutoff (Hz)	Upper cutoff (Hz)	0.8 mm wall	1 mm wall	1.2 mm wall	1.4 mm wall	1 mm wall 2 mm skeleton	1 mm walls 5 mm skeleton
224	282	84	64	52	44	48	27
282	355	102	82	64	57	67	43
355	447	129	105	86	73	89	38
447	562	165	128	108	90	178	50
562	708	216	167	140	117	197	82
708	891	277	220	177	150	249	105
891	1122	353	276	226	194	287	333
1122	1413	461	361	299	253	360	392
1413	1778	148	110	89	73	136	64
	Sum:	**1935**	**1513**	**1241**	**1051**	**1611**	**1134**

Table 4.: Number of modes of various steel cavity versions with different wall- and skeleton thicknesses

After determining the final geometry, some modifications were made for the practical use of the cavity. Pick-up plates were added to the bottom reinforcements to mount the apparatus on airbags for vibration isolation. The front cover plate`s mounting is riveted to the structure, with the threaded rods welded on. These have the same bolt pattern as on the concrete structure, so the test plate specimens can be exchanged. Two openings are made on the side for cables and acoustic excitations, and pick-up points are added for lifting to the side reinforcements. The final design is shown on Figure 40.

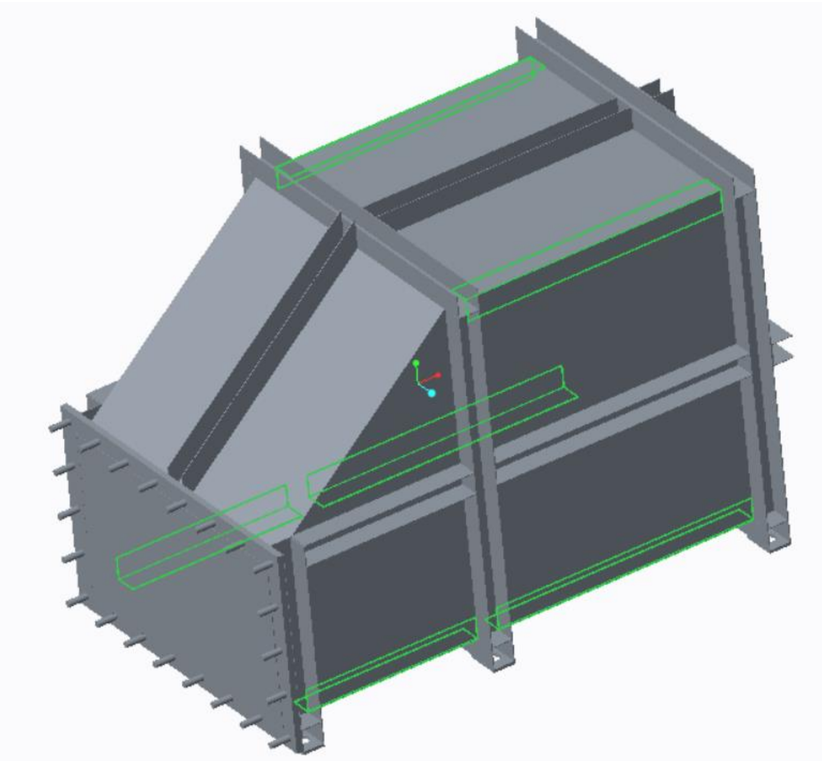

Figure 40: Final steel cavity design with attached front cover plate and highlighted edge stiffeners

Final weight of the designed metal cavity was 91.33 kg, with a total number of modes up to 1800 Hz being over 1600. The two manufactured cavities are shown on Figure 41.

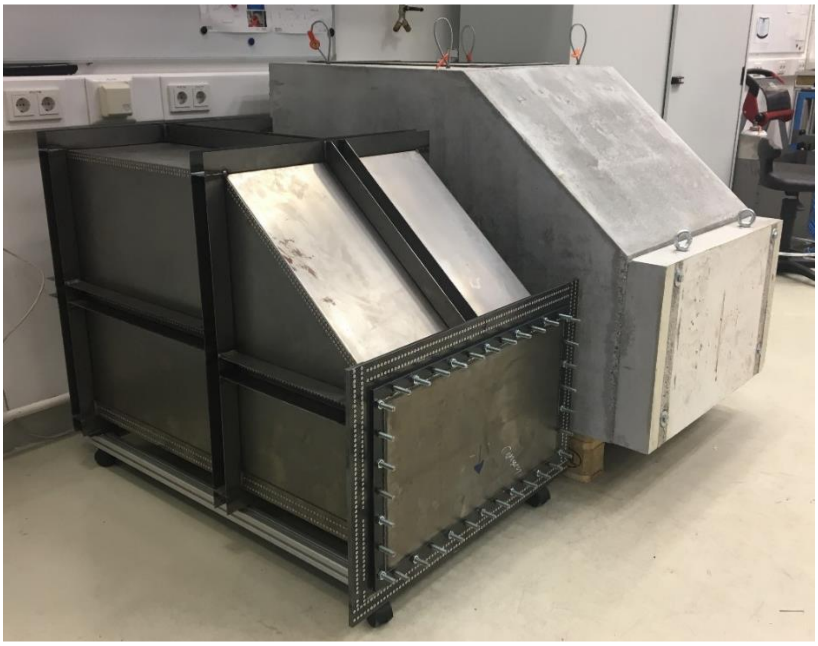

Figure 41.: Manufactured versions of Test Cases 2a (concrete cavity, far right) and 2b (steel cavity, nearside left)

Test Cases 2a and 2b were designed within the framework of a larger research program aimed to improve mid-frequency acoustic simulations of porous elastic material trims applied on metal structures. Within the research campaign, a distinct need emerged to investigate a panel-air cavity setup with a trapezoidal cavity cross-section. Due to the nature of the research project, an apparatus capable of replicating conditions both in finite element methods and statistical energy analysis was required. The conflicting requirements of the two computational methods resulted in the design of two separate cavity apparatuses: one made of concrete with a single flexible wall, and another made of steel with reinforcements to replicate a vehicle body on a smaller scale.

During the design of the apparatuses, modal analysis was carried out using ANSA EPILYSIS. As SEA requires at least 3 modes in each third-octave band, the cavity interior volume was defined such that it fulfils this requirement. A final cavity volume was selected from 36 investigated versions, with dimensions of 650 mm width, 1150 mm length and 750 mm height. This became the basis of the steel and concrete cavities, whose final designs were also the results of extensive modal analysis.

In case of the rigid walled cavity, multiple wall thicknesses with various reinforcements were studied. It was found that the wall thickness has the most profound effect on the modal behaviour, however, there was not a significant increase in the number of modes with decreasing the wall thickness to the minimum limit of manufacturability, 100 mm. This resulted in a relatively practical, 1 ton overall weight, significantly lower than the approximately 3.6 tons of the version with 300 mm thick walls. A welded steel insert is moulded into the cavity opening wall with threaded rods, able to hold both a plate specimen and a 100 mm thick concrete cover used for pure acoustic material investigations.

The steel cavity`s main role was to provide a structure with acoustically participating elements, i.e. compliant walls and reinforcements, to allow calculation of a complex set of subsystems` response in SEA and to investigate power flow and a car-like simpler structure in FEM. With multiple wall thicknesses and reinforcement thicknesses- as well as locations studied, the final version achieved the goals of having a total number of modes similar to that of a vehicle body structure.

3.1.1. Thesis 1:

I designed a scaled passenger car interior model for the purposes of acoustic FEM-PEM and SEA simulation validation in the mid-frequency (400 -1000 Hz) range. Three key design guidelines have been established to achieve this:

a) *The optimum volume of the cavity can be achieved when the criteria of minimum 3 fluid eigenmodes in third-octave frequency bands above 282 Hz center frequency (enabling SEA validation) is met, while minimizing the total number of fluid eigenmodes (enabling FEM-PEM validation).*

b) *For validating fluid-PEM interaction, rigid walls are required. For a reinforced concrete structure, the wall thickness should be selected to find a compromise between the total number of structural eigenmodes and the minimum thickness dictated by the manufacturability.*

c) *For validating fluid-structure-PEM interaction, acoustically flexible walls are required.*

4. Frequency-dependent poroelastic material parameters

As demonstrated in the literature review, and highlighted as a gap in the current state-of-the-art knowledge, a conclusive effect of frequency dependent PEM parameters has not yet been identified. Literature already indicates that large variation may exist in certain PEM parameters, but their overall effect in complex acoustic systems is not shown. Within the research group, another researcher's dedicated field was the measurement of the behavior of poroelastic materials (Schweighardt and Vehovszky, 2021). Results of these measurements were applied in FEM simulations in the current research, specifically the frequency-dependent parameter results. In this section, the goal is to apply these measured frequency-dependent material parameters – namely Young's modulus and damping – to trim materials on all three levels of test case complexity (Test Cases 1, 2 and 3) and to understand their effect

Individual cases are simulated and compared with measurements to establish the effect frequency dependent parameters have on frequency response functions.

Based on measurement data, a frequency dependent Young's modulus and damping curve was compiled, and then applied to the foam material in simulations. Material measurement was carried out within the research group and is detailed in (Schweighardt and Vehovszky, 2021). Figure 42. shows the two curves along with the constant values that were used for comparison in the simulations. Both damping and Young's modulus varied significantly in a progressive manner over the frequency range of interest. Young's modulus increased by 800% while damping increased by over 200% to the upper frequency range limit.

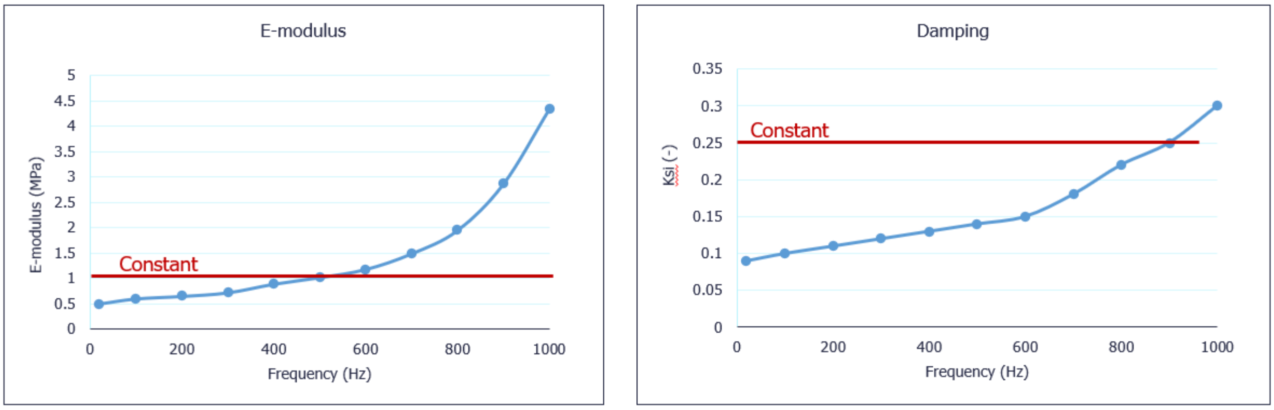

Figure 42.: Measured frequency dependent material parameter curves (Data source: Schweighardt and Vehovszky, 2021)

As detailed before, simulations for Test Cases 1 and 2b were carried out using ESI VPS solver, while Test Case 3 was computed using NASTRAN-PEM. Evaluation of results was carried out in BETA CAE Meta tool throughout.

Recall that the results of damping loss factor measurements for Test Case 1 indicated that a large relative variation existed in the structural damping of a simple flat plate. Before the application of frequency dependent trim parameters, a simple investigation was carried out to examine, whether changes in structural damping coefficient affect the structural frequency response of an untrimmed plate. However, it is important to note, that damping loss factor is not equivalent with structural damping coefficient in the solver: there is a simple relation of $DLF = 2 * \xi$ between the two.

In Section 2.1. and (Kun et.al. 2020) it was detailed that the half-power bandwith measurement method was used to determine the damping values. In VPS, the modal frequency response method only supports the inclusion of frequency dependent material parameters for poroelastic materials. Frequency dependent damping for structures can only directly be applied using direct frequency response method, however, for the sake of similarity, the frequency response calculation method was not changed. Rather, modal frequency response method was used, separately for each third-octave band with the appropriate structural damping coefficient applied to the flat plate. Table 5. shows the values obtained through measurement, with Figure 43. showing them graphically.

Center frequency	**DLF**	ξ
200	0.00116	0.00058
250	0.00056	0.00028
315	0.00099	0.00050
400	0.00058	0.00029
500	0.00056	0.00028
630	0.00062	0.00031
800	0.00050	0.00025
1000	0.00068	0.00034

Table 5.: Measured damping loss factors, their corresponding center frequencies and structural damping coefficients used in the FE-solver.

Two distinct peaks at 200 and 315 Hz center frequencies exist, where the damping doubles. While relative changes are large due to the inherently low damping value that such a structure possesses, in absolute terms, changes were on the order of 10^{-5} .

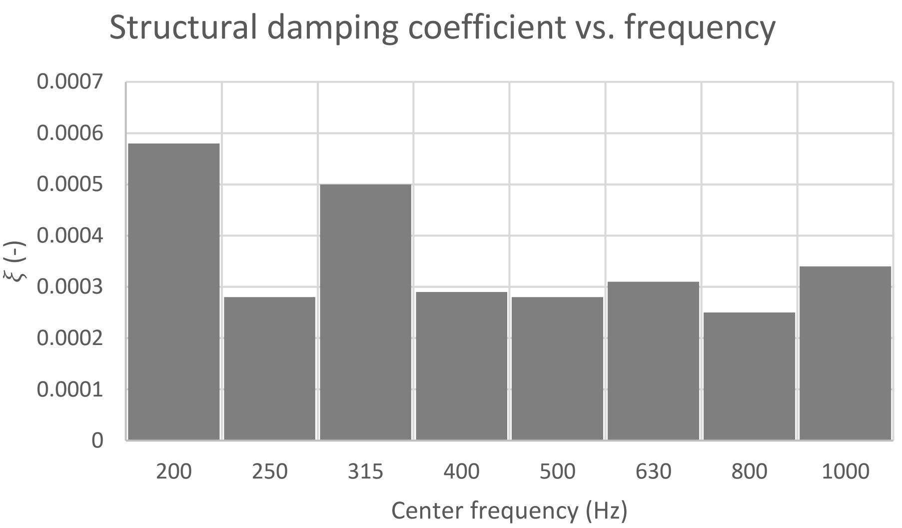

Figure 43.: Structural damping coefficient for third-octave frequency bands.

As the DLF measurement resulted in frequency response function curves, they provided a good basis for comparison with simulations. Figure 44. shows baseline results for complex translational acceleration compared with measurement, which used an averaged structural damping coefficient of 0.034 % based on measurement results in the simulation. Results from each response points were averaged for both the measurement and the simulation. Highly modal behavior can be observed with many peaks within frequency bands, as expected from such a lightly damped structure. Correlation was found to be acceptable already for this case, however, some issues were noted: some peaks were missed by the computation, and at higher frequencies the peak locations became less and less accurate, while peak heights also showed a variation from the measured values. This is consistent with the expectation of the modal frequency response method's application for a lightly damped, highly modal structure in the higher frequency range.

The application of the frequency dependent structural damping coefficient affected the heights of peaks at the modal locations. Most pronounced was the effect at higher frequencies, with the 800 – 1000 Hz range shown on Figure 45. With this magnified range, two conclusions can be drawn for the untrimmed plate:

- Correlation between simulation results and measurement is good overall but starts to decline over ~740 Hz.
- The application of frequency dependent structural damping coefficient somewhat improves correlation, but not significantly enough to offset the high computational effort in its application for modal frequency response.

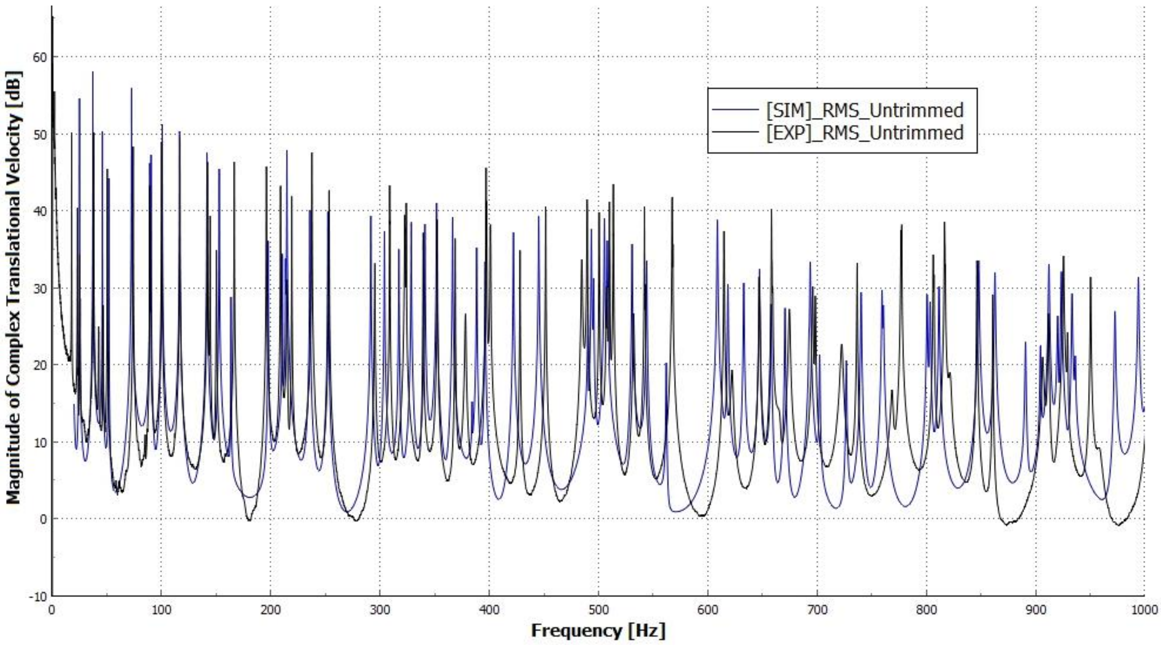

Figure 44: Simulated (blue) and measured (black) baseline response of flat plate with constant material properties in the range of 20-1000 Hz.

It must be noted that while the measurement attempted to establish a free-free boundary condition (like in the simulation), in reality, this was difficult to achieve. This imperfection in the boundary condition, as well as an imperfection in plate curvature and the previously investigated material tolerance effects all contribute to the discrepancies between simulation and measurement.

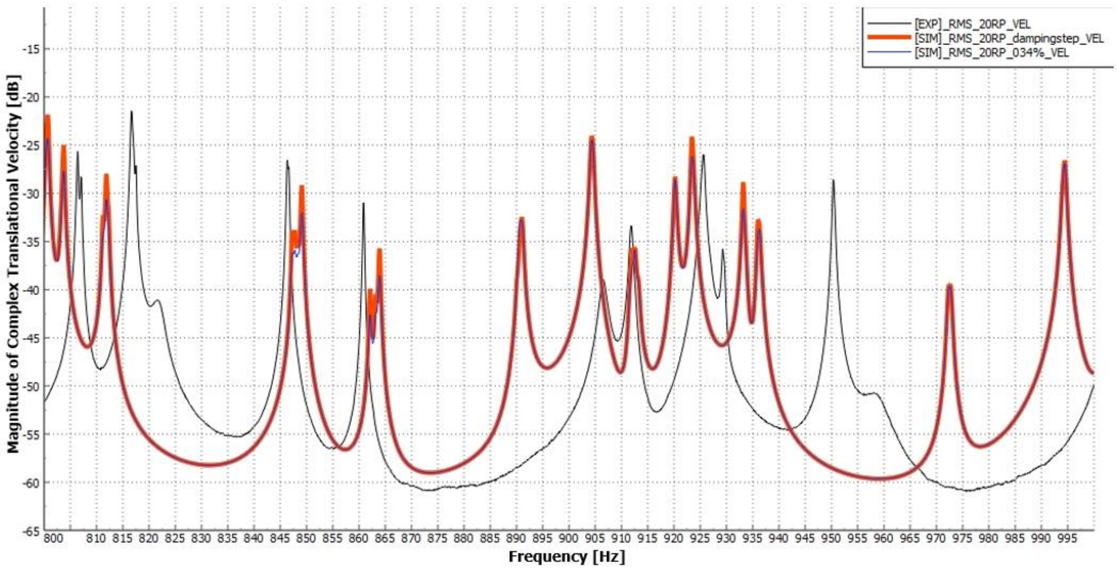

Figure 45.: Effect of frequency dependent damping between 800 and 1000 Hz on RMS velocity magnitude response (red: frequency dependent damping simulation, blue: baseline simulation, black: measured response – blue and red curves overlap due to the minimal effect of frequency dependency).

As it has been established that even in the most damping-sensitive case, changes in structural damping coefficient do not significantly affect results, focus was placed on trimmed cases. Structural damping coefficient was considered constant in all further investigations. Firstly, Test Case 1, the trimmed flat plate was investigated.

A simulation campaign was conducted for the trimmed flat plate test case. Goal of this campaign was to understand how frequency dependent damping and the frequency dependent Young's modulus affect the response of such a lightly damped system. A single-material foam trim was applied, with three different thicknesses, with and without separately applied frequency dependent damping and Young's modulus. 10, 30 and 50 mm thick trims were investigated. These are not feasible thicknesses (especially 30 and 50 mm) in the automotive industry, but the exaggerated cases were used to highlight effects. Other Biot-parameters of the material were assumed to be equal to that of an industrially used sound absorbing foam. Beside the single material foam trim, a 10 mm foam trim with 2 mm thick heavy layer case was also investigated, with constant and frequency-dependent parameters. A foam-heavy layer material combination is often used in whole vehicles, therefore it was of interest for the current research. In the simulation setup, the full trim surface was coupled to the plate, with pure STICK condition. This meant that both the out-of-plane and in-plane movement of the trim nodes was coupled with the structure.

First configuration to be examined was the pure foam trim. Initially, a 65 kg/m^3 density foam was tested, with the three different thicknesses explained earlier. As expected, attenuation increased with thickness, as Figure 46. shows. At some peaks, over 30 dB velocity reduction was achieved with 50 mm thick trim.

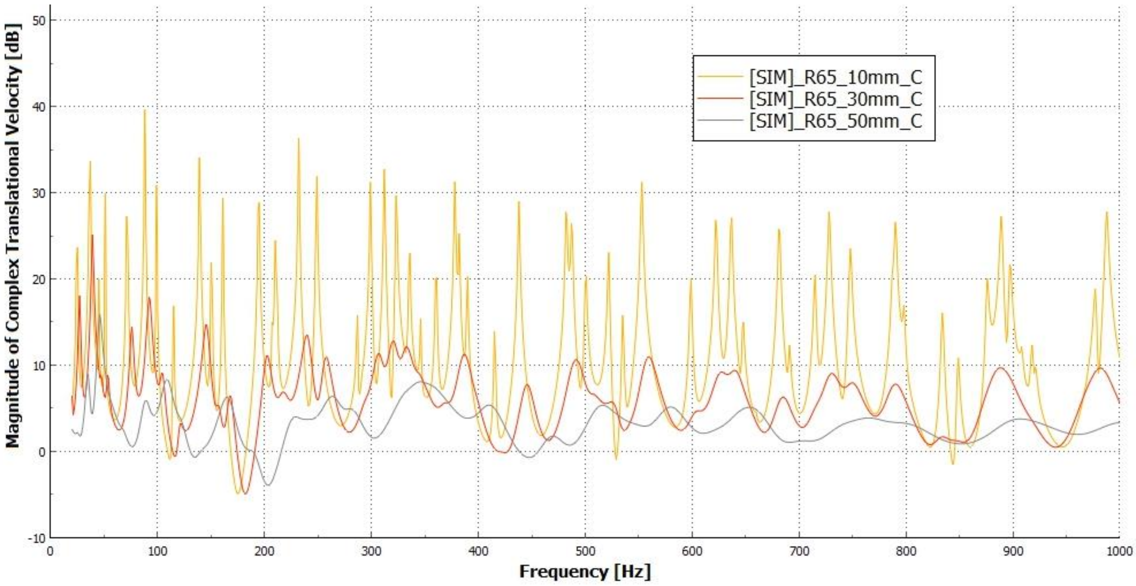

Figure 46.: Effect of 65 kg/m3 foam trim on Test Case 1 structural response, with 10 mm, 30 mm and 50 mm trim thickness and constant material properties.

As the Young's modulus of the foam acts similarly to a spring constant in a mass-spring system. This effect can manifest itself not only by reducing modal peaks, but also in changing resonant frequencies and thereby shifting peaks to different frequencies. Therefore it was expected to have significant effect on the results, and even more so in a foam-heavy layer configuration. However, results indicate that its significance was greatly exaggerated with thicknesses unfeasible in automotive applications, shown on Figures 47-49.: while at 10 mm trim thickness, it mainly manifested in peak reduction (Figure 47.), at 30 mm (Figure 48.) and especially at 50 mm thickness (Figure 49.), variable Young's modulus resulted in significantly different curves, with shifted peak locations as well as reduced attenuation compared to the constant parameter's results. Compared constant assumed Young's modulus was 4 MPa for this given case, which can be observed as the curves converge towards the upper frequency limit, 1000 Hz.

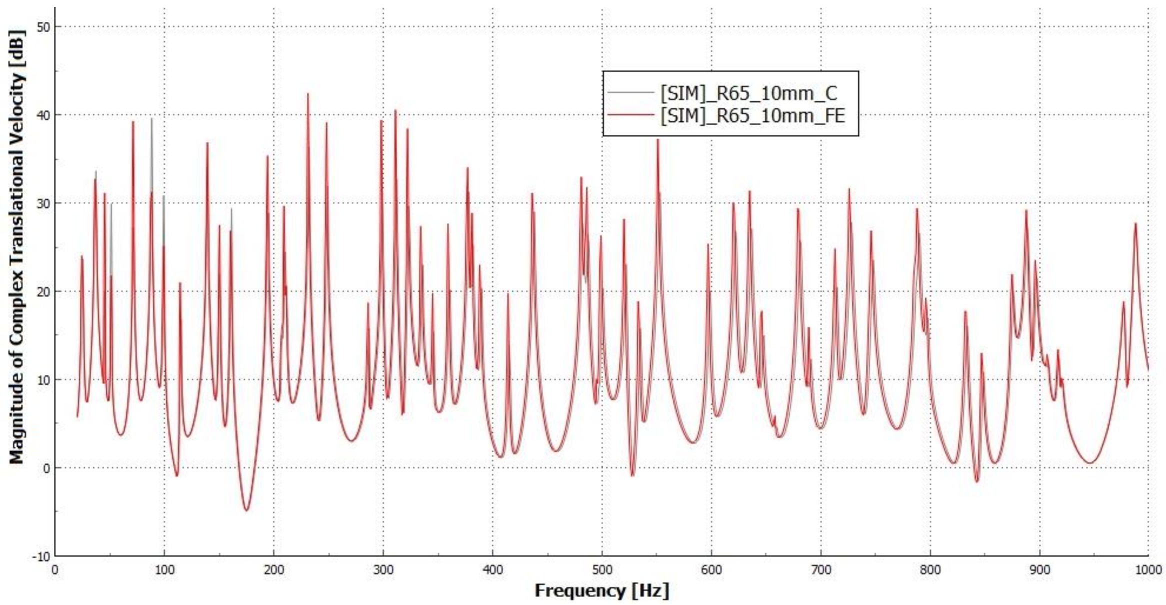

Figure 47.: Structural response of Test Case 1 for 10 mm trim thickness with constant (grey) and frequency-dependent Young's modulus (red). Differences in peak heights between 50 and 300 Hz can be observed, up to 8 dB. In the majority of the frequency range, the two curves overlap.

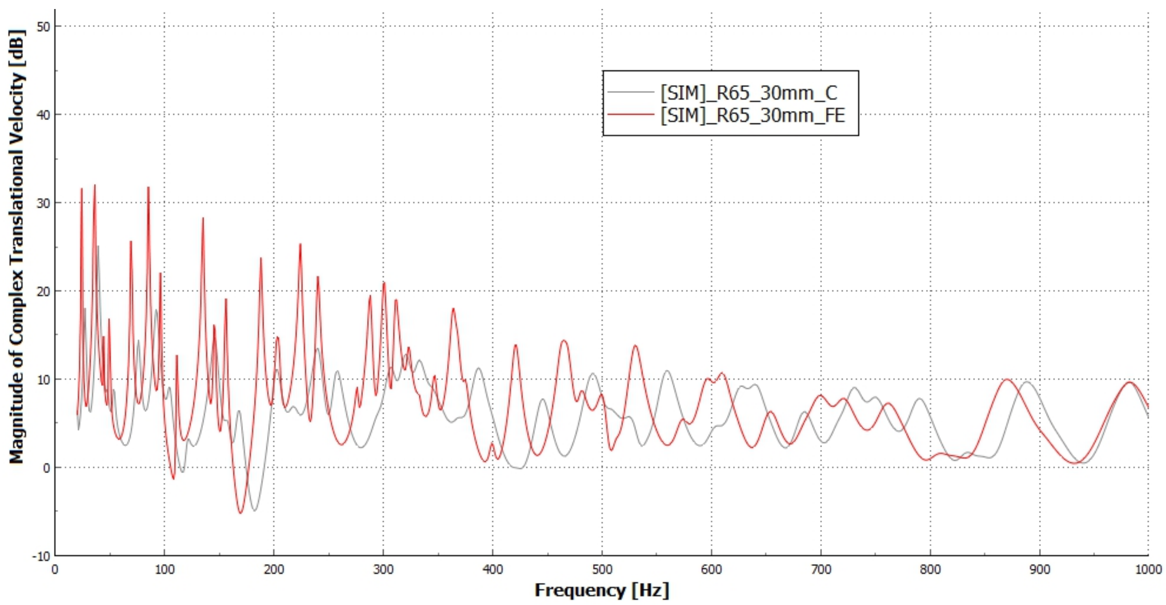

Figure 48.: Structural response of Test Case 1 for 30 mm trim thickness with constant (grey) and frequency-dependent Young's modulus (red).

Frequency dependent damping for trim parts has already been a research topic of interest, so it was similarly investigated for the three different trim thicknesses. The frequency dependency curve was obtained from measurement, just like in the case of the Young's modulus, and applied to the material. Damping mainly affects the peak values of a response, however it does not influence resonance locations.

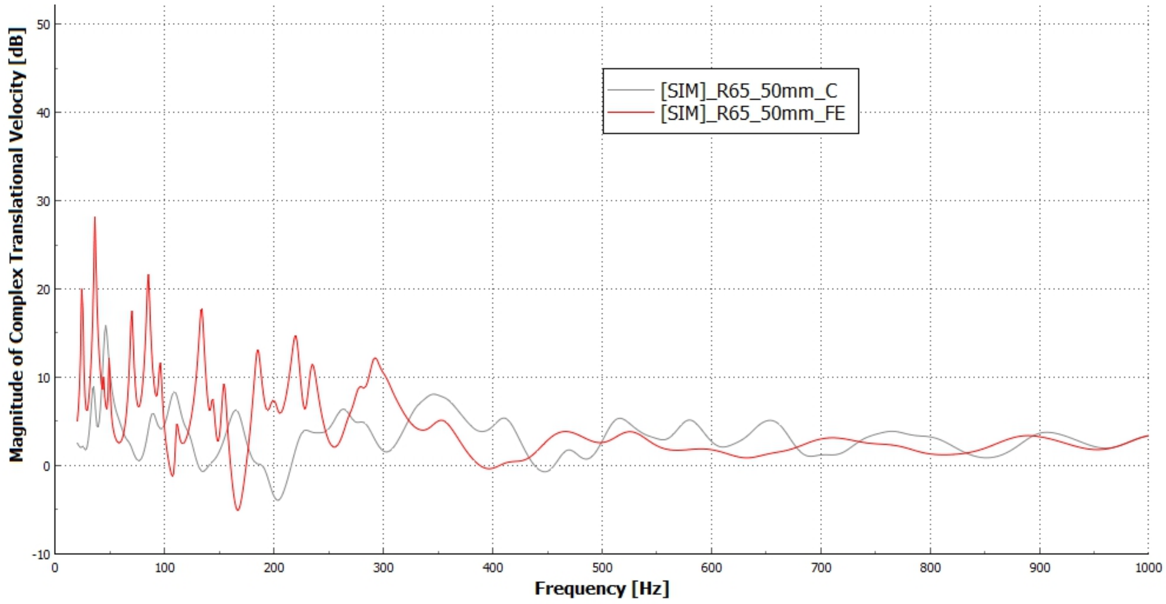

Figure 49.: Structural response of Test Case 1 for 50 mm trim thickness with constant (grey) and frequency-dependent Young's modulus (red).

Frequency dependent damping's effect was also more pronounced for the 50 mm thick trim (Figure 50.), with low-frequency peaks under 500 Hz being much more pronounced due to the lower damping values in that region. For 30 mm thickness, shown on Figure 51., the effect was just as significant.

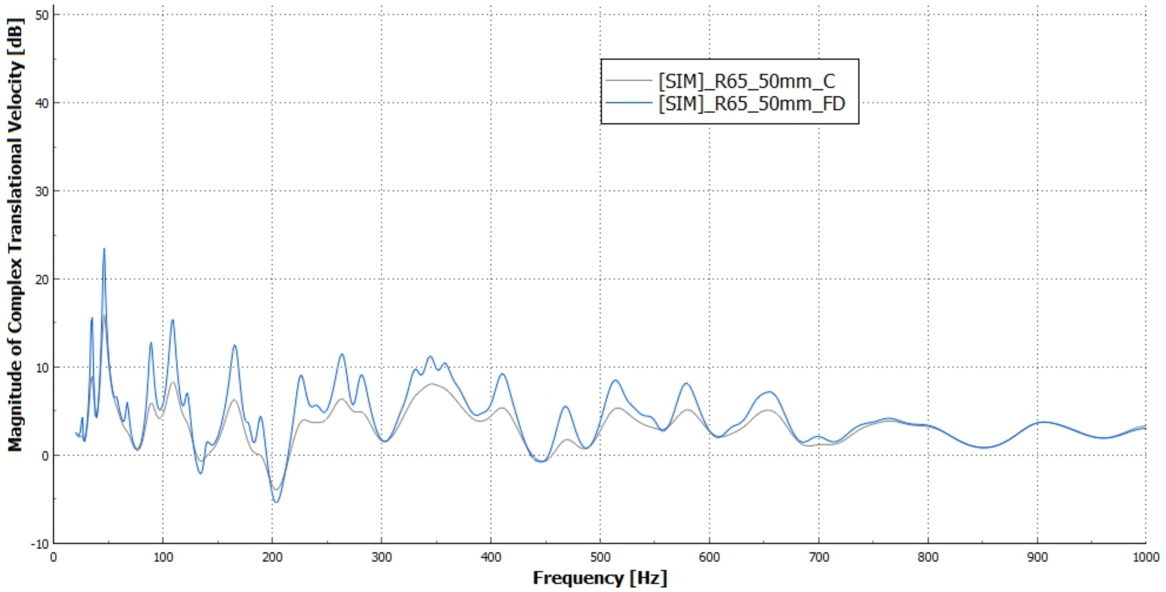

Figure 50.: Structural response of Test Case 1 for 50 mm trim thickness with constant (grey) and frequency-dependent damping (blue).

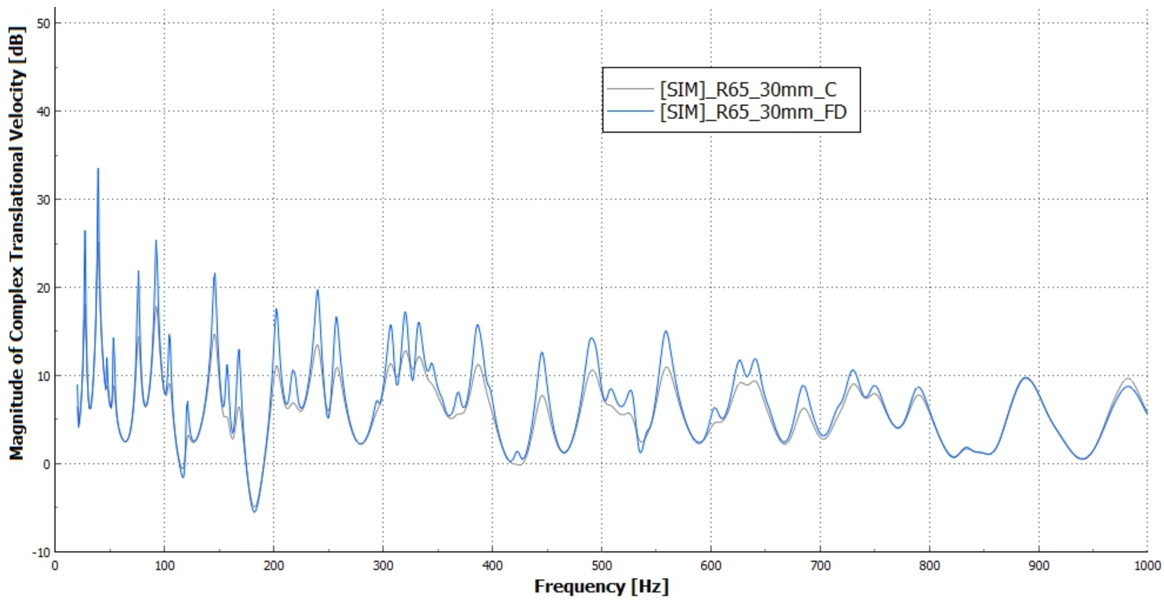

Figure 51.: Structural response of Test Case 1 for 30 mm trim thickness with constant (grey) and frequency-dependent damping (blue).

These initial results suggested that frequency dependency both in Young's modulus as well as damping could effectively be used to alter responses of structures in given frequency ranges, dependent upon the attenuating material's behavior. However, these were decidedly academic cases, where a simple structure was 100% directly covered on its surface with a simple acoustic treatment.

Generally, an acoustic treatment consists of an underlying foam covered with a solid, elastic so-called heavy layer, therefore such a setup was also considered for the flat plate investigation. This configuration can be effective for noise reduction, as the system can be tuned as a mass-damper system. A frequency-dependent material could alter this system's eigenfrequency, extending the attenuation range. For this purpose, a 55 kg/m^3 density foam was used, with previously used nominal material parameters and 20 mm thickness for a closer-to-production investigation. On its free side, a heavy layer was applied, with 2 mm thickness and 5500 kg/m^3 density, directly coupled to the foam nodes. Comparison this time was made with a 1 MPa constant Young's modulus. Results indicated a significant effect, especially beyond 700 Hz where up to 10 dB difference was observed between the constant- and frequency dependent material. Figure 52. shows the RMS velocity magnitude results of the response points.

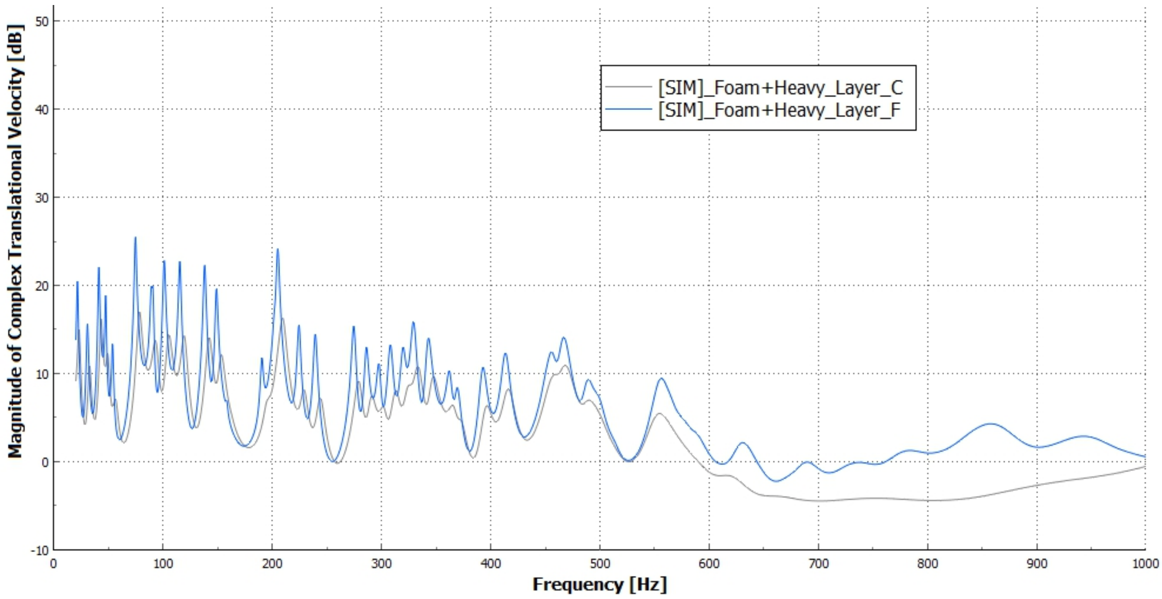

Figure 52.: Structural response of Test Case 1 for 20 mm foam trim with 2 mm heavy layer applied, with constant (grey) and frequency-dependent parameters (blue).

Altogether, investigations on Test Case 1 indicated that frequency dependent damping and Young's modulus for trim materials can be a promising tool to increase FEM acoustic simulation accuracy in the higher frequency range, as both have significant effects on responses. The following complexity step was Test Case 2b, the model interior cavity with acoustically participating walls.

One loadcase was examined, on the firewall-like front panel with a point-loaded unit excitation. Responses were computed from 20 Hz up to 1000 Hz, with 6 response locations recording interior sound pressure levels. Simulations were conducted with two different foam configurations, as well as a foam-heavy layer treatment. Experimental data was also collected for the pure foam configuration. Frequency dependency was added both to damping and Young's modulus, to replicate more realistic conditions for the trim material.

The two foams differed in density as well as Young's modulus: Foam 1 was 55 kg/m^3 density with 1 MPa constant Young's modulus.Foam 2 resembled most the vehicle industry standard, had 60 kg/m^3 density with 0.2 MPa constant Young's modulus and was procured for experimental measurement as well. Both foams used the same Biot parameters, with a constant damping coefficient of 0.25. Frequency dependency was applied using the previously established measured curves. Trim was 20 mm thick throughout all cases. For the foam and heavy layer configuration, Foam 1 was used along with a 2 mm thick heavy layer with 5500 kg/m^3 density, just like for Test Case 1.

First, the investigation of the frequency dependent parameters was repeated on this test apparatus as well, with analysis of results between constant and frequency dependent parameters. Figure 53. shows RMS-averaged frequency response sound pressure levels for Test Case 2b, trimmed with Foam 1. Yellow corresponds to constant, while blue represents frequency dependent parameters.

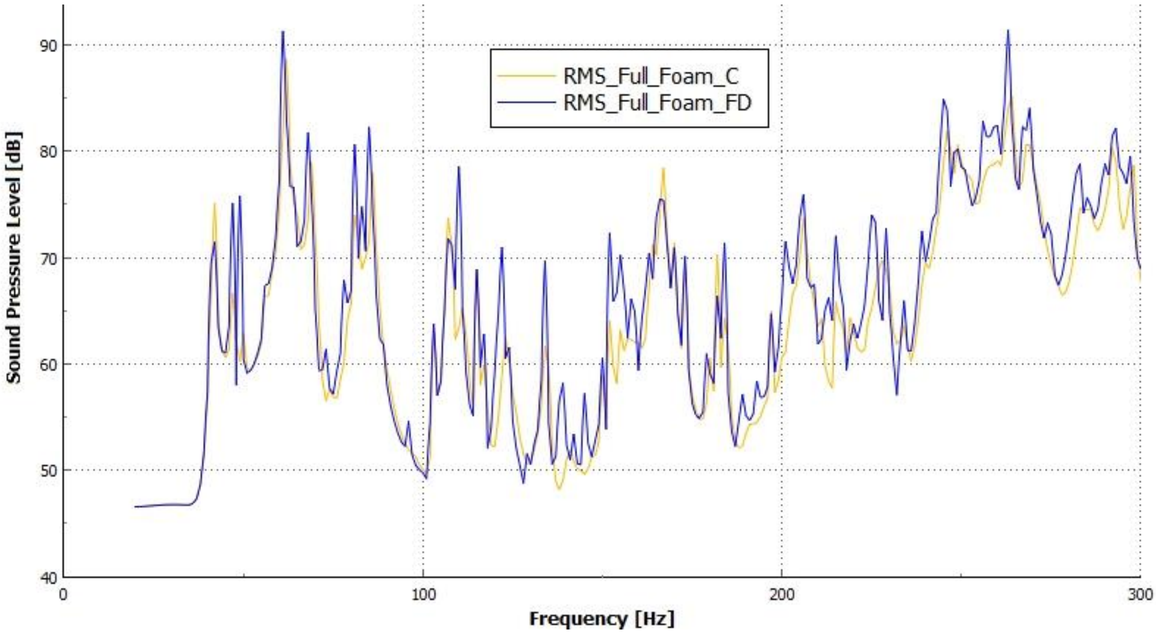

Figure 53.: Test Case 2b RMS sound pressure level for foam trim with constant- and frequency dependent Young's modulus and damping, 0-300 Hz

For ease of visualization, a frequency range up to 300 Hz is chosen, since the differences between the results are minor. With both damping and Young's modulus lower than the constant value, peaks are higher for the frequency dependent case. However, the overall effect is less pronounced, than before, which is only reinforced when looking at Figure 54., showing the same results between 700-1000 Hz.

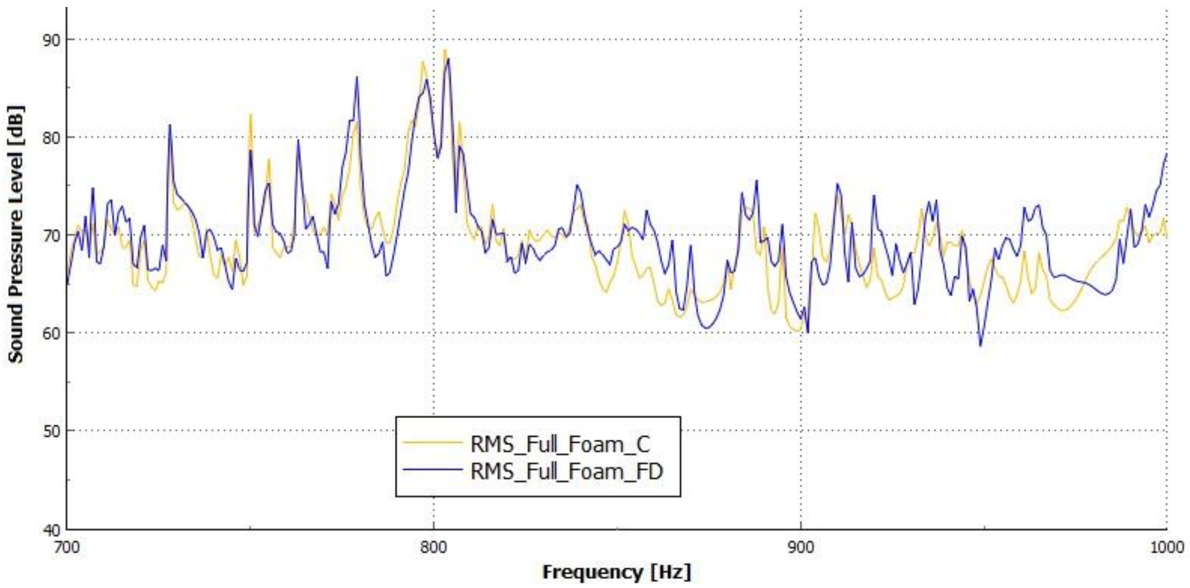

Figure 54.: Test Case 2b RMS sound pressure level for foam trim with constant- and frequency dependent Young's modulus and damping, 700-1000 Hz

At high frequencies, even peak heights correlate, and there is no significant difference between the results – a first indication that the more complex the case is, the less significance there is of frequency dependency. It is also to be noted, that in Test Case 2b, just like in a whole vehicle, a comparatively much smaller area is directly covered with acoustic treatment than in Test Case 1, further reducing its effect.

A foam and heavy layer configuration was also tested, with Figure 55. showing low-frequency response up to 300 Hz, and Figure 56. displaying the high frequency results from 700 Hz to 1 kHz. Dark blue represents frequency dependent results, while green corresponds to constant parameters.

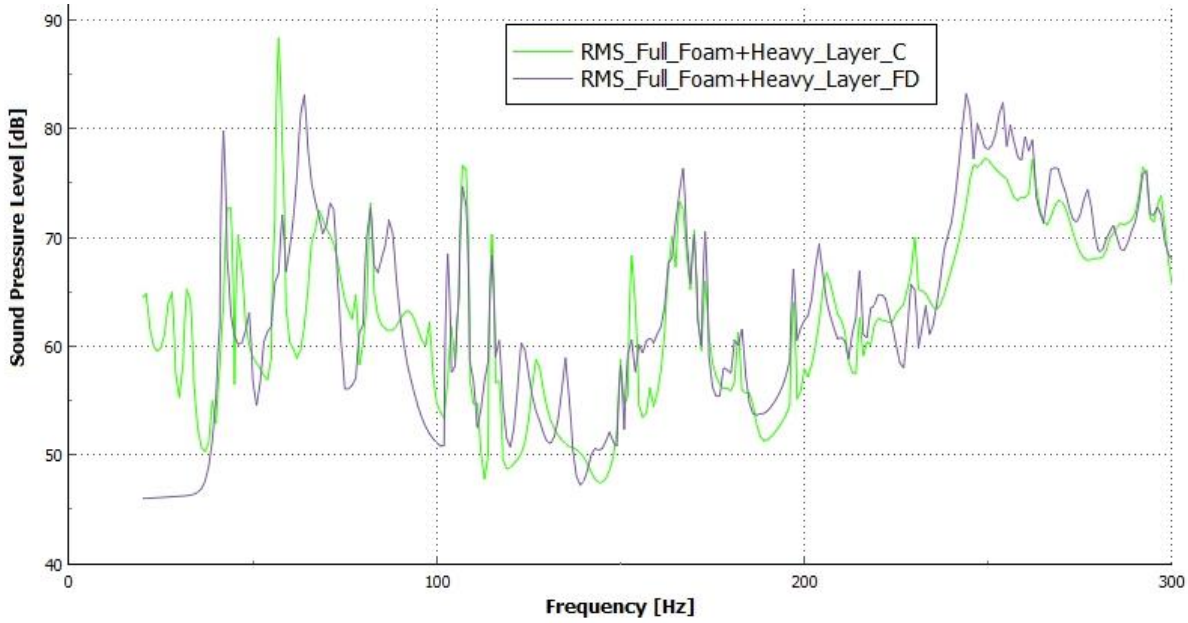

Figure 55.: Frequency dependent and constant results for Test Case 2b with foam and heavy layer trim configuration, 0-300 Hz.

At very low frequency, below 50 Hz, the low Young's modulus of the frequency dependent foam results in complete attenuation of the small resonances, while between 200 and 300 Hz, differences on the magnitude of 5 dB(A) are seen locally. However, despite the over 300% increase in Young's modulus, at higher frequency, the effect of frequency dependency is almost negligible.

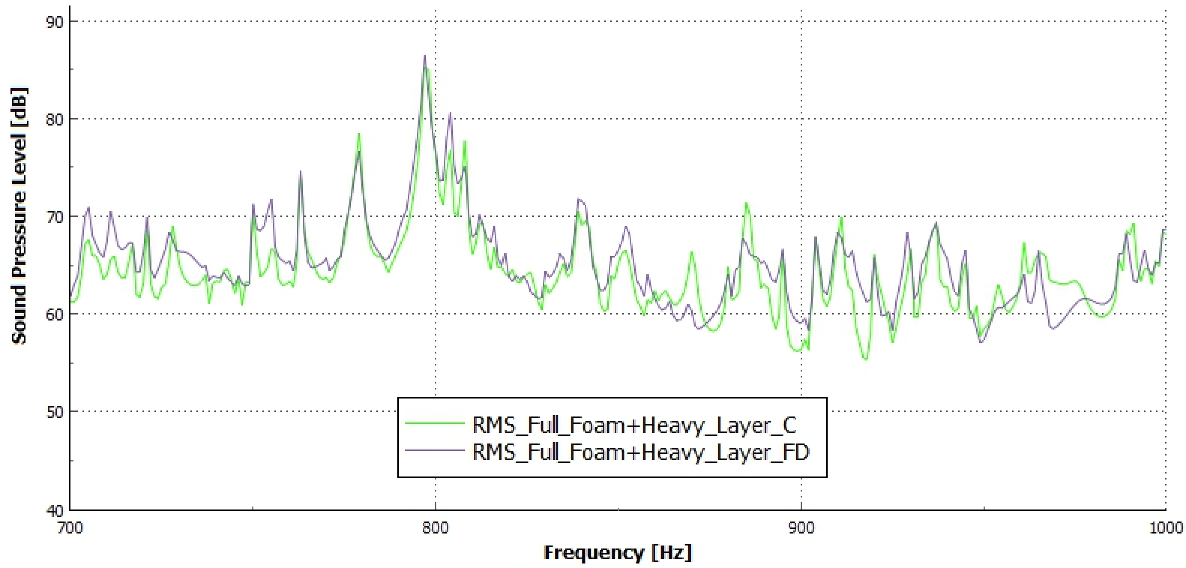

Figure 56.: Frequency dependent and constant results for Test Case 2b with foam and heavy layer trim configuration, 700-1000 Hz.

For more representative data, the previously described Foam 2 material was procured and custom made for experimental analysis. The arrangement within the cavity was the same as for Foam 1, and naturally the configuration in the simulation was the same as the measurement, which was described in Section 2. Sound pressure level RMS results were calculated for constant and frequency dependent parameters, and compared to measurement on Figure 57.

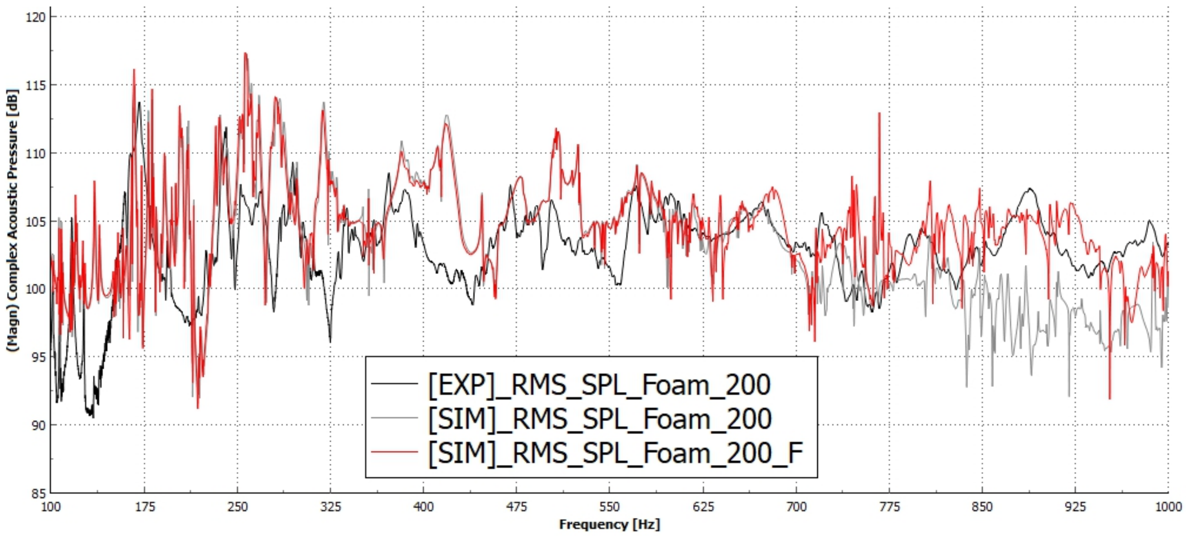

Figure 57.: RMS interior sound pressure levels in dB(A) for Test Case 2b in foam trim configuration. Figure shows measurement (black), simulation with constant (grey) and frequency dependent (red) parameters.

Measurements and simulation show large differences, especially above 500 Hz. The goal of applying frequency dependent parameters was to improve correlation between simulation and experiment. However, with the realistic, measurement-based Young's modulus and damping curves, it can be concluded that the correlation is not significantly improved for a complex acoustic case. While the frequency dependent parameter does impact the results, its effects are small and very localized compared to the difference between measurement and simulation.

Although Test Case 2b already indicated that with increasing structure and trim complexity, the effect of frequency dependent parameters is decreasing, it was still the ultimate goal to apply these parameters to a fully trimmed vehicle structure, so that their effect in a realistic vehicle model can be understood. To that extent, Test Case 3, a fully trimmed production vehicle model was used. The particular configuration omitted front seats and the HVAC system's detailed model behind the instrument panel, but otherwise was complete. Corresponding to the real vehicle, the FE-model of the bodywork consisted almost exclusively of 2D QUAD elements except for door hinges and certain small cast parts. Figure 58. shows the body-in-white without doors and trunklid.

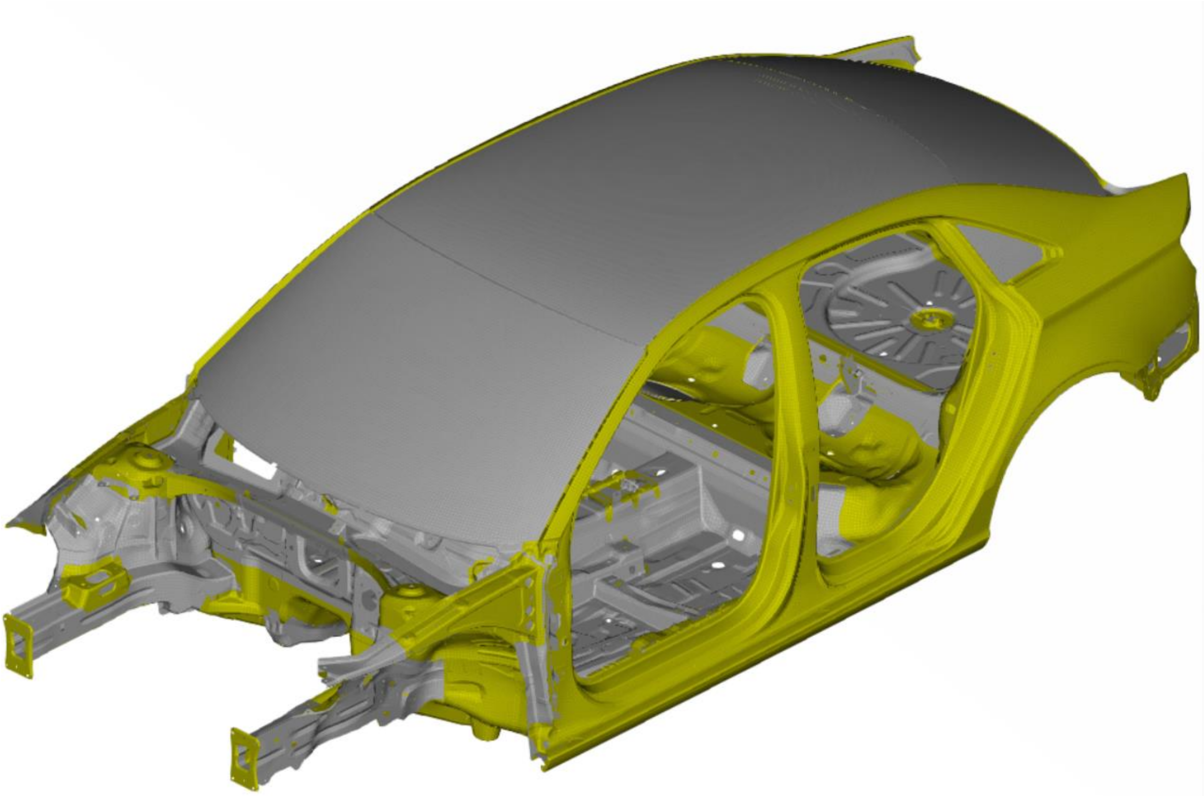

Figure 58.: Audi A3 Limousine body-in-white finite element model without doors and trunklid.

Trims and interior cavities were modelled using solid elements. Front hood and fenders were represented using point masses, the four doors and the trunklid were modelled explicitly. Glued or welded connections were realized using RBE3-HEXA-RBE3 representation. Total element count exceeded 700.000, with over 4 million degrees of freedom for the body in white, while trims were represented by over 3 million solid 3D TETRA elements. The fully meshed FE-model was provided by the industrial partner of the research. Figure 59. shows the finite element model of all parts classified as trim within the model.

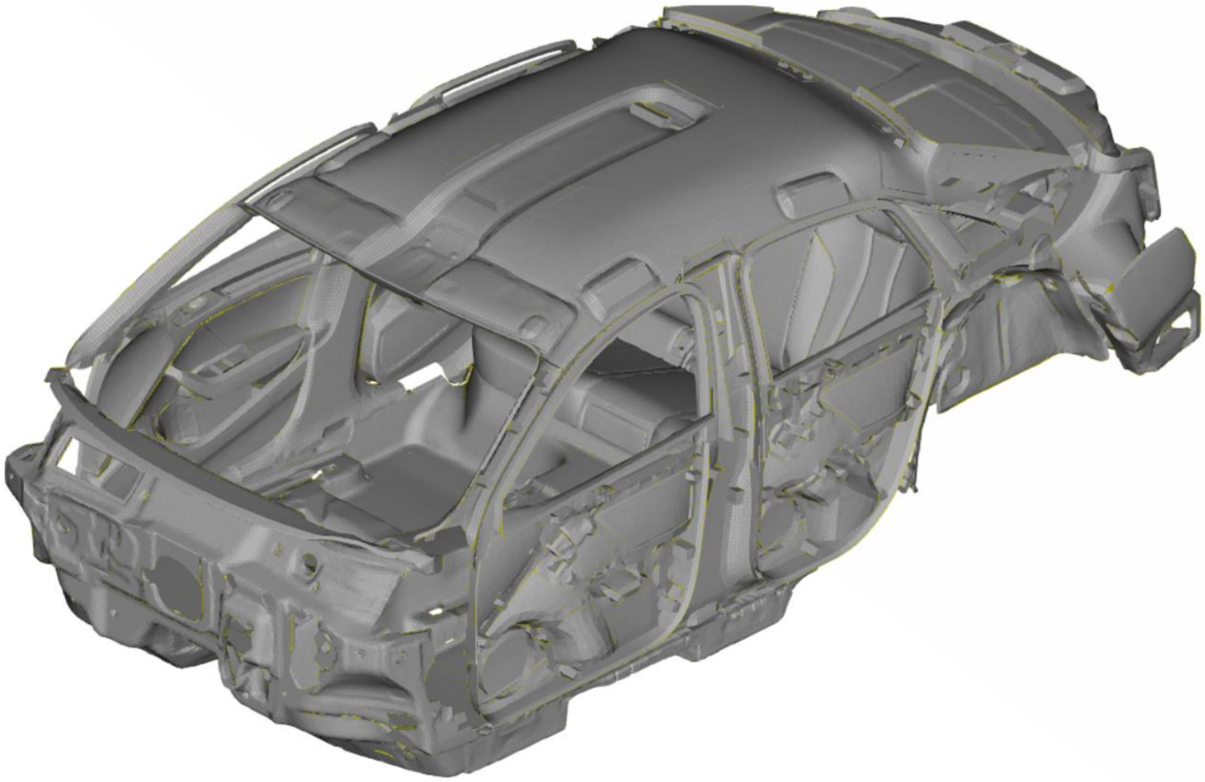

Figure 59.: Finite element model of all trim parts in the Audi A3 Limousine

A fundamental difference between Test Case 2b and Test Case 3 was the material complexity: in a full vehicle, beside foam trim and steel, a variety of materials can be found including glass, plastic interior parts as well as various foam- and heavy layer configurations. Unlike in Test Case 2, foams are rarely in direct contact with the interior air cavity, rather covered by a heavy layer or felt-like material. Furthermore, the geometry is also highly complex, with a variety of local enclosures (like front passenger- and driver footwells, trunk) and irregular surfaces. Therefore the relative surface covered by trim, as well as the ratio of trim mass to non-trim mass was much lower than in other cases. Frequency dependent damping and Young's modulus was applied to all foam parts of the interior. Table 6. contains trim parts, their constant Young's moduli and the element count, signifying their size within the vehicle. Frequency dependency in the simulation itself was considered using MATF material card, which referenced a table of frequencies and corresponding material property. This in turn was interpolated and the values used for trim impedance calculation.

Trim part	Frequency dependency	Element count	Constant E-modulus (MPa)
Firewall	YES	224049	0.044
Carpet	YES	206799	0.064
Rear seat bench	YES	239521	0.046
Rear seatback	YES	341662	0.046
Front door cards	YES	4820	8.9
Rear door cards	YES	5364	8.9
Headlining&pillars	YES	24187	0.030
Side trim	YES	29920	52
Trunk floor	NO		
Trunk side cover	YES	140432	0.046
Trunk cover	NO		
Wheelhouse cover	YES	9632	52
Loudspeaker cover	NO		
Parcel shelf	YES	12067	0.046

Table 6.: List of all trim materials for the given configuration, their frequency dependency, element count and Young's modulus. The trunk floor, trunk cover and the loudspeaker cover parts did not contain porous materials, so were not modified for frequency dependency.

The most significant trim parts with the largest surface area as well as element count were the firewall, the carpet, and the full rear seat. All frequency dependent parameters were defined so that the nominal value corresponded to the value at 500 Hz for the frequency dependent curve. A-weighted sound pressure level results in dB were evaluated as RMS results of all interior response points. Loadcases 1, 24 and 34 are shown on figures 60., 61. and 62.

respectively, comparing measurement and simulation results with constant and frequency dependent parameters.

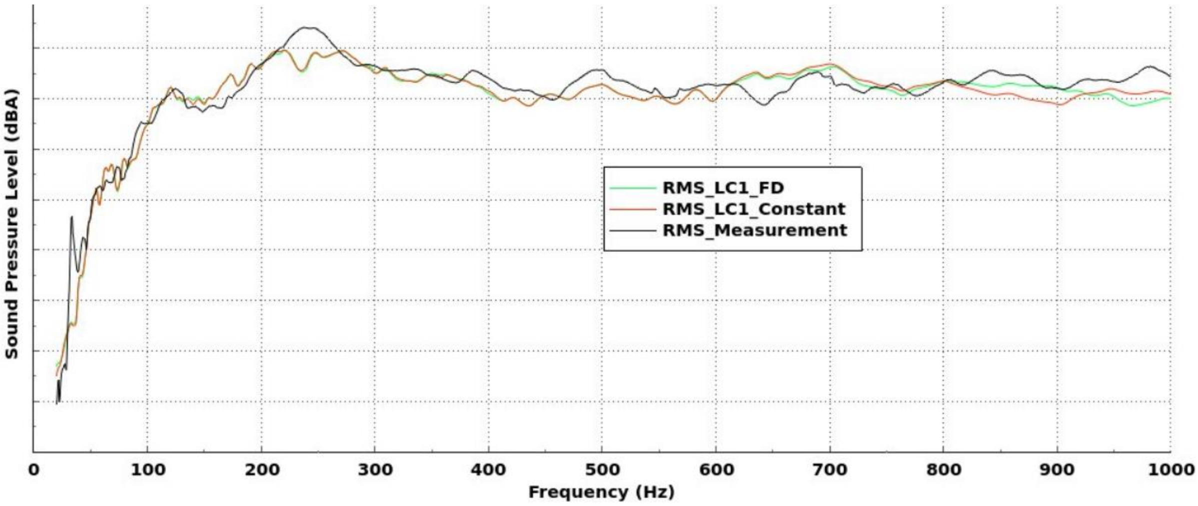

Figure 60.: Constant and frequency dependent sound pressure level results for Loadcase 1., showing negligible effect on the response.

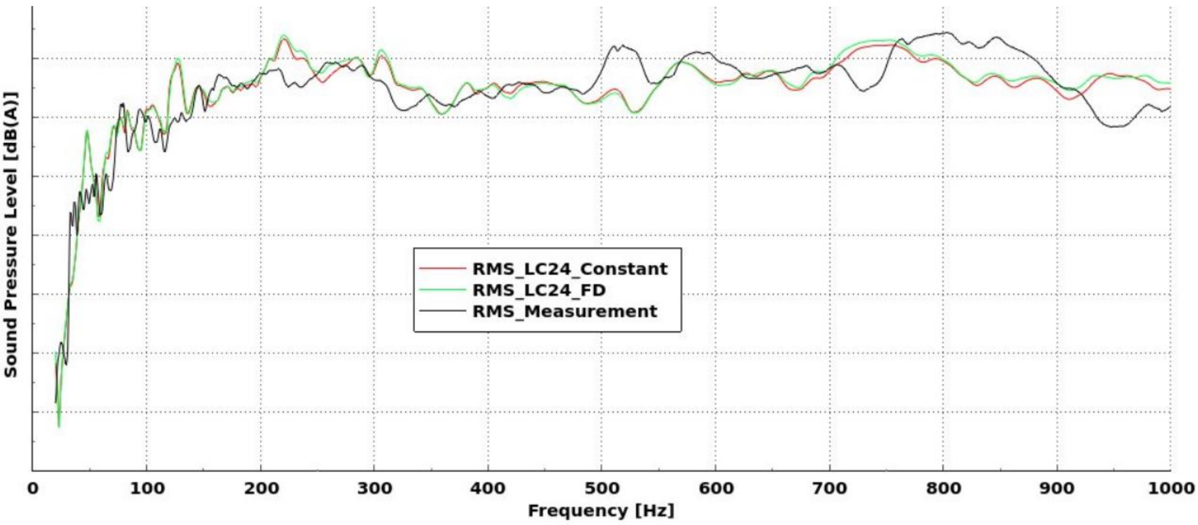

Figure 61.: Constant and frequency dependent sound pressure level results for Loadcase 24., showing negligible effect on the response.

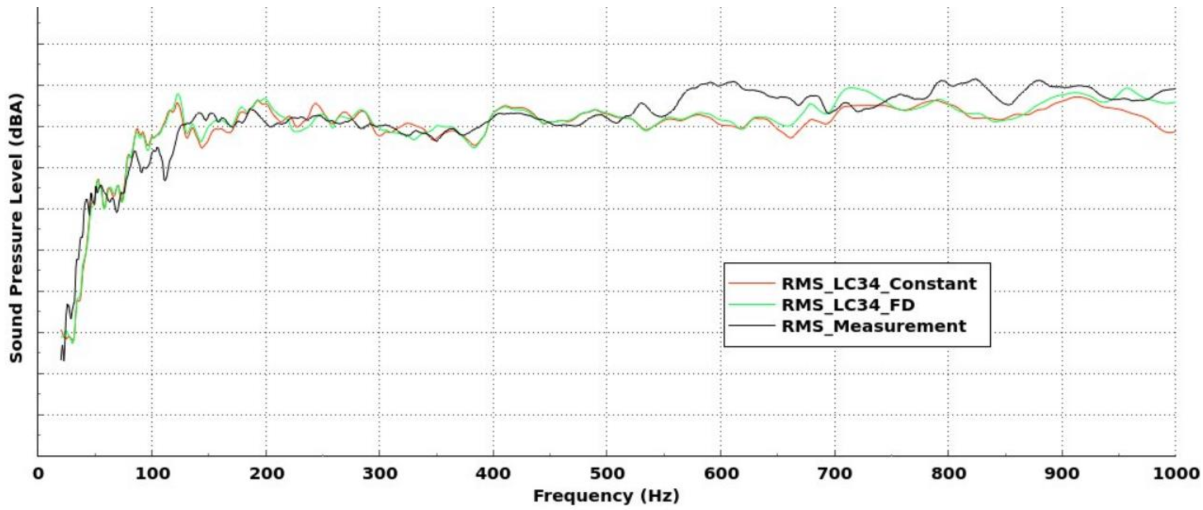

Figure 62.: Constant and frequency dependent sound pressure level results for Loadcase 34., showing negligible effect on the response.

Two conclusions can be drawn from the results:

1. In general, simulation results show relatively good agreement with the measurements up to 500 Hz.
2. Overall, the effect of frequency dependent parameters applied to foam trim parts in the overall vehicle did not have sufficient effect on the results to bridge the gap between simulation and measurement in the high frequency region. Except for the frequency range above 920 Hz to 1000 Hz for Loadcase 34, frequency dependency resulted in less than 2 dB(A) difference compared to constant parameters.

To summarize the findings of this chapter, a multi-scale computational campaign was conducted to examine the effects of applying frequency dependent damping and Young's modulus to trim materials on three different structures with increasing complexity. A flat plate, a vehicle-interior like model steel cavity and a full-scale vehicle in fully trimmed configuration were investigated. The purpose for the increasing complexity was to understand the effects of frequency dependency on various structures, with varying structure-trim ratios and decreasing level of abstraction from a practical industrial problem. Ultimate goal was to investigate if frequency dependent materials can improve the accuracy of an interior acoustic simulation for a whole vehicle case. Foam and foam + heavy layer configurations were investigated for the academic cases, while production configuration with various combinations of foam, heavy layer and felt were found in the full vehicle case.

While on the academic case of a flat plate fully covered with trim, the effect was promising, with increasing structure complexity and less relative trim area, the effect became less and less pronounced. In the whole vehicle, overall significantly less than 2 dB(A) difference could be observed between the constant and frequency dependent solutions, which was not sufficient to improve the accuracy of the prediction.

4.1.1. Thesis 2:

Frequency-dependent damping and/or Young's modulus of poro-elastic materials (PEM) can significantly affect the amplitude and resonance frequencies of the response of geometrically simplified pure foam trim-structures. This effect was observed to be in the order of 3-5 dB difference in amplitude and 10-40 Hz shift in frequency up to 1000 Hz for the academic test cases considered in this thesis. However, for a complex vibro-acoustic system, such as a trimmed body passenger vehicle structure consisting of multi-material trim elements including foam, heavy layer and felt elements, it has been proven that their combined effect on the response is below the audible threshold of sound pressure level difference [2 dB(A)].

5. Effects of material parameter tolerances

Comparisons with measurements for both Test Case 2b and Test Case 3 indicated a noticeable discrepancy between simulation and experiments. Some peaks that exist in measurements do not exist in simulations, and the overall levels are also not captured correctly. Discrepancies existed already at the body-in-white level, as shown on Figure 63.

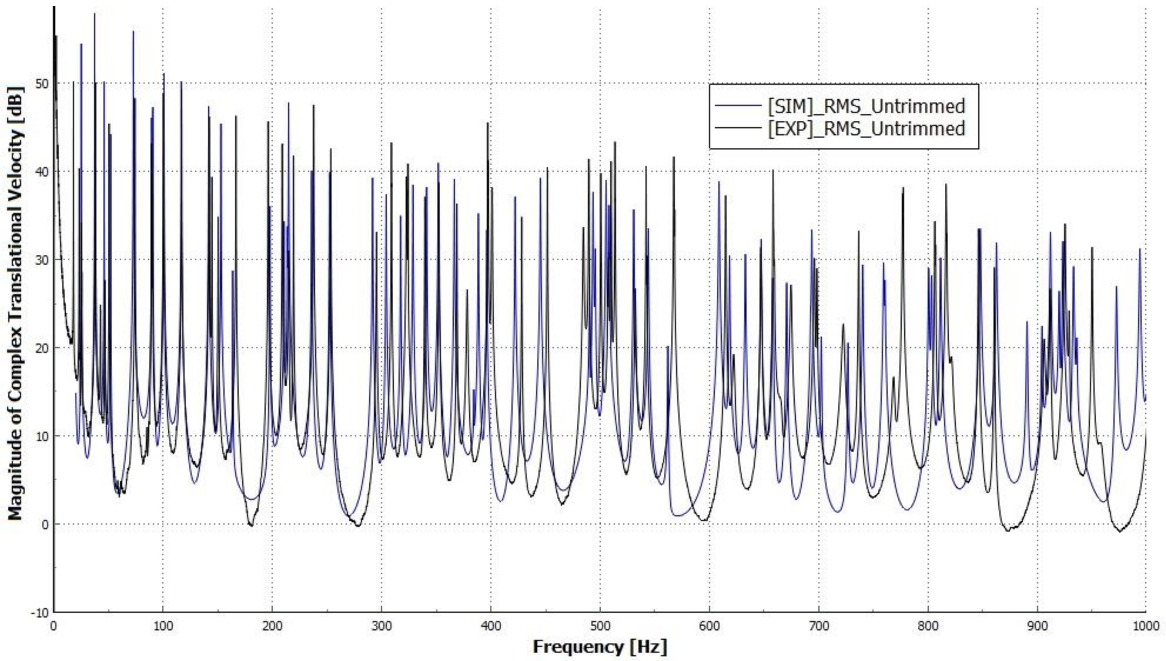

Figure 63.: Comparison of measurement (black) and simulation (blue) results for untrimmed Test Case 1. While agreement overall is good, at higher frequencies, discrepancies arise.

Such discrepancies may have several reasons: modal density can be too high at high frequencies, while at lower frequencies imperfections may exist in the measurement boundary conditions that introduce unexpected resonances. Both of these issues would result in localized, identifiable resonances with distinct peaks. However, discrepancies exist more generally along the frequency spectrum in the shown results. Therefore, another root cause had to be identified. It has also been established that frequency dependent parameters are unable to close this gap. A less considered, however, in mass production quite relevant effect can be attributed to manufacturing tolerances. As Schmid and Luegmar, as well as Scram et.al. have noted in literature, concentrating on the optimization of a finite element method for a single, nominal vehicle may lead to overconstraining the model (Luegmair and Schmid, 2020, Schmid and Luegmair, 2020, Scram et.al., 2022). Becoming perfectly tailored for a single application can result in even lower agreement across the range of manufactured vehicles. All parts and joining methods possess tolerances, which, added together, may result in significantly varied acoustic response. A variety of geometric and material properties, such as material thickness, material composition, inhomogeneity, geometric location and geometric accuracy all influence acoustic behavior. Currently, these tolerances are not directly included or considered significantly during acoustic design process – in other words, only the response of a nominal vehicle is optimized, without consideration for the statistical spread of mass production. A computational campaign was carried out to investigate the effect of these statistical values, specifically focusing on thickness tolerances. Modal frequency analysis was used to compute the results. Test cases 1, 2b and 3 were investigated.

After the initial simulations were conducted for the flat plate academic case, one direction to improve simulation accuracy was the application of frequency dependent parameters, detailed in Section 4. However, already the body-in-white results showed some discrepancy in the high frequency range. While flatness inaccuracy and replication of the free-free boundary condition in an experimental setting both could contribute to this, one of the most important input parameters, namely plate thickness was investigated. Thickness directly influences bending stiffness and thereby eigenfrequencies of the plate. Measurements of a set of 6 steel plates with nominal 2 mm thickness indicated a statistical spread of thickness, with a mean of 2.057 mm and standard deviation of 0.055 mm. 76% of samples was above nominal thickness. Plate thickness was recorded in 24 locations for each plate. Distribution of the measurement results is shown on Figure 64.

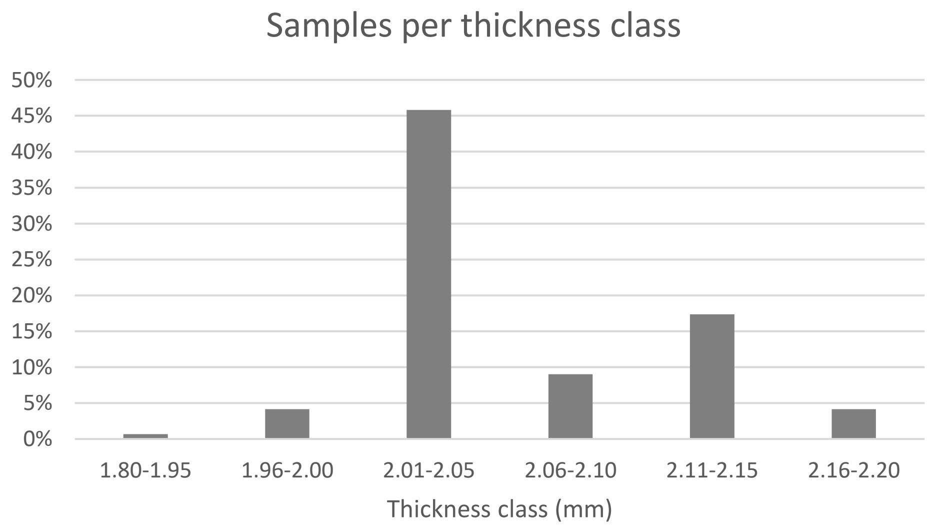

Figure 64.: Samples in thickness classes, based on measurements of 144 measurement points on 6 steel plates. 76% of samples lay above the nominal 2 mm thickness.

Despite the manufacturer specified 0.1 mm tolerance and a nominal thickness of 2 mm, the mean thickness of the plates was different. Some were beyond the specified tolerance level. Therefore a simulation was run with the increased thickness. Even though only a 5% deviation from the nominal value was applied, its effect was very significant, as shown on Figure 65. Peaks at high frequencies were shifted by as much as 50 Hz higher than their original values.

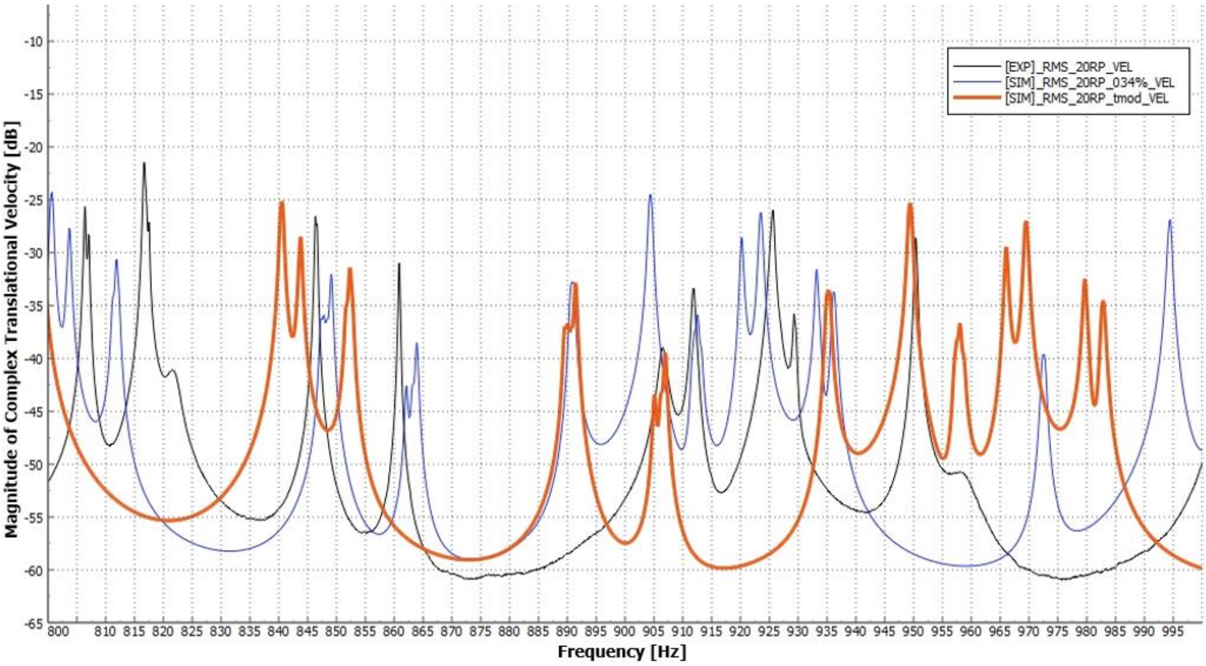

Figure 65.: Effect of 5% thickness increase between 800 and 1000 Hz (black: measured response, blue: baseline simulation, orange: increased thickness).

In the case of the currently investigated plate, it seems then that local imperfections in the thickness, e.g. small scratches or minimal unevenness in its thickness existed. These have contributed to frequency shifts of resonance peaks compared to the idealized simulation assuming a perfectly smooth plate with homogeneous nominal thickness.

Throughout the investigation of frequency-dependent parameters, it was evident that the effects did not transfer through the increasing complexity of test cases in the same magnitude. Effects on overall stiffness and local modal behavior are all expected, and especially in the case of a full vehicle, are not straightforward to predict. Although results for the flat plate seem trivial, they point out an improvement potential in the setup of FEM acoustic simulations. During metal forming processes, material thickness undergoes some deformation. As shown by these results, even a very small thickness variation causes significant modification of the response of a plate structure. Therefore it was vital to understand the effect small material thickness variations have on frequency responses of more complex structures.

Test Case 2b provided the next step of complexity for this campaign. As a riveted steel sheetmetal structure with bent sheetmetal stiffeners, it provided the complex interaction between parts of various stiffness. Furthermore, the structure had higher damping and stiffness, more closely replicating a production vehicle. A further advantage for this investigation in this apparatus was the very clear distinction between non-load-bearing and load-bearing elements. Boundaries of the interior air cavity were formed from 1 mm sheetmetal and retained a simple geometry bounded by flat surfaces. In contrast, the stiffeners had a bent U-shaped cross-section, as well as 2 mm thickness, and provided the overall support for the structure. Not only were they fastened to the cavity but also welded to one another at the contact surfaces. Therefore, in this analysis, effects of thickness tolerances were separately considered for the load-bearing and non-load-bearing parts. With the enclosed air volume, Test Case 2b enabled investigation of interior sound pressure levels, one of the most relevant metrics to a vehicle interior acoustic investigation. Trimmed and untrimmed variations were both investigated, to understand if structural manufacturing tolerances still play a role in the presence of an acoustic package. Evaluated response of interest was the RMS interior sound pressure level in the 6 previously used response locations.

Changes in thickness influenced the total weight of the examined structure in the simulations. Table 7. summarizes the resultant weight differences. Worst case scenarios were considered, so thickness was uniformly modified by 0.1 mm in each direction to represent extreme cases of tolerance.

Configuration	Wall thickness	Weight	Relative difference
Nominal	Nominal	91.33 kg	0 %
Cavity	1.1 mm	94.5 kg	+ 3.5 %
	0.9 mm	88.13 kg	- 3.5 %
Stiffener	2.1 mm	92.9 kg	+ 1.7 %
	1.9 mm	89.8 kg	- 1.7 %

Table 7.: Weight differences between simulated configurations

Although the 3.5 % relative maximum mass difference is an extreme outlier in a manufacturing environment, this academic case was still a proof of concept for whether such a variation would at all affect sound pressure levels. Further goal was to examine whether tolerances of the walls or of the stiffeners have a more pronounced effect. Results computed for variations in cavity sheetmetal thickness and skeleton thickness were plotted separately, and compared with nominal results both for body-in-white (Figures 66-67.) and trimmed (Figures 68-69.) configurations.

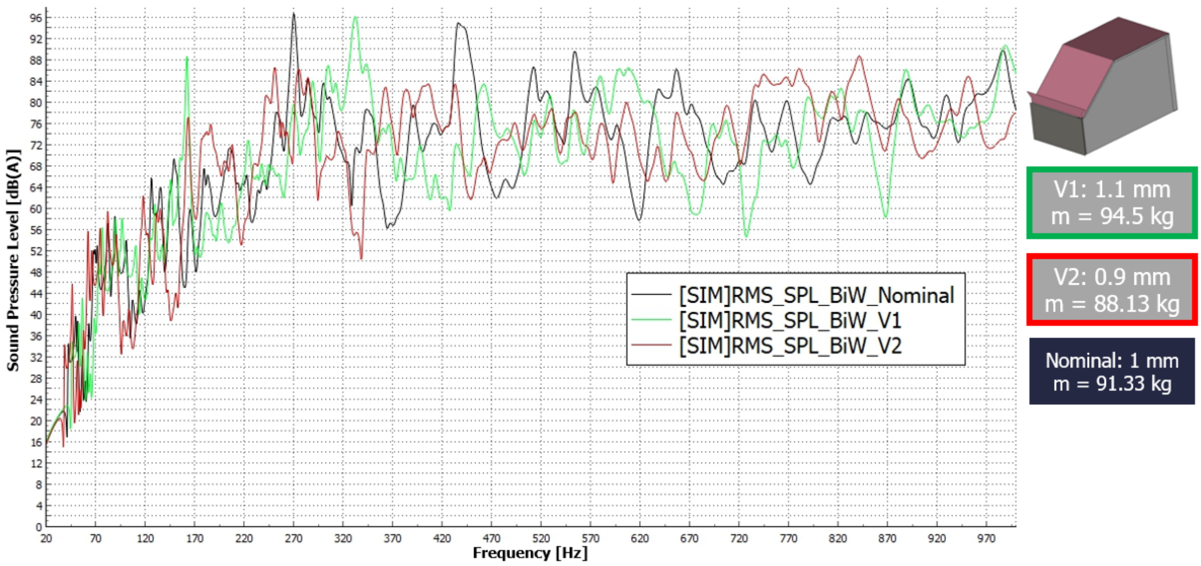

Figure 66.: RMS-averaged sound pressure levels for body-in-white configuration with consideration of manufacturing tolerance extremes on cavity walls.

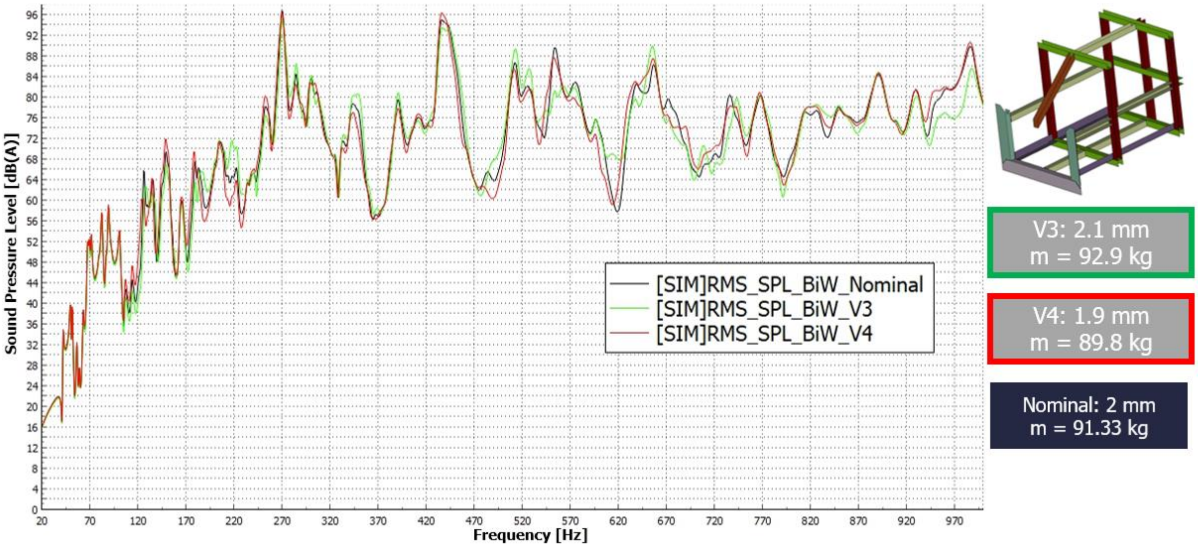

Figure 67.: RMS-averaged sound pressure levels for body-in-white configuration with consideration of manufacturing tolerance extremes on skeleton structure.

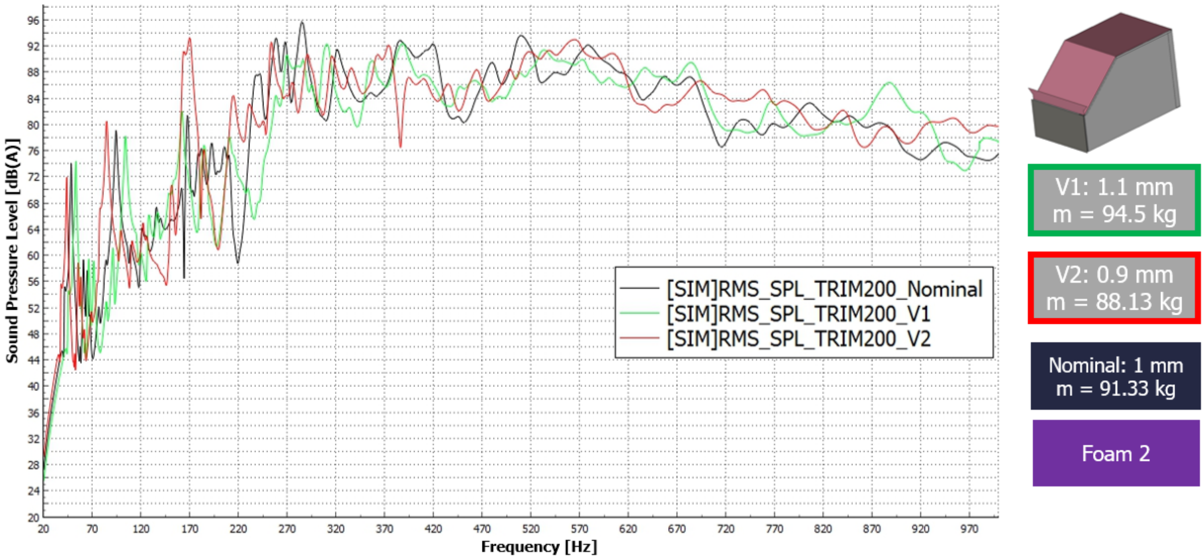

Figure 68.: RMS-averaged sound pressure levels for trimmed body configuration with consideration of manufacturing tolerance extremes on cavity walls.

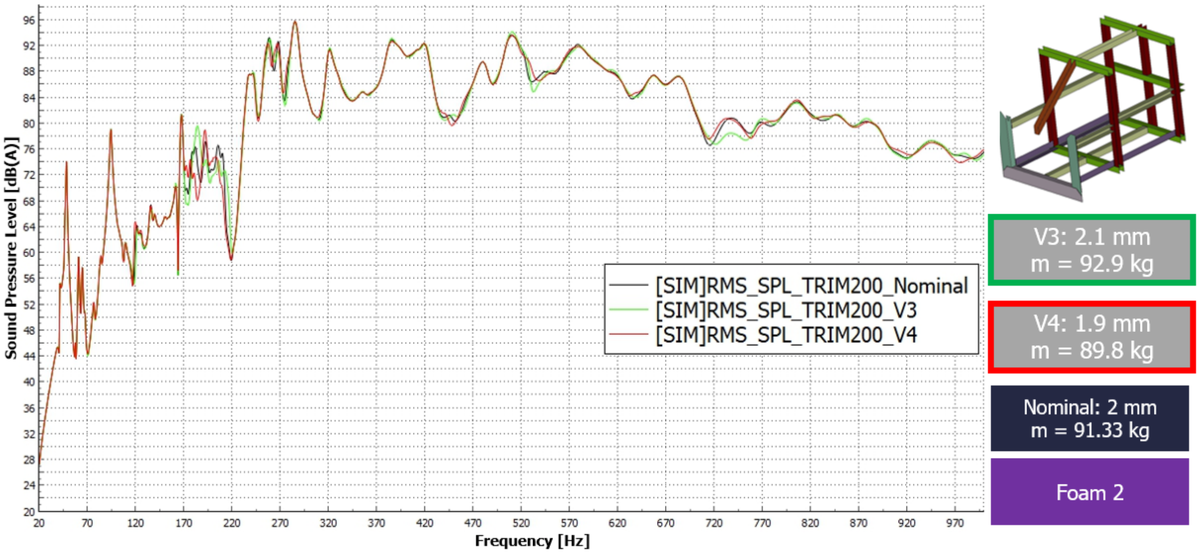

Figure 69.: RMS-averaged sound pressure levels for trimmed configuration with consideration of manufacturing tolerance extremes on skeleton structure.

Simulation results overwhelmingly indicate that in a structure with clearly distinguishable body and skeleton, tolerances of the body influence interior sound pressure levels significantly more than that of the skeleton. This is attributed in part to the higher mass difference, as well as the larger reflective surface into the cavity volume. Especially in the trimmed configuration, variations in skeleton thickness have almost negligible impact on results, influencing SPL by less than 1 dB at most frequencies. In stark contrast, effects of cavity wall tolerance are much more pronounced, fundamentally altering the response. In certain locations, up to 6 dB difference can be observed, overall resonant peaks are moved in the spectrum with significantly altered peaks. This stark effect furthered the investigation into applying similar logic to Test Case 3, a full scale car.

Modern passenger vehicles are almost exclusively constructed in a unibody philosophy, with no easily separable load bearing structure. Therefore such a clean consideration of load-bearing and non-load-bearing elements, as for Test Case 2b, is not as clear to define. However, monocoque constructions still use external body panels for cosmetic purposes, and formed structures primarily optimized for load carrying and overall stiffness. For optimal material use, such modern structures employ a variety of sheetmetal thicknesses for the large amount of individually formed parts that are finally welded or joined together to form the vehicle structure. As these ranged from 0.6 mm up to 5 mm, the classification in Table 8. was used for the appropriate materials (V and F Co. UK, 2023).

Thickness (mm)	Tolerance (mm)
0.6 - 0.79	0.05
0.8 - 0.99	0.06
1.0 - 1.19	0.07
1.2 - 1.49	0.08
1.5 - 1.99	0.09
2.0 - 2.49	0.1
2.5 - 2.99	0.12
3.0 <	0.14

Table 8.: Tolerance classes applied to parts corresponding to part thicknesses on Test Case 3.

To preserve the sensitivity study, parts of the monocoque body were classified as cosmetic and load-bearing following the analogy described in the previous section. Of the more than 350 different parts of the bodywork, 24 were classified as cosmetic – referred simply to as skin, and 287 were classified as load-bearing – referred to as skeleton. The goal was to estimate, whether the previously observed trend of dominant effects from non-load-bearing parts prevails on such a complex case as well. As this was a quantitative classification, Figures 70. and 71. illustrate how the final division of the bodywork resulted in the two part groups that were separately analysed for tolerance sensitivity.

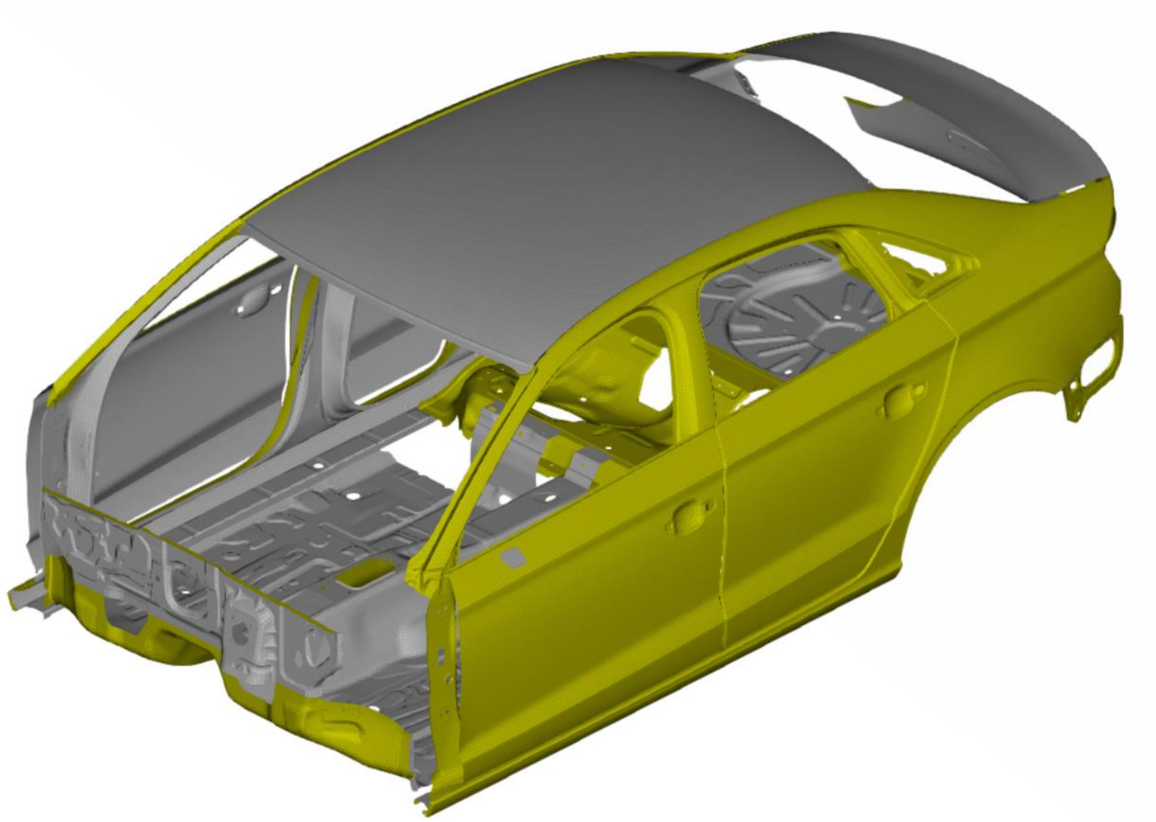

Figure 70.: Parts of the Audi A3 Limousine bodywork included in the skin part group.

Of the total body-in-white bodywork weight, 22% by weight was included in the skin- and 55% in the skeleton group. Weight change compared to the nominal trimmed body total weight was 4.6% for skin part tolerances, while 5.6% for skeleton parts. Thicknesses were modified within the input files, and simulations were separately run for the extreme cases at each end of the tolerance spectrum. Once again, only the extreme cases were simulated, to establish sensitivity. Approximate simulation run time was ~120 hours.

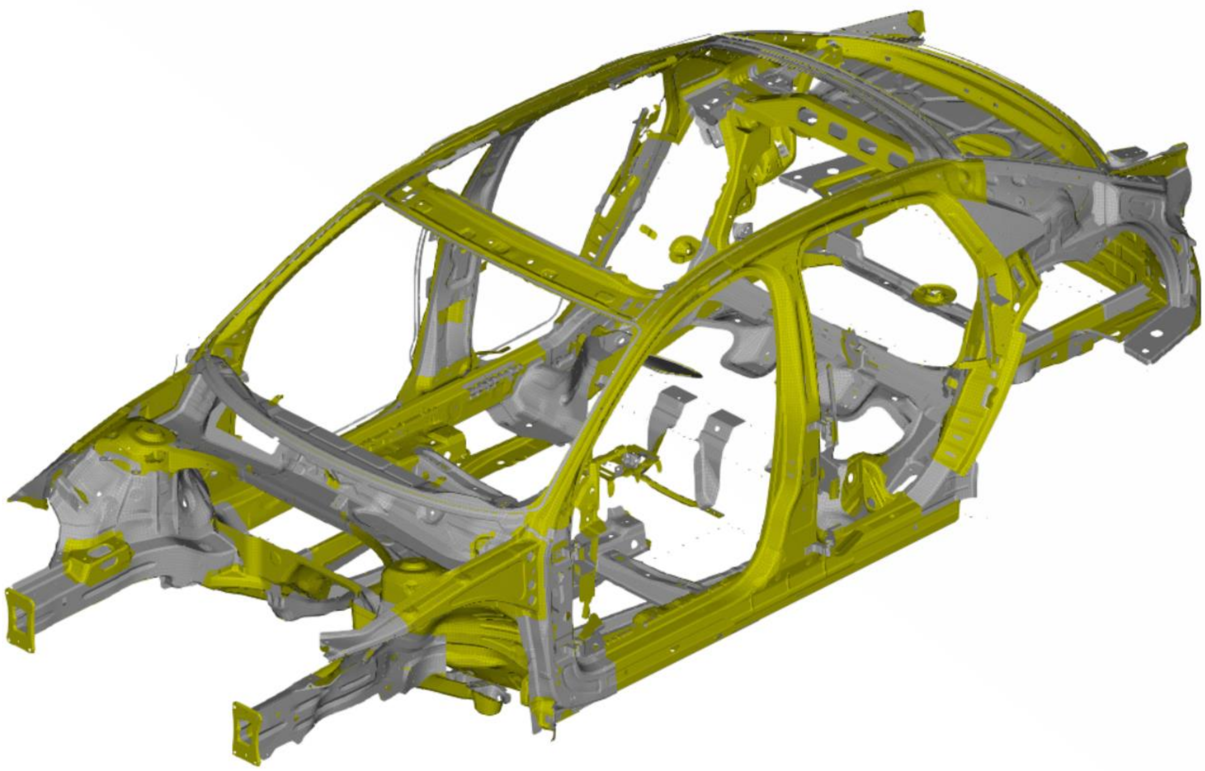

Figure 71.: Parts of the Audi A3 Limousine bodywork included in the skeleton part group.

Sound Pressure Level results were examined for each load case as RMS of all response points. Each graph below on Figures 72-77. shows comparisons of extreme cases for both skeleton and skin tolerances for each load case. All results shown are simulation results. On all graphs, the color legend explained in Table 9. was used:

Result curve	Color
Constant	
Skin upper tolerance limit (Skin+)	
Skin lower tolerance limit (Skin-)	
Skeleton upper tolerance limit (Skeleton+)	
Skeleton lower tolerance limit (Skeleton-)	

Table 9.: Color legend for result graphs

Loadcase 1:

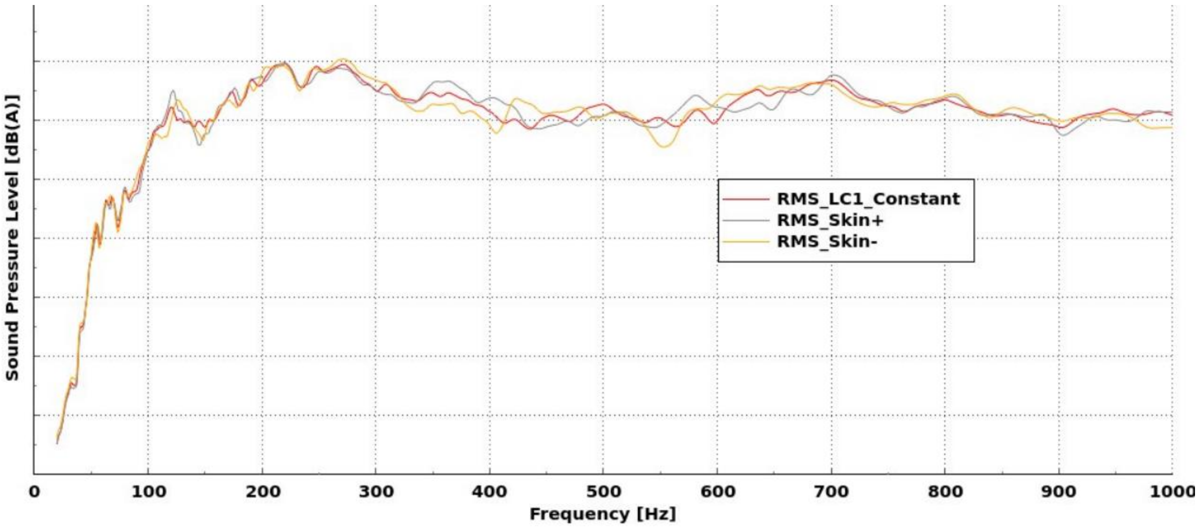

Figure 72.: RMS Sound Pressure Levels in dB(A) for skin tolerance extreme cases and nominal vehicle body.

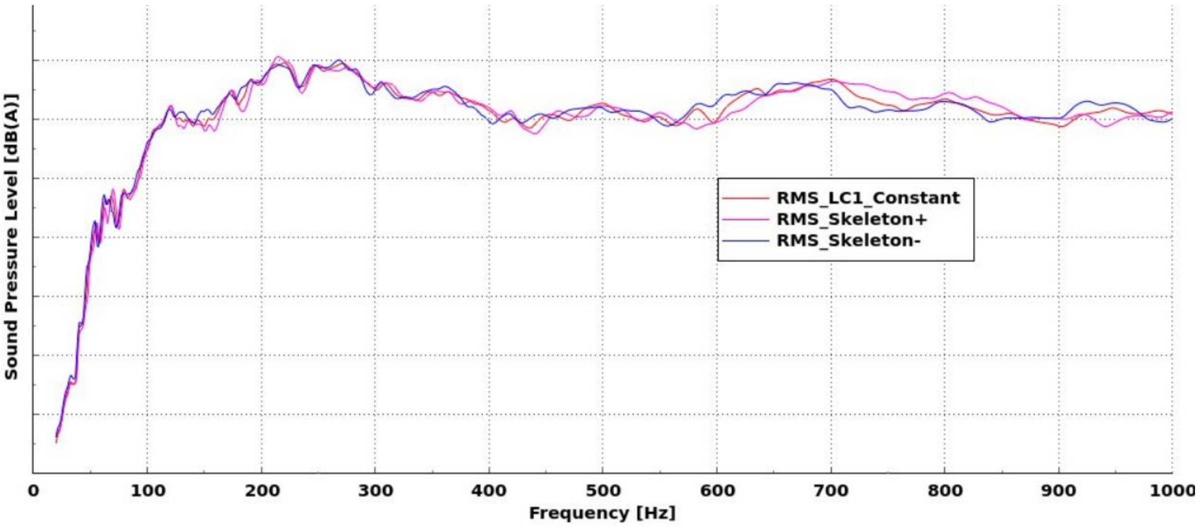

Figure 73.: RMS Sound Pressure Levels in dB(A) for skeleton tolerance extreme cases and nominal vehicle body.

Loadcase 24:

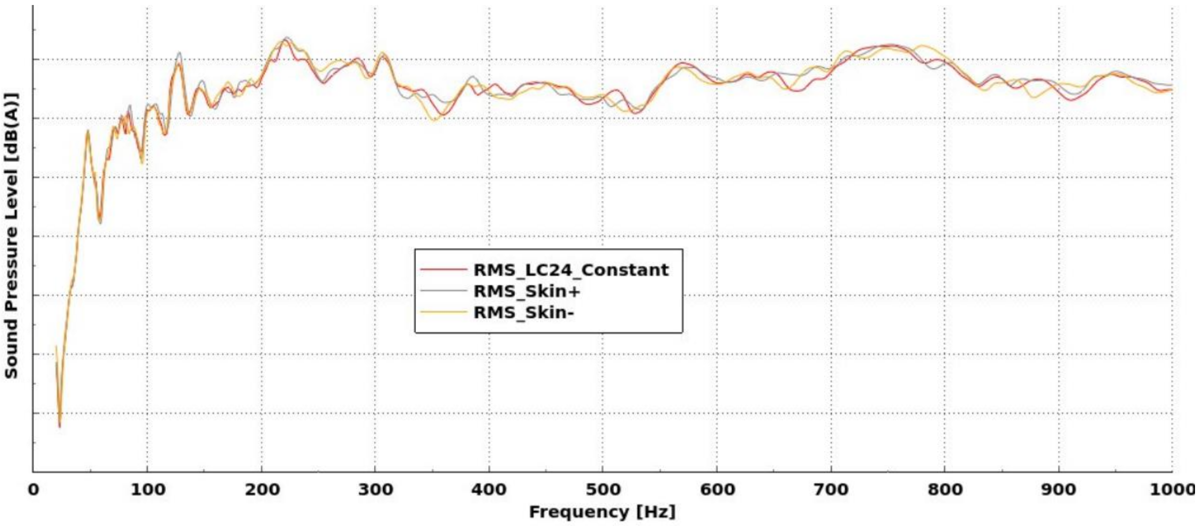

Figure 74.: RMS Sound Pressure Levels in dB(A) for skin tolerance extreme cases and nominal vehicle body.

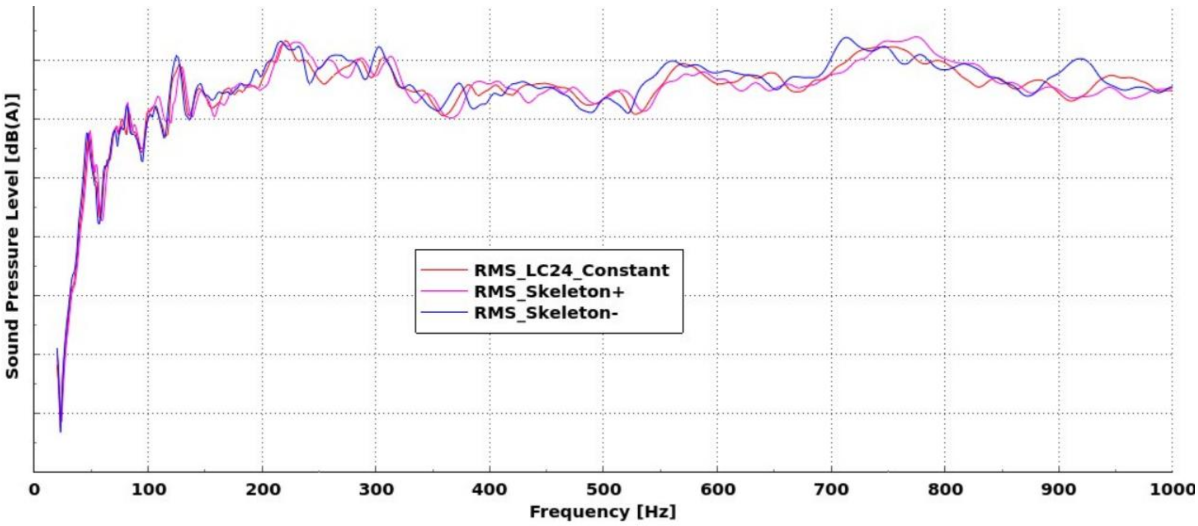

Figure 75.: RMS Sound Pressure Levels in dB(A) for skeleton tolerance extreme cases and nominal vehicle body.

Loadcase 34:

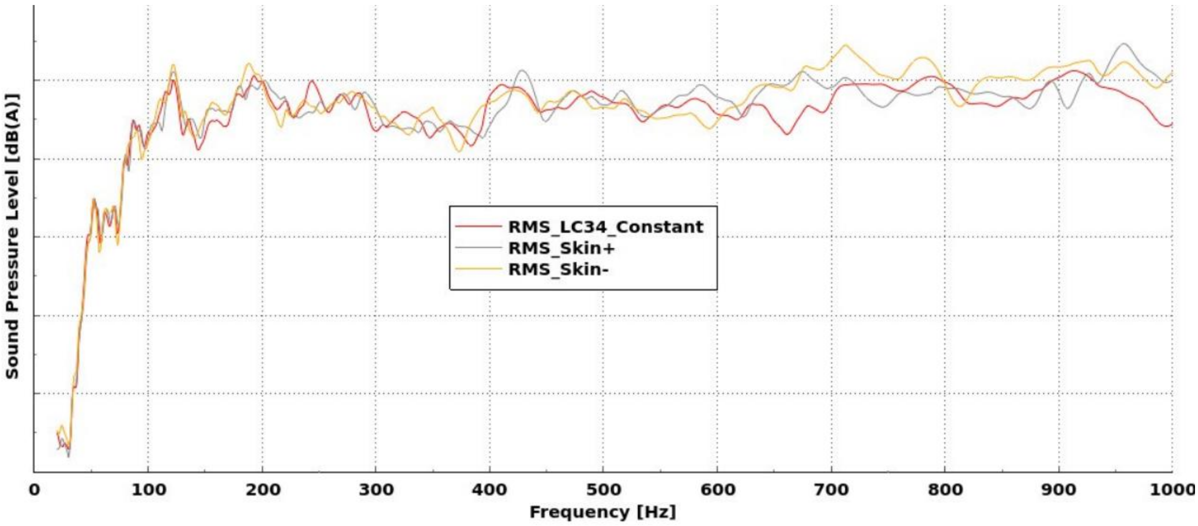

Figure 76.: RMS Sound Pressure Levels in dB(A) for skin tolerance extreme cases and nominal vehicle body.

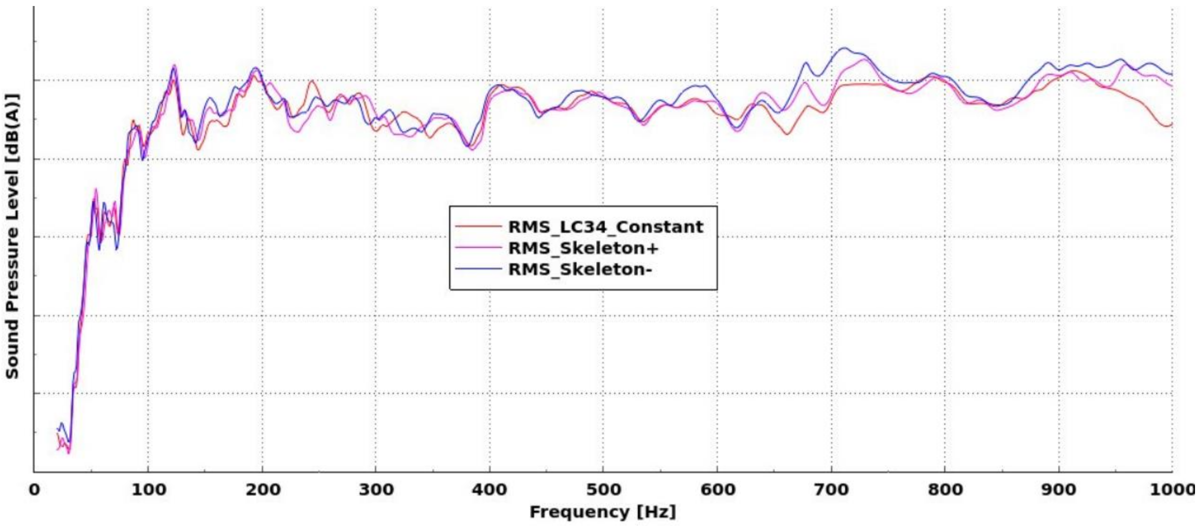

Figure 77.: RMS Sound Pressure Levels in dB(A) for skeleton tolerance extreme cases and nominal vehicle body.

While results for the full vehicle do not show as clear a trend as for Test Case 2b, conclusions can still be drawn. Since monocoque constructions do not have as clearly divisible skin and skeleton parts as the metal cavity did, it would be difficult to argue that one or the other is more sensitive to tolerances. While some differences exist between load cases – Loadcase 24 seems more sensitive to tolerances of skeleton parts, while skin tolerances have a more pronounced effect for Loadcase 34 – a generalized statement regarding tolerance sensitivity cannot be made. What is clear, and shows a significant difference to the behavior seen on Test Case 2b is that the effect of tolerances is negligible below 400 Hz. This means that manufacturing uncertainties can be one of the significant reasons for the discrepancy between simulation and measurement in the mid-frequency range.

To summarize the findings of this chapter, a simulation campaign was carried out to investigate whether thickness variations on the magnitude of manufacturing tolerances influence acoustic responses of primarily sheetmetal structures. Initial investigations carried out on a flat plate sample indicated that structures with low damping are particularly sensitive to small (<5%) variations of thickness. As mainstream vehicle structures currently almost exclusively employ formed sheetmetal structures, the implications of this initial finding were investigated on Test Cases 2b and Test Case 3 as well. As Test Case 2b was clearly divided into a load-bearing skeleton consisting of thicker and stiffer elements and a cosmetic interior cavity with large flat surfaces, sensitivities of each of these parts to a nominal 0.1 mm thickness variation was simulated in both trimmed and untrimmed configurations. Results of RMS aggregate interior sound pressure levels indicated that tolerances of the cosmetic (skin) parts had a very pronounced effect on the response, while the skeleton's tolerances – especially in trimmed configuration – had negligible effect on the response. Despite current vehicle monocoque structures not having such a clear division between load-carrying and non-load-carrying parts, a quantitative divison was still made, as exterior panels generally are thin parts with large surface area and low damping, as opposed to structural elements like A-, B- and C-pillars. However, the observed behavior on Test Case 2b did not transfer to the full vehicle case: there was no clear indication that skin or skeleton parts would be particularly more sensitive to manufacturing tolerances. What the results did indicate, however, is that on a fully trimmed vehicle structure, sheetmetal thickness manufacturing tolerances do have an impact on the responses in the 400 – 1000 Hz mid-frequency region.

5.1.1. Thesis 3.:

In a mass production environment, the thicknesses of sheet metal components exhibit a statistical deviation from the nominal thickness values. It has been found, that this may have the following effects on the acoustic response in simulations:

a) *For structures with clearly separable load carrying elements (beams, stiffeners, frame, etc.) and non-load carrying panels made of sheetmetal, the deviations from the nominal thickness of the non-load caryying panels may significantly influence the SPL response* *in the interior volume enclosed by the structure. This effect was observable for the full frequency range up to 1000 Hz.*

b) *For vehicle-like structures, where the load carrying elements (beams, stiffeners, frame, etc.) and non-load carrying panels made of sheetmetal are not clearly separable due tot he monocoque nature of the structure. the deviations from the nominal thickness had a significant impact on the interior SPL frequency response only above 400 Hz. This may contribute to the uncertainty of mid-frequency range FEM-PEM simulations.*

6. Conclusion and outlook

As the literature review has shown, a major challenge for acoustic FEM-based simulations of vehicles is the deviation between experimental and simulation results in the mid-frequency (400-1000 Hz) range. Thus, the overall goal of the research presented in this Dissertation was to develop methods improving the accuracy of vehicle acoustic simulations specifically in the mid-frequency range.

It was hypothesized, that in a multi-level complexity simulation methodology campaign using FEM-PEM approach, the effects of frequency-dependent damping and Young's modulus as well as the sensitivity to sheetmetal thickness tolerances needs to be evaluated. However, in order to enable the thorough investigation these phenomena, the need for an intermediate level test apparatus – in between complexity of the highly academic flat plate case and the full complexity whole vehicle - was required. This prompted the design of a scaled model vehicle interior cavity, whose volume was chosen to be suitable not only for FEM-PEM but also for statistical method validation as well. To further the applicability of the apparatus, it was conceptualized and realized as a twin apparatus, with one version manufactured with concrete walls for simplified boundary conditions while another took the form of a bent and riveted sheetmetal structure to replicate the behavior of a vehicle body on a small scale.

Next, the frequency dependent material parameters were applied not only for the academic cases of a flat plate and a model vehicle interior cavity with acoustically participating walls, but also for a fully trimmed full-scale production vehicle, a 2015 Audi A3 Limousine. It was found that although frequency dependency of damping and Young's modulus of foam trims has a significant impact in academic cases with low damping and comparatively high amount of trim application, in a production vehicle, these effects become negligible and are unable to bridge the gap between experimental results and simulations.

To attempt to remedy this discrepancy, sensitivity of acoustic responses to material thickness tolerances was examined. Showing significant – up to 50 Hz – shifts in resonance frequencies for the academic case, extreme cases of positive and negative tolerance models were found to be sensitive to this parameter, with up to 5 dB differences between cases even for the fully trimmed, most complex vehicle model. A further finding of the study was that for structures with clearly divisible load-carrying and non-load-carrying parts, tolerances of the non-load-carrying cosmetic parts are decisive factors in acoustic response. This shows great promise in the further development of acoustic methodology for vehicles in mass production. A statistical application of these tolerances based on production data could reveal the true spread in a mass produced vehicle and provide a better estimate of its true acoustic performance. The particular challenge to overcome is the high computational effort of each version requiring a full FEM-PEM simulation run including modal base calculation for the structure. Naturally, beside sheetmetal thickness, a host of other tolerances like geometric accuracy, spotweld location and size, etc. may play a role, to which the sensitivity of a vehicle structure is yet to be identified, further expanding the list of open question in the field.

7. References

[1] Allard, J.F. and Atalla, N.: Propagation of Sound in Porous Media, John Wiley & Sons Ltd. 2009. ISBN 978-0-470-746615-0

[2] Atalla, Noureddine, et al. “Enhanced Weak Integral Formulation for the Mixed (u_,p_) Poroelastic Equations.” The Journal of the Acoustical Society of America, vol. 109, no. 6, 2001, pp. 3065–3068., doi:10.1121/1.1365423.

[3] Atalla, Noureddine, et al. “On the Modeling of Sound Radiation from Poroelastic Materials.” *The Journal of the Acoustical Society of America*, vol. 120, no. 4, 2006 doi:10.1121/1.2261244.

[4] Audi Media Center, „Lightweight Construction”, Web.: https://www.audi-mediacenter.com/en/leightweight-construction-246, accessed on: 28th of February, 2023

[5] Audi Media Center, „Sharpened design and innovative technologies for the flagship: the enhanced Audi A8”, Web.: https://www.audi-mediacenter.com/en/press-releases/sharpened-design-and-innovative-technologies-for-the-flagship-the-enhanced-audi-a8-14358, accessed on: 28th of February, 2023

[6] Berardi, Umberto, Ginno Iannace, and Maria Di Gabriele. "Challenges and Solutions in Acoustical Measurements and Design: Paper ICA2016-238 Characterization of Sheep Wool Pane." Characterization of Sheep Wool Panels for Room Acoustic Applications. Proc. of 22nd International Congress on Acoustics, Buenos Aires. Buenos Aires: ICA, 2016.

[7] Bergen, B., Schaefer, N., Van de Rostyne, K., and Keppens, T., “Vehicle Acoustic Performance Analysis towards Effective Sound Package Design in Mid-Frequency,” SAE Technical Paper 2018-01-1495, 2018, doi:10.4271/2018-01-1495.

[8] Biot, M. A. “Theory of Propagation of Elastic Waves in a Fluid-Saturated Porous Solid. I. Low-Frequency Range.” *The Journal of the Acoustical Society of America*, vol. 28, no. 2, 1956, pp. 168–178., doi:10.1121/1.1908239.

[9] Biot, M. A. “Theory of Propagation of Elastic Waves in a Fluid-Saturated Porous Solid. II. Higher Frequency Range.” *The Journal of the Acoustical Society of America*, vol. 28, no. 2, 1956, pp. 179–191., doi:10.1121/1.1908241.

[10] Bonfiglio, P., Pompoli, F., „Frequency-dependent mechanical modelling of poro-elastic materials for sound transmission loss simulations", Journal of Noise Control Engineering, 64, 5(2016), 627 – 633

[11] Burlayenko, V., Altenbach, H., & Sadowski, T. (2015). An evaluation of displacement-based finite element models used for free vibration analysis of homogeneous and composite plates. *Journal of Sound and Vibration, 358*, 152-175. doi:10.1016/j.jsv.2015.08.010

[12] Buy-a-car UK, „Audi A3 Saloon (2013-2020)", Web.: https://www.buyacar.co.uk/audi/a3/a3-saloon/1430/audi-a3-saloon-2013-2020, accessed on: 28th of February, 2023

[13] Champoux, Yvan, and Jean-F. Allard. "Dynamic Tortuosity and Bulk Modulus in Air-Saturated Porous Media." *Journal of Applied Physics*, vol. 70, no. 4, 1991, pp. 1975–1979., doi:10.1063/1.349482.

[14] Chen, S., Wang, D., Zuo, A., Chen, Z., Zan, J., Sun, Y., "Design and optimization of vehicle interior sound package," 2010 International Conference On Computer Design and Applications, Qinhuangdao, China, 2010, pp. V4-30-V4-34, doi:10.1109/ICCDA.2010.5541504.

[15] Cram, S., Luegmair, M., Schmid, J.D., Marburg, S. " Sensitivity Analysis of NVH Simulations with Stochastic Input Parameters for a Car Body" SAE Technical Paper 2022-01-0951, 2022, https://doi.org/10.4271/2022-01-0951

[16] Dandaroy, I., Hartley, D., Hund, R., "Interior Noise Prediction Of Hawker Horizon Aircraft Using Statistical Energy Analysis", Noise-Con 04. The 2004 National Conference on Noise Control Engineering

[17] Deckers, E., et al. "Modelling Techniques for Vibro-Acoustic Dynamics of Poroelastic Materials." Archives of Computational Methods in Engineering, vol. 22, no. 2, 2014, pp. 183–236., doi:10.1007/s11831-014-9121-0.

[18] Dejaeger, L., Rondeau, J-F., Chanudet, P., Auffray, B. „Transmission Loss trim FEM simulation of lightweight automotive dashboard insulators with consideration of the

instrument panel”. Société Française d’Acoustique. Acoustics 2012, Apr 2012, Nantes, France. 2012.

[19] Dowell, E. H., & Voss, H. M. (1963). The Effect Of A Cavity On Panel Vibration. *AIAA Journal, 1*(2), 476-477. doi:10.2514/3.1568

[20] Duval, A., Rondeau, J-F., Lhuillier, F., Deshayes, G., Dejaeger, L., “VEHICLE ACOUSTIC SYNTHESIS METHOD: A Hybrid Approach to Simulate Interior Noise of Fully Trimmed Vehicles.” Congrès SIA Confort Automobile Et Ferroviaire 2004, Nov. 2004.

[21] Duvigneau, F., Spannan, L., Lloret, M., Woschke, E., Gabbert, U., „Characterization of the frequency-dependent properties of damping materials”, Proceedings in Applied Mathematics and Mechanics, 18 (2018)

[22] Ege, K., Henry, V., Leclere, Q., Rinaldi, R.G., Sandier, C., “Vibrational behavior of multilayer plates in broad-band frequency range: comparisons between experimental and theoretical estimations”, InterNoise 2015, Aug 2015, San Francisco, United States. pp.218. ffhal-01215310f

[23] Eshmatov, B. (2007). Nonlinear vibrations and dynamic stability of viscoelastic orthotropic rectangular plates. *Journal of Sound and Vibration, 300*(3-5), 709-726. doi:10.1016/j.jsv.2006.08.024

[24] Farag, N. H., & Pan, J. (1998). On the free and forced vibration of single and coupled rectangular plates. *The Journal of the Acoustical Society of America*, *104*(1), 204-216. doi:10.1121/1.423270.

[25] Forssén, J., Tober, S., Corakci, A.C., Frid, A., Kropp, W., „Modelling the interior sound field of a railway vehicle using statistical energy analysis”, Applied Acoustics, 73, 4 (2012), 307-311

[26] Göransson, Peter. “A 3-D, Symmetric, Finite Element Formulation of the Biot Equations with Application to Acoustic Wave Propagation through an Elastic Porous Medium.” International Journal for Numerical Methods in Engineering, vol. 41, no. 1, 1998, pp. 167–192. doi:10.1002/(sici)1097-0207(19980115)41:1<167::aid-nme285>3.0.co;2-t.

[27] Graham, W.R.; „Boundary Layer Induced Noise in Aircraft, Part I: the Flat Plate Model”, Journal of Sound and Vibration, 192, 1 (1996.), 101-120. https://www.sciencedirect.com/science/article/abs/pii/S0022460X96901789

[28] Graham, W.R.; „Boundary Layer Induced Noise in Aircraft, Part II: the Trimmed Flat Plate Model”, Journal of Sound and Vibration, 192, 1 (1996.), 121-138.

[29] Guellec, A., Cabrol, M., Jacqmot, J., and Van den Nieuwenhof, B., “Optimization of Trim Component and Reduction of the Road Noise Transmission Based on Finite Element Methods,” SAE Technical Paper 2018-01-1547, 2018 doi:10.4271/2018-01-1547.

[30] Hamdi, M. A, et al. “An Efficient Finite Element Formulation for the Analysis of Acoustic and Elastic Waves Propagation in Sound Packages.” *SAE Transactions*, vol. 110, 2001, pp. 1481–1488. *JSTOR*, www.jstor.org/stable/44731003.

[31] Hamdi, M. A., et al. “Integration of Acoustic Absorbing Porous Components in Vehicle Environment Using a Novel Finite Element Solver.” *Journal of the Canadian Acoustical Association*, vol. 28, no. 3, 2000.

[32] Hörlin, N.-E., et al. “A 3-D Hierarchical Fe Formulation Of Biots Equations For Elasto-Acoustic Modelling Of Porous Media.” *Journal of Sound and Vibration*, vol. 245, no. 4, 2001, pp. 633–652., doi:10.1006/jsvi.2000.3556.

[33] Hughes, Thomas J. R. *The Finite Element Method: Linear Static and Dynamic Finite Element Analysis*. Dover Publication, Inc, 2007.

[34] Ihlenburg, Frank. *Finite Element Analysis of Acoustic Scattering*. Springer, 1998.

[35] Jain, S.K., Joshi, M.P., Shravage, P.G:, Yadav, P.S., Karanth, N.V., “Evaluation of Acoustic Performance of Automotive Seats by Experimental and Simulation Techniques”, Symposium on International Automotive Technology, India, 2013

[36] Jin, G., Liu, Z., & Yang, T. (2009). Active control of sound transmission into an acoustic cavity surrounded by more than one flexible plate. *Noise Control Engineering Journal*, *57*(3), 210. doi:10.3397/1.3097762

[37] Jocker, Jeroen, and David Smeulders. "Ultrasonic Measurements on Poroelastic Slabs: Determination of Reflection and Transmission Coefficients and Processing for Biot Input Parameters." Ultrasonics 49.3 (2008): 319-30. Web. 15 Dec. 2016.

[38] Johnson, David Linton, et al. “Theory of Dynamic Permeability and Tortuosity in Fluid-Saturated Porous Media.” *Journal of Fluid Mechanics*, vol. 176, no. -1, 1987, p. 379., doi:10.1017/s0022112087000727.

[39] Kagami, Naokatsu, et al. “Analysis of Booming Noise in Van-Type Vehicle by Component Mode Synthesis Method.” *SAE Technical Paper Series*, 1988, doi:10.4271/880079.

[40] Kim, S.h., et al. “Structural-Acoustic Modal Coupling Analysis And Application To Noise Reduction In A Vehicle Passenger Compartment.” Journal of Sound and Vibration, vol. 225, no. 5, 1999, pp. 989–999. doi:10.1006/jsvi.1999.2217.

[41] Koners, Gregor, and Ralf Lehmann. “Investigation of Tire-Road Noise with Respect to Road Induced Wheel Forces and Radiated Airborne Noise.” *SAE International Journal of Passenger Cars - Mechanical Systems*, vol. 7, no. 3, 2014, pp. 1194–1197. doi:10.4271/2014-01-2075.

[42] Kumar, B., Ranjan, V., Azam, M.S. et al., "A Comparison of Vibroacoustic Response of Isotropic Plate with Attached Discrete Patches and Point Masses Having Different Thickness Variation with Different Taper Ratios", Shock and Vibration, vol. 2016, Article ID 8431431, 12 pages, 2016. https://doi.org/10.1155/2016/8431431

[43] Kumar, B., Ranjan, V., Azam, M.S. et al. Acoustic Response of Thin Plate with Discrete Patches with Variable Thickness in Water Medium. J. Vib. Eng. Technol. 8, 27–34 (2020).

[44] Lee, H. R., Kim, H. Y., Jeon, J. H., Kang, Y. J.”Application of global sensitivity analysis to statistical energy analysis: Vehicle model development and transmission path contribution.” Applied Acoustics, 146 (2019), 368–389

[45] Lennström, D., Lindbom, T., & Nykänen, A. (2013). Prominence of tones in electric vehicle interior noise. In Internoise 2013 : Noise Control for Quality of Life (Vol. 1, pp. 508–515). Innsbruck: ÖAL Österreichischer Arbeitsring für Lärmbekämpfung.

[46] Li, Y. Y., & Cheng, L. (2004). Modifications of acoustic modes and coupling due to a leaning wall in a rectangular cavity. *The Journal of the Acoustical Society of America, 116*(6), 3312-3318. doi:10.1121/1.1823331

[47] Li, Y., & Cheng, L. (2007). Vibro-acoustic analysis of a rectangular-like cavity with a tilted wall. *Applied Acoustics,68*(7), 739-751. doi:10.1016/j.apacoust.2006.04.005

[48] Liu, Y., and Li, Y., "Vibration and Acoustic Response of Rectangular Sandwich Plate Under Thermal Environment". Shock and Vibration, 20., 5 (2013), 1011 – 1030.

[49] Liu, Z., Fard, M., & Davy, J. (2015). "The effects of porous materials on the noise inside a box cavity." Proceedings of the 22nd International Congress on Sound and Vibration (ICSV22 2015), 1–8.

[50] Liu, Z., Fard, M., Davy, J. L., „Prediction of the acoustic effect of an interior trim porous material inside a rigid-walled car air cavity model", Applied Acoustics, 165 (2020)

[51] Lloret, M.G., Duvigneau, F., Müller, G., Gabbert, U., "On the numerical modelling of poroelastic layers in spring-mass systems", Applied Acoustics, 157 (2020)

[52] Lloret, M.G., Gabbert, U., Müller, G., "Evaluation of Sound Transmission Models for Automotive Applications" DAGA 2017 – 43. Jahrestagung für Akustik, 2017, Kiel

[53] Luegmair, M., Schmid, J.D., „Challenges in Vibroacoustic Vehicle Body Simulation Including Uncertainties", 11th International Styrian Noise, Vibration & Harshness Congress: The European Automotive Noise Conference, 2020, Graz

[54] Magliacano, D., Ashani, S., Ouisse, M., Deckers, E., Petrone, G., Desmet, W., De Rosa, S., „Formulation and validation of the shift cell technique for acoustic applications of poro-elastic materials described by the Biot theory", Mechanical Systems and Signal Processing, 147 (2021)

[55] Marburg, Steffen, and Bodo Nolte. *Computational Acoustics of Noise Propagation in Fluids: Finite and Boundary Element Methods*. Springer, 2008.

[56] Martin, V. and Bodrero, A. (1997). An Introduction To The Control Of Sound Fields By Optimising Impedance Locations On The Wall Of An Acoustic Cavity. *Journal of Sound* and Vibration, 204(2), 331-357. doi:10.1006/jsvi.1997.0963

[57] Miller, V. R., and L. L. Faulkner. "Prediction of aircraft interior noise using the statistical energy analysis method." Journal of Vibration, Acoustics, Stress and Reliability in Design, 105, 4 (1983): 512-518.

[58] Moeller, M. and Miller, T., "TBL Modeling for Aircraft Interior Noise Prediction Using Statistical Energy Analysis," SAE International Journal of Passenger Cars - Mechanical Systems, 6, 2 (2013), 1239-1250, https://doi.org/10.4271/2013-01-1931.

[59] Musser, C., Manning, J.E., Peng, G.C., Predicting Vehicle Interior Sound with Statistical Energy Analysis, Sound & Vibration, December (2012)

[60] N. Atalla, R. Panneton, and P. Debergue. A mixed displacement-pressure formulation for poroelastic materials. Journal of the Acoustical Society of America, 104 (3) 1444-1452, 1998.

[61] NASTRAN Basic Dynamic Analysis User’s Guide, Siemens Product Lifecycle Management Software Inc., 2014

[62] Olivier Dazel: Numerical methods for the Biot theory in acoustics, Uniersity of Maine – Le Mans, 2011

[63] Panneton, R., and Atalla, N. “An Efficient Finite Element Scheme for Solving the Three-Dimensional Poroelasticity Problem in Acoustics.” The Journal of the Acoustical Society of America, vol. 101, no. 6, 1997, pp. 3287–3298., doi:10.1121/1.418345.

[64] Peretti, L. F., & Dowell, E. H. (1992). „Asymptotic modal analysis of a rectangular acoustic cavity excited by wall vibration” *AIAA Journal, 30* (5), 1191-1198. doi:10.2514/3.11050

[65] Petrone, G., Melillo, G., Laudiero, A., De Rosa, S., “A Statistical Energy Analysis (SEA) model of a fuselage section for the prediction of the internal Sound Pressure Level (SPL) at cruise flight conditions”, Aerospace Science and Technology, 88 (2019), 340 – 349

[66] Pietrzyk, A., "Prediction of Airborne Sound Transmission into the Passenger Compartment," SAE Technical Paper 2015-01-2266, 2015, doi:10.4271/2015-01-2266.

[67] Priebsch, Hans H., et al. “Structure Borne Noise Prediction Techniques.” SAE Technical Paper Series, 1990, doi:10.4271/900019.

[68] Prosser, W. H., Hamstad, M. A., Gary, J., & O`Gallagher, A. (1999). Finite element and plate theory modeling of acoustic emission waveform. *Journal of Nondestructive Evaluation, 18*(3).

[69] Radcliffe, C. J., and Huang, X. L. "Putting Statistics into the Statistical Energy Analysis of Automotive Vehicles." ASME. Journal of Vibration and Acoustics, October 1997; 119(4): 629–634.

[70] Raju, B.B., „Vibration of thin elastic plates of linearly variable thickness”, International Journal of Mechanical Sciences, 8, 2 (1966), 89 – 94

[71] Raju, K.K., „Large amplitude vibrations of circular plates with varying thickness”, Journal of Sound and Vibration, 50, 3(1977), 399-403

[72] Rigobert, S., et al. “Investigation of the Convergence of the Mixed Displacement-Pressure Formulation for Three-Dimensional Poroelastic Materials Using Hierarchical Elements.” *The Journal of the Acoustical Society of America*, vol. 114, no. 5, 2003, p. 2607., doi:10.1121/1.1616579.

[73] Rondeau, J., Dejaeger, L., Guellec, A., Caillet, A. et al., "Cockpit Module Analysis Using Poroelastic Finite Elements," SAE Technical Paper 2014-01-2078, 2014 doi:10.4271/2014-01-2078.

[74] Roy, P.K., Ganesan, N., „Dynamic stress analysis of a tapered cantilever square plate under impact load”, Computers & Structures, 49, 2 (1993), 275 – 281.

[75] Roy, P.K., Ganesan, N., „Studies on dynamic stress in parabolically varying thickness square plate”, Journal of Sound and Vibration, 157, 3 (1992), 545 – 548.

[76] Roy, P.K., Ganesan, N., „Studies on the response of a square plate with variable thickness excited by uniformly distributed load”, Computers & Structures, 45, 3 (1992), 593 – 603.

[77] Schmid, J., Luegmair, M., Sepahvand, K., Marburg, S., "Uncertainty Quantification in Vibroacoustic Analysis of a Vehicle Body Using Generalized Polynomial Chaos Expansion," SAE Technical Paper 2020-01-1572, 2020, https://doi.org/10.4271/2020-01-1572.

[78] Schrader, P., Duvigneau, F., Lloret, M., Rottengruber, H., Gabbert, U. „Finite Element Analysis of the Acoustic Behavior of Poroelastic Materials Based on Experimentally Determined Frequency-Dependent Material Properties", International Conference on Noise and Vibration Engineering – ISMA 2018, Leuven

[79] Schweighardt, Attila ; Vehovszky, Balazs, Investigation of frequency dependent mechanical properties of porous materials using dynamic mechanical analyzer and frequency-temperature superposition theory, In: INTER-NOISE 50th International Congress and Exposition of Noise Control Engineering, Washington DC, United States of America: Institute of Noise Control Engineering (2021) pp. 4851-4862. , 12 p.

[80] SGM-Techno, „Sound absorber materials", Web.: https://sgm-techno.com/catalog/sound-absorber-materials-cars, accessed on: 28th of February, 2023

[81] Shome, Mahadev and Tumuluru, Muralidhar, Welding and Joining of Advanced High Strength Steels (AHSS),Woodhead Publishing, 2015, ISBN 9780857094360, https://doi.org/10.1016/B978-0-85709-436-0.12001-6.

[82] Song, Chul Ki, et al. "Active Vibration Control for Structural–Acoustic Coupling System of a 3-D Vehicle Cabin Model." Journal of Sound and Vibration, vol. 267, no. 4, 2003, pp. 851–865., doi:10.1016/s0022-460x(02)01553-5.

[83] Subramanian, S., et al. "Optimization of Damping Treatment for Structure Borne Noise Reduction." SAE Technical Paper Series, 2003, doi:10.4271/2003-01-1592.

[84] Sum, K. S., & Pan, J. (2006). Effects of the inclination of a rigid wall on the free vibration characteristics of acoustic modes in a trapezoidal cavity. *The Journal of the Acoustical Society of America, 119*(4), 2201-2210. doi:10.1121/1.2166707

[85] Sun, W., Thompson, D. J., Zhang, Z., Squicciarini, G., „A practical approach to modelling railway vehicle interior acoustics", Applied Acoustics, 200 (2022)

[86] Sung, S. H., Nefske D. “Assessment of a Vehicle Concept Finite-Element Model for Predicting Structural Vibration.” SAE Technical Paper Series, 2001, doi:10.4271/2001-01-1402.

[87] Sung, Shung H., et al. “Development and Experimental Evaluation of a Vehicle Structural-Acoustic Trimmed-Body Model.” SAE Technical Paper Series, 1999 doi:10.4271/1999-01-1798.

[88] V and F Co. UK., „”Sheet metal thickness”, Web: http://www.vandf.co.uk/design-data/sheet-metal-thickness-tolerances/, accessed on: 28th February, 2023.

[89] W. Strawderman, R. S. Brand, „Turbulent-Flow-Excited Vibration of a Simply Supported Rectangular Plate”, Journal of the Acoustical Society of America, 45, 177 (1969.)

[90] Wang, Y., Lu, C., Qin, X., Huang, S., Fu, G., Ni, X. “Analysis and Control of Structure-Borne Noise for a Trimmed Body by Using Panel Acoustic Participation Method.” Thin-Walled Structures, vol. 119, 2017, pp. 828–838., doi:10.1016/j.tws.2017.08.001.

[91] Wolf, J. A., Jr., & Nefske, D. J. (1975). NASTRAN modeling and analysis of rigid and flexible walled acoustic cavities. In *NASTRAN: User`s Experiences* (pp. 615-631). Warren, MI: NASA.

[92] Wolkesson, Martin. Evaluation of Impedance Tube Methods - A Two Microphone In-situ Method for Road Surfaces and the Three Microphone Transfer Function Method for Porous Materials. Thesis. Chalmers University of Technology, 2013. Göteborg: Division of Applied Acoustics

[93] Zhang, J., Xiao, X., Sheng, X., Zhang, C., Wang, R., Jin, X., „SEA and contribution analysis for interior noise of a high speed train”, Applied Acoustics, 112 (2016), 158-170

[94] Zienkiewicz, Olgierd C., and Robert L. Taylor. *The Finite Element Method*. Butterworth-Heinemann, 2003.